Cooperative Effects of Loss of *Vhl* and Loss of the Primary Cilium on Renal Cyst Formation and Renal Cancer Initiation

Dissertation

zur

Erlangung der naturwissenschaftlichen Doktorwürde

(Dr. sc. nat.)

vorgelegt der

Mathematisch-naturwissenschaftlichen Fakultät

der

Universität Zürich

Von

Holger Lehmann

aus

Deutschland

Promotionskomitee

Prof. Dr. Ian J. Frew

(Vorsitz und Leitung der Dissertation)

Prof. Dr. Eric Féraille

Prof. Dr. Olivier Devuyst

PD. Dr. Andreas Serra

Zürich 2014

Summary

von Hippel-Lindau (VHL) disease is an autosomal-dominant monogenetic disorder caused by inheritance of mutations of the *VHL* gene. Amongst other clinical manifestations, VHL patients have an increased risk of developing renal cysts and bilateral multifocal solid or cystic clear cell renal cell carcinomas (ccRCC). ccRCC in VHL patients is believed to arise from cystic precursor lesions in some cases and independently of cysts in other cases. The *VHL* gene is also biallelically inactivated in up to 90% of sporadic ccRCC cases, approximately 5% of which are multilocular cystic renal cell carcinomas. This suggests that sporadic ccRCC may also form through cyst-dependent as well as cyst-independent pathways. The protein product of the *VHL* gene (pVHL) is involved in many molecular processes, including HIFα regulation and stabilization of the microtubule network. The latter function seems to be particularly important for the cyst-dependent progression model due to the role of pVHL in regulating the stability of the primary cilium, a specialized microtubule structure that functions as a cellular antenna. Genetic mutations that compromise the structure or signalling functions of the primary cilium cause diverse types of polycystic kidney diseases, indicating that the primary cilium is an organelle that suppresses the formation of renal cysts. This thesis tested the cooperative effects of loss of *Vhl* function and loss of the primary cilium in mouse kidneys, to attempt to model the initial cellular changes that occur in the development of ccRCC.

We first developed a µCT imaging approach and validated this technique as a suitable tool to quantitatively monitor cyst formation and progression longitudinally and non-invasively *in vivo* in mice. This technique will likely be generally beneficial for all future studies of polycystic kidney diseases in rodent models. We show that renal epithelial-specific co-deletion of *Vhl* together with *Kif3a*, a key component of the primary cilium, shortens the latency of cyst initiation and enhances cyst formation and size. In addition, combined deletion of *Kif3a* and *Vhl* resulted in an ~4 fold increase in the formation of atypical cysts compared to *Kif3a* deletion alone. These lesions appear similar to the lesions that are proposed to be the precursor lesions of ccRCC in humans. One possible mechanism that may account for the increased formation of simple cysts and increased rate of progression to atypical cysts is an increased frequency of non-planar cellular divisions in *Vhl/Kif3a* double mutant mice. These studies give rise to a new model of initiation of ccRCC whereby loss of the primary cilium represents a secondary event in *VHL* mutant cells that cooperates with additional cellular changes that arise due to loss of pVHL function to induce simple and atypical cyst formation. It appears that additional genetic alterations are necessary to allow neoplastic transformation and progression of these precursor lesions to cystic or solid ccRCC.

A second aim of this thesis was to investigate the hypothesis that HIF1α may play a general role in cyst formation in the kidney, based on observations that HIF1α is stabilized in cystic epithelial cells due to microenvironmental hypoxia. Recent studies proposed that HIF1α activation functions to promote cyst formation. In contrast to these studies, we found that cystic lesions induced by *Kif3a* deletion are not characterized by HIF1α stabilization. Moreover, deletion of *Hif1a* in the *Kif3a* knockout model of cyst formation did not alter the timing of initiation or extent of growth of cysts, nor did it affect the frequency of atypical cysts. It appears that HIF1α stabilization in renal cysts may be limited to more severe cystic phenotypes or that additional cellular signaling changes induced by mutations of the *PKD1/PKD2* genes in autosomal dominant polycystic kidney disease may contribute to HIF1α activation. Our genetic studies in a physiologically relevant model of polycystic kidney disease clearly indicate that HIF1α stabilization does not modify cystic phenotypes.

Zusammenfassung

Die von Hippel-Lindau (VHL) Erkrankung ist eine autosomal dominante Erbkrankheit, welche durch Mutationen des *VHL* Gens verursacht wird. Neben anderen klinischen Erscheinungsformen haben VHL Patienten ein erhöhtes Risiko beidseitig Nierenzysten und multilokuläre solide oder zystische klarzellige Nierenzellkarzinome (NZK) zu entwickeln. Es wird angenommen, dass NZK in VHL Patienten in einigen Fällen aus zystischen Vorläuferläsionen und in anderen Fällen unabhängig von Zysten entstehen. Das *VHL* Gen ist außerdem in bis zu 90% der sporadischen NZK Fälle biallelisch inaktiviert, ungefähr 5% davon sind multilokulär zystische Nierenzellkarzinome. Dies deutet daraufhin, dass sporadische NZK wahrscheinlich zysten-abhängig, wie auch –unabhängig, entstehen. Das Proteinprodukt des *VHL* Gens (pVHL) ist in viele molekulare Prozesse involviert, unter anderem auch in die HIFα Regulierung und die Stabilisierung des Mikrotubulinnetzwerkes. Die letztere Funktion scheint besonders wichtig für das zysten-abhängige Entstehungsmodell zu sein, da pVHL eine Rolle in der Regulierung der Stabilität der primären Zilie, eine spezialisierte Mikrotubulistruktur, welches als zelluläre Antenne funktioniert, spielt. Genetische Mutationen, welche die Struktur oder die Signalfunktionen der primären Zilie stören, führen zu diversen Arten von polyzystischen Nierenerkrankungen. Dies deutet daraufhin, dass die primäre Zilie ein Organell ist, welches die Entstehung von Nierenzysten unterdrücken kann. Diese Doktorarbeit untersucht den kooperativen Effekt des Verlustes der *Vhl* Genfunktion und des Verlustes der primären Zilie in Maus Nieren, um ein Modell für die initialen zellulären Veränderung, welche während der Entwicklung von NZK entstehen, zu entwickeln.

Zuerst haben wir einen Ansatz für bildgebende µCT Daten entwickelt und diese Technik zur quantitativen Überwachung von Zystenbildungen und –entwicklung als geeignetes Mittel zur wiederholten nicht invasiven *in vivo* Methode in der Maus validiert. Diese Technik wird generell für alle zukünftigen Studien von polyzystischen Nierenerkrankungen in kleinen Nagern nützlich sein. Wir zeigen, dass nierenepithelspezifische zeitgleiche Deletion von *Vhl* und *Kif3a*, einer wichtigen Komponente der primären Zilie, die Latenzzeit des Zystenbeginns verkürzt und die Zystenentstehung, sowie die Zystengröße, erhöht. Zusätzlich führt die gleichzeitige Deletion von *Vhl* und *Kif3a* zu einer ~4 fachen Erhöhung der Entstehung von atypischen Zysten im Vergleich zur Einzeldeletion von *Kif3a*. Diese Läsionen scheinen ähnlich zu den Läsionen zu sein, welche als Vorläuferläsionen für NZK im Menschen gelten. Ein möglicher Mechanismus, der die erhöhte Entstehung von einfachen Zysten und die erhöhte Rate zum Übergang in atypische Zysten erklären kann, ist die erhöhte Frequenz von nicht-planaren Zellteilungen in *Vhl*/*Kif3a* doppelmutanten Mäusen. Diese Studien zeigen ein

neues Modell der Initiierung von NZK auf, wobei der Verlust der primären Zilie ein sekundäres Ereignis in *VHL* mutierten Zellen ist, welches mit weiteren zellulären Veränderungen kooperiert, die durch den Verlust der pVHL Funktion entstehen und zu einfachen, sowie atypischen Zysten führen. Es scheint, als wären weitere genetische Veränderungen nötig, um neoplastische Transformation und die Entwicklung von Vorläuferläsionen in zystische oder solide NZK zu erzeugen.

Ein zweites Ziel dieser Doktorarbeit war es die Hypothese, dass HIF1α eine eher generelle Rolle in der Zystenentstehung in der Nieren spielen soll, zu untersuchen. Diese Hypothese beruht auf Beobachtungen, dass HIF1α in zystischen Epithelzellen durch Hypoxie stabilisiert ist. Jüngste Studien schlagen vor, dass HIF1α Aktivität die Entstehung von Zysten fördert. Im Gegensatz zu diesen Studien haben unsere zystischen Läsionen, induziert durch *Kif3a* Deletion, keine HIF1α Stabilisierung gezeigt. Zusätzlich unterschieden sich die Mäuse mit Deletion von *Hif1a* im *Kif3a* knockout Modell für Zystenentstehung weder im Zeitpunkt der Zystenentstehung, dem Ausmaß des Wachstums noch in der Frequenz von atypischen Zysten. Es scheint, als wäre HIF1α Stabilisierung in Nierenzysten auf schwerere zystische Phänotypen beschränkt oder dass zusätzliche zelluläre Mechanismen, wie z.B. durch Mutationen in *PKD1/PKD2* Genen, verantwortlich für autosomal dominante polyzystische Nierenerkrankung, die Stabilisierung von HIF1α unterstützen. Unsere genetischen Studien in einem physiologisch relevanten Model für polyzystische Nierenerkrankungen zeigen deutlich, dass die Stabilisierung von HIF1α den zystischen Phänotyp nicht beeinflusst.

Acknowledgements

First, I would like to thank Ian Frew for giving me the opportunity to work with him in his lab. I very much appreciated Ian´s constant support, how he handled the lab and that his door was always open. This made it a truly exciting and stimulating time.

Thanks to Olivier Devuyst, Eric Féraille and Andreas Serra for valuable input during my PhD committee meetings and for providing cells and methods to support my work. Thanks to Vartan Kurtcuoglu for replacing Olivier Devuyst in my PhD exam. I would also like to thank Roli Wenger for valuable discussions during our lab meetings and for the support with the SPS travel grant.

I would like to acknowledge all current and former members of our and the Wenger lab who all helped to create a positive working atmosphere and also a special thanks for the not work related memories. I have enjoyed the friendships and will continue to do so. I really appreciate the help in the lab and the contributions made to this thesis including spare aliquots of adenoviruses (Tomas), taking care of cell lines during holidays (Tomas, Joachim, Laura, Désirée and Sabine), statistical consultations (Michal) or providing data for Fig. 5 and Fig. S7 (Ian).

The staff of the mouse facility and the ZIRP center deserves a big thank you for their countless hours of work that allowed me to study mice and perform experiments.

I would like to thank all my friends in Zurich and back in Germany for common trips (short or long) and for the occasional distraction from work. Special thanks to everyone who joined me or whom I could join for the occasional run.

Thanks to my family who supported me all the way and who I can rely on when I need to.

Last but not least, thanks to Mareike who always supported me and made me feel at home. I would not be where I am now if it was not for you.

Table of Contents

Abbreviations

ADPKD	Autosomal-dominant polycystic kidney disease
AE1	Anion exchanger 1
Aqp2	Aquaporin 2
ATPV1B1	ATPase H+ transporting lysosomal V1 subunit B1
ARPKD	Autosomal-recessive polycystic kidney disease
BSA	Bovine serum albumin
µCT	micro Computed Tomography
DABCO	1,4-diazabicyclo[2.2.2]octane
DBA	Dolichos Biflorus Agglutinin
DICOM	medical imaging file format
DMEM	Dulbecco´s modified Eagle's medium
DTT	Dithiothreitol
EDTA	Ethylenediamine tetra acetic acid
EGF	epidermal growth factor
FCS	fetal calf serum
H&E	haematoxylin and eosin
HBSS	Hank´s balanced salt solution
HC	hydrocortisone
HEPES	4-(2-hydroxyethyl)-1-piperazineethanesulfonic acid
HGF	hepatocyte growth factor
HIF	hypoxia-inducible factor
i.v.	intravenously
IF	immunofluorescence
IFT	intraflagellar transport
LTA	Lotus tetragonolobus agglutinin
NaN_3	sodium azide
NaPi	Sodium/phosphate cotransporter
NCC	sodium-chloride symporter
NKCC2	Na-K-Cl cotransporter 2
PAGE	polyacrylamide gel electrophorese

PBS	phosphate buffered saline
PCP	planar cell polarity
Pen/Strep	Penicillin/Streptamycin
PGE1	prostaglandin 1
PKD	Polycystic kidney disease
PMSF	Phenylmethanesufonyl fluoride
RIPA	Radioimmunoprecipitation assay protein lysis buffer
SBA	sodium boric acid
SDS	sodium dodecyl sulfate
SRB	Sulforhodamine B sodium salt
SS	sodium selenite
T3	Triiodothyronine
TBS	Tris buffered saline
TEMED	N,N,N´,N´-Tetramethylethylenediamine
TF	transferrin
THP	Tamm-Horsfall protein
VHL	von Hippel-Lindau

1 Introduction

1.1 VHL disease

Von Hippel-Lindau (VHL) disease is an autosomal dominant inherited genetic condition with an incidence of 1:36,000 live births (1, 2). VHL patients have an increased risk of developing benign and malignant tumours, including haemangioblastomas, renal cysts, renal carcinomas and phaeochromocytoma (3). VHL disease is caused by germline mutations (deletions, missense or splicing defects) of the *VHL* tumour suppressor gene located on chromosome 3p25 (4, 5). In addition to hereditary VHL disease, the *VHL* gene is inactivated in up to 90% of sporadic cases of clear cell renal cell carcinoma (ccRCC) (6-11). Approximately two-thirds of patients with VHL disease develop renal cysts and clear cell renal cell carcinoma (ccRCC) (3, 12, 13). VHL disease can be split into two distinct clinical phenotypes based on the risk of patients for phaeochromocytoma (14-16). Type 1 VHL disease exhibits low risk of phaeochromocytoma whereas type 2 VHL disease is characterized by a high risk of developing phaeochromocytoma. Both of these subtypes can be further divided by their mutation status and their risk of RCC. Type 1A disease is characterized by a high risk of RCC and truncating mutations or missense mutations that impair pVHL (the *VHL* gene product) folding whereas type 1B shows a low risk for RCC and large deletions of the *VHL* gene. Type 2 can be divided into three groups, all of which are caused by missense mutations. The risk of developing RCC is low in Type 2A, high in Type 2B and extremely low in Type 2C patients (14-16). Mutations of the *VHL* gene are distributed over all three exons (9).

Several models of deletion of the mouse VHL homologue, *Vhl,* have been generated. The germline deletion of *Vhl* resulted in embryonic lethality due to dysfunctional placental vasculature (17). Mosaic deletion of *Vhl* (β-actin-Cre) resulted in hepatic vascular tumours and increased angiogenesis in the kidney (18). Specific *Vhl* inactivation in the proximal tubule cells (Pepck-Cre) resulted in the development of a small number of renal cysts in about 20% of mice after one year of age (19). Furthermore, deletion of *Vhl* in all nephron segments (Pax8-Cre), all segments but the proximal tubules (Ksp1.3-Cre) or the thick ascending limb only (Thp-Cre) did not lead to ccRCC formation (20-23). Thus, *Vhl* deletion alone in renal epithelial cells does not cause proliferative dysregulation or the formation of ccRCC. Recently, combined deletion of *Vhl* and *Pten* in renal epithelia was shown to cause polycystic kidneys and the combined deletion of *Vhl* and *Trp53* in the kidney resulted in cyst formation and also the induction of neoplasms, mimicking apparent precursor lesions of ccRCC but not causing ccRCC (see section 1.1.4) (20, 24). These studies collectively show that *Vhl* inactivation alone is not sufficient to induce ccRCC formation in the mouse and that

additional mutations most likely need to occur to induce malignant transformation. This project aims to investigate using mouse genetics the initial events that occur in the formation of ccRCC precursor lesions and also seeks to contribute to the longer term goal of generating the first autochthonous mouse model of ccRCC.

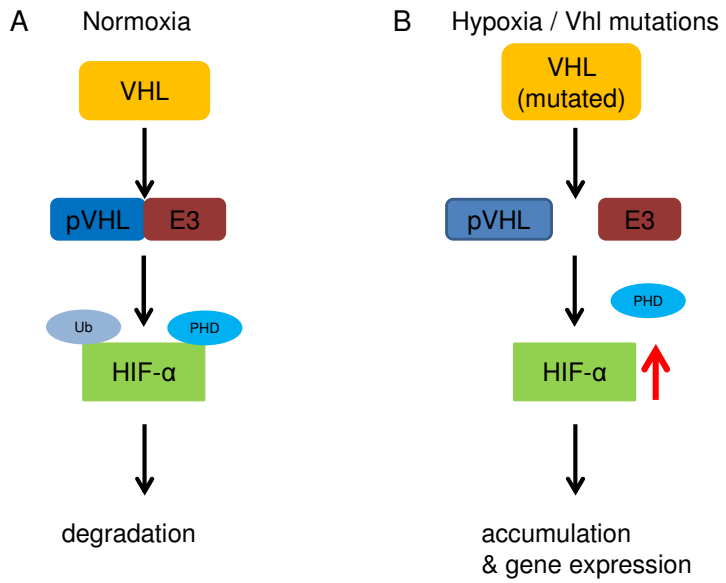

Figure 1.1: Regulation of HIFα by pVHL. (A) In normoxia, HIF-αs are hydroxylated by the PHD enzymes. pVHL forms an E3 ubiquitin ligase complex that binds the α-subunits of the HIF-α protein and marks them with ubiquitin. This results in the proteasomal degradation of the HIF-α. (B) Under hypoxic conditions, HIF-α are not hydroxylated by the PHD enzymes therefore escaping pVHL dependent degradation. In addition, mutations of the VHL gene that prevent the binding of HIF-α or the association with the other E3 ubiquitin ligase complex members lead also to the accumulation of HIF-α. This accumulation results in gene expression of HIF-α target genes. E3 = members of the E3 ubiquitin ligase complex; HIF-α = hypoxia-inducible factors α; PHD = prolyl hydroxylases; VHL = von Hippel-Lindau tumour suppressor.

1.1.1 VHL gene product (pVHL)

The *VHL* gene was first isolated in 1993 (4). Two gene products are transcribed from the *VHL* gene locus due to an internal translation start at codon 54. This results in two proteins with an apparent molecular weight of 30kDa and 19kDa, respectively (25-28). The term pVHL refers to both *VHL* gene products. pVHL consists of two major structural domains: an N-terminal β-domain and a smaller C-terminal α-domain (29). The β-domain contains mainly β-sheets whereas the α-domain spans the amino acids 155 to 192 and comprises α-helices. The most studied function of pVHL is its role as the substrate-binding subunit of an E3 ubiquitin ligase complex that targets substrates for proteasomal degradation. In addition to pVHL, the complex consists of elongin C, elongin B, Cullin 2 and Rbx1 (10, 29-33). Under normoxic conditions this ubiquitin ligase complex binds to the α-subunits of the hypoxia-inducible factors (HIF1α, HIF2α and HIF3α) and marks them for ubiquitination and proteasomal degradation. The mechanism of this will be discussed in section 1.1.2. In addition, there is evidence that pVHL is also involved in regulating other cellular processes,

including microtubule stability (34). pVHL´s influence on microtubules and therefore on the function of the primary cilium and will be addressed in section 1.3.

1.1.2 Regulation of HIFα by pVHL

The hypoxia-inducible transcription factors (HIFs) consist of three HIFα members (HIF1-3α) and HIF1β which is also called ARNT (aryl hydrocarbon receptor nuclear translocator) (33, 35, 36). HIFα and ß contain the same domains including a basic helix-loop-helix domain for DNA binding, a PAS domain for dimerization and a C-terminal transactivation domain (CTAD) for the interaction with other proteins. In normoxia, the HIFα subunits are rapidly degraded through interaction with prolyl hydroxylases (PHDs) and the pVHL/E3 ubiquitin ligase complex. The newly synthetized HIFα´s are hydroxylated at two conserved proline residues through one of the four mammalian PHDs (35, 37, 38). Only after hydroxylation at these proline residues are the HIFα´s recognized by the pVHL/E3 ubiquitin complex and targeted for degradation by direct interaction of the proline hydroxylated region of HIFα with the HIFα oxygen-dependent degradation domain (ODD) of pVHL. In normoxia and mild hypoxia, factor-inhibiting HIF (FIH) is able to hydroxylate an asparaginyl residue within the CTAD and thereby inhibits HIF transactivation activity by altering protein-protein interactions with the co-activators p300 and CREB-binding protein (CBP) (39). Under hypoxia, the unhydroxlated HIFα cannot be bound by pVHL and therefore accumulates in the cell. The HIFα´s translocate into the nucleus and form heterodimers with the constitutively expressed HIF1β. The HIFα/HIFβ complex recruits p300 and CBP and binds to nuclear DNA, so called hypoxia response elements (HREs) (40). Binding of HIF complexes to HREs increases gene expression involved in but not limited to cell proliferation, survival, angiogenesis and energy metabolism (Glut1). To date more than 70 different genes have been shown to be directly regulated by HIF (41). Inactivation or functional loss of pVHL results in the accumulation of HIFα and in HIFα target gene expression. In addition, HIF1α accumulation was detected in large cysts of rodent PKD (polycystic kidney disease) models due to the presence of hypoxic regions in these cystic kidneys (42). There is conflicting data concerning whether HIF1α has a direct influence on cyst formation or not. One study showed that deletion of HIF1α leads to decreased cyst formation in *in vitro* cyst formation models and that HIF1α overexpression leads to increased chemical induced cyst formation *in vivo* (43). On the other hand, data from a genetic model involving *Vhl* deletion showed that deletion of Hif1a does not suppress formation of cysts *in vivo* (19). One aim of this project is to investigate whether HIF1α is activated in cysts that form due to the absence of the primary cilium (due to *Kif3a* deletion) and whether co-deletion of *Hif1a* affects cyst formation or progression *in vivo*.

1.1.3 PI3K/mTOR pathway in cancer

The phostatidylinositol-3-kinase (PI3K) and the mammalian target of rapamycin (mTOR) signaling pathways regulate cell growth and cell survival in physiological and pathophysiological conditions. Mutations in either of these pathways enable cell growth that is unrestricted by extracellular cues and ultimately drive tumourigenesis through enhanced protein synthesis, cell cycle progression and changes in metabolism (44, 45). Activating mutations of receptor tyrosine kinases and PI3K subunits or inactivating mutations of negative regulators like PTEN are found in up to 30% of human tumours including breast and colon cancer but also kidney cancer (45). Cowden´s disease is a dominant inherited cancer syndrome with germline mutations in *PTEN* and a high percentage of sporadic cancers displays with PTEN mutations (46, 47). The activation of PI3K leads to the generation of phosphatidylinositol 3,4,5 triphosphate (PtdIns(3,4,5)P3) that activate the AKT1, AKT2, and AKT3 kinases (48, 49). AKTs are able to inactivate pro-apoptotic factors, negatively regulate TP53 through MDM2 activation, cause mTOR activation and inhibit GSK3β which regulates cell cycle progression, metabolism and is a part of the primary cilium maintaining network (see chapter 1.3) (48, 50, 51). mTOR forms dimers and participates in large protein complexes. In humans, two mTOR complexes (mTORC1 and mTORC2) with distinct functions are known. mTORC1 is activated in about 60-85% of ccRCCs (52, 53). mTORC1 is a key component of the cell´s metabolic and growth regulatory signalling networks (54-56). It is able to promote protein synthesis by phosphorylation and activation of S6 kinase and phosphorylation and inactivation of 4E-BP1 (57, 58). Regulation of mTORC1 is achieved by negative inhibition of Rheb through the tuberous sclerosis complex 1 (TSC1) and 2 (TSC2) tumour suppressor proteins (55). In turn, one pathway that regulates TSC2 is PI3K signaling. Given the frequency of activation of the PI3K/mTOR pathway in ccRCC, it appears likely that this may act cooperatively with pVHL loss to cause ccRCC (see section 1.1.4).

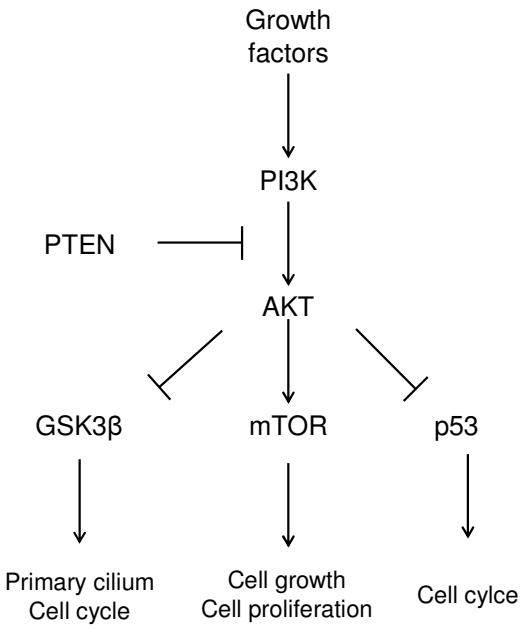

Figure 1.2: PI3K-mTOR pathway: Activation of the PI3K pathway through growth factors results in the activation of AKT. Active AKT is able to directly inhibit GSK3β, indirectly inhibit p53 and activates mTOR. This results in enhanced proliferation, cell growth, it influences the cell cycle progression and has an effect on the maintenance of the primary cilium.

1.1.4 clear cell Renal Cell Carcinoma (ccRCC)

The term RCC describes the set of cancers that arise from the renal tubular epithelia. There are 3 main histopathological entities. ccRCC accounts for ~65-80% of all reported cases followed by papillary RCC (~15-20%) and chromophobe RCC (5%) (59). Histological characteristics of ccRCC include glycogen and lipid-rich clear cells and a network of small blood vessels (60). On computed tomography (CT) images, ccRCC presents as typically hypervascular and heterogeneous lesions due to central necrosis, hemorrhage and/or calcification (Figure 1.1) (61). In addition to solid ccRCC several other subtypes are described. Some ccRCC display a cystic appearance with ccRCC tumour cells growing along the wall of the cyst within the cystic space and also growing as small clusters between cysts. These cases with no solid ccRCC and only cystic appearance are termed multilocular cystic RCC and account for 5% of all ccRCC (62). Some pVHL-deficient cysts that arise in patients with VHL disease also contain micro-foci of ccRCC. It appears that, at least in some cases, cystic regions represent a precursor lesion of malignant familial and sporadic cases of ccRCC (63, 64). The presence of renal cysts, the cystic appearances and the solid entities in many sporadic ccRCC suggest a not mutually exclusive concept of cyst-dependent and cyst-independent progression models of ccRCC formation. This progression model is described in more detail in Figure 1.2 (65, 66). This thesis aims to test the hypothesis that cysts represent precursor lesions of ccRCC using a mouse genetic approach.

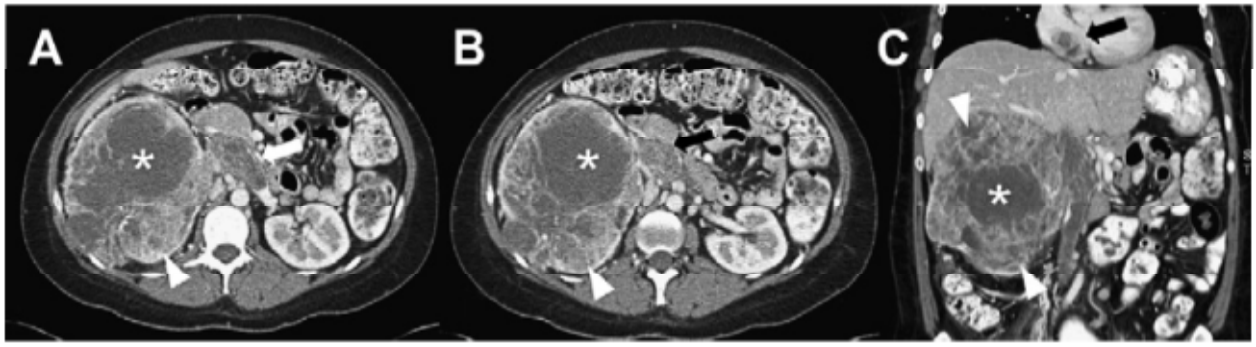

Figure 1.3: CT image of a ccRCC patient. Contrast-enhanced CT images show a large right renal mass with features typical of ccRCC, including central necrosis (asterisk) and peripheral heterogeneously hyperenhancing tissue (arrowheads). Axial (A, B) and coronal (C). Nephrectomy was performed and histopathology showed ccRCC, grade IV. Image from Krajewski *et al.* (67).

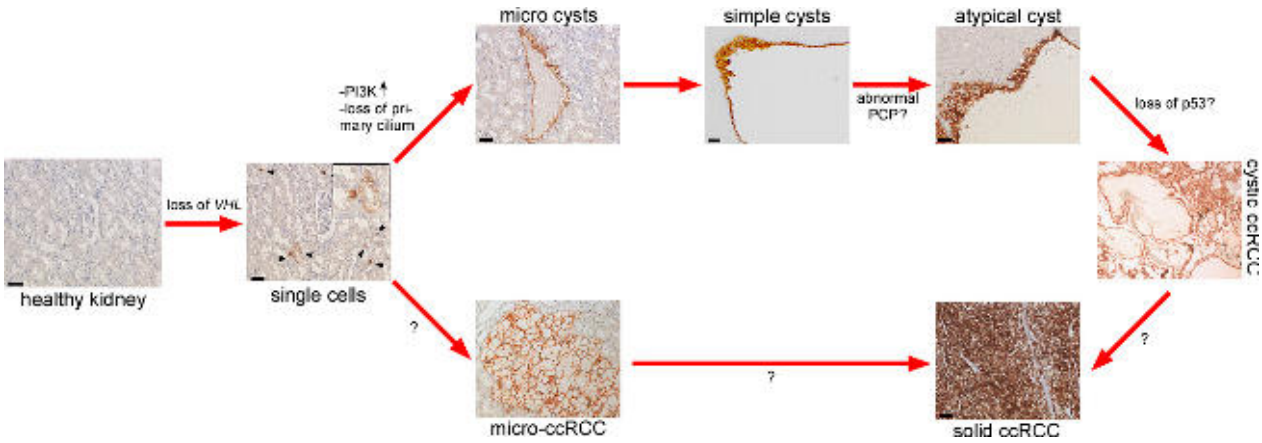

Figure 1.4: Current model of ccRCC development and progression. Homozygous loss of *VHL* occurs frequently in VHL patients but only a small proportion of these *VHL* null cells progress into micro-cysts and the majority of *VHL* mutant cells appear to remain as single cells or as small clusters of cells. Micro-cysts are characterized by upregulated PI3K signalling and loss of the primary cilium. Cyst expansion leads to the enlargement of micro-cysts into larger simple cysts that are lined by a single epithelial layer. It is believed that some simple cysts can progress to form atypical cysts, which are characterized by regions of disorganized and multilayered epithelial growth, potentially reflecting a loss of epithelial planar cell polarity (PCP). It is likely additional pro-proliferative mutations, such as *TP53* mutations, are needed for the development of cystic ccRCC and probably further mutations may turn cystic ccRCC into solid ccRCC. This may occur through neoplastic growth completely filling the former cystic lumen. Little is known about the mechanisms by which *VHL* null cells may progress to form micro-ccRCC lesions with a solid appearance which may then directly go on to form solid ccRCC. In summary, it is believed that ccRCCs can form via cyst-dependent and cyst-independent precursor lesions.

Bi-allelic loss of *VHL*, either through mutations, deletions, methylation or chromosomal loss, appears in most hereditary and sporadic cases of ccRCC. A recent study estimates the frequency of *VHL* loss in ccRCC to be up to 91% of cases (9). Very recently, The Cancer Genome Atlas consortium characterized ccRCC on a genome-wide molecular level (68). The analysis of over 400 tumours revealed that in addition to VHL mutations, ccRCCs frequently harbor activating mutations in the PI3K/mTOR pathway, mutations that impair normal cell cycle regulation (TP53, RB1, CDKN2A, MYC) as well as mutations in several genes involved in epigenetic regulation (PBRM1, SETD2 and BAP1). Thus, since these mutations occur in

different combinations in ccRCC, it appears that there are numerous different molecular subtypes of these tumours, which are described in more detail below.

Dysfunctional pVHL prevents the degradation of HIF1α and HIF2α leading to their constitutive overexpression. Genetic data suggests that HIFα activation is an oncogenic driving force in ccRCC (69-71). However, several studies indicate that HIF1α and HIF2α carry out different roles in ccRCC development. Comparing *Vhl*-wild type and *Vhl*-deficient mouse tumor xenografts suggests that loss of pVhl function causes a growth disadvantage (72, 73). This effect may in part be based on the activation of HIF1α which exerts a growth disadvantage in MEFs *in vitro* and in human ccRCC xenografts (70, 74). This is likely to be at least partly mediated by opposing the cell cycle promoting activity of MYC through direct binding, transcriptional regulation of a MYC inhibitor (MXI-1) and promotion of MYC degradation (74, 75). HIF2α, in contrast, promotes MYC activity and promotes proliferation in MEFs and ccRCC xenografts (69-71, 75). In regard to cell cycle properties in ccRCC, HIF1α seems to inhibit tumour proliferation whereas HIF2α promotes tumour proliferation. ccRCC expressing both HIF1α and HIF2α display reduced MYC activity and are less proliferative than ccRCCs expressing HIF2α only (76). Several factors may contribute to this imbalance of HIF1α to HIF2α expression. ccRCCs frequently present with single copy loss of the *HIF1A* gene locus and ccRCC cell lines often harbor biallelic inactivation of the *HIF1A* locus (77, 78). The hypoxia-associated factor (HAF) selectively targets HIF1α for proteasomal degradation and rather enhances HIF2α´s gene transactivation ability (79, 80). In various *in vitro* studies the expression of HIF1α and HIF2α seem to be mutually exclusive (70, 81). In addition, there is a differentially dependency of HIF1α and HIF2α on PI3K/mTOR activity which is frequently upregulated in ccRCC cases (82). In summary, it appears that HIF1α acts like a tumour suppressor, whereas HIF2α acts as an oncogene in established ccRCC tumours. However, the involvement of these proteins in tumour initiation has yet to be established.

The PI3K pathway is upregulated in malignant and pre-malignant regions in the kidney of VHL patients (20). Mutations throughout the whole PI3K/mTOR pathway leading to activation of mTORC1 occur in ~28% of analyzed ccRCCs (68). Supporting the idea that cooperative effects of loss of pVHL function and activation of the PI3K pathway may contribute to ccRCC, the generation of a mouse with renal epithelial-specific combined deletion of *Vhl* and *Pten* caused a strong cystic kidney phenotype (20). Loss of primary cilium due to the diminished microtubule stabilization by *Vhl* deletion and inactivation of GSK3ß was proposed to contribute to the development of this cystic phenotype (see also chapter 1.3) (51). Interestingly, these *Vhl/Pten*-deficient animals also developed multiple begin malignancies in the genital tract due to activity of the Cre driver in the embryonic structures

that gives rise to these tissues, further emphasizing the cooperative functions of the VHL and PTEN-controlled pathways in tumour formation (20).

ccRCC can also be viewed as one of the so-called ciliopathies, diseases that are associated with dysfunction of the primary cilium (83). VHL disease, like the collection of polycystic kidney diseases (PKD), presents with renal cysts. ccRCC associated with loss of *VHL* shows a reduced frequency of cilia compared to papillary RCC (84). The primary cilium is linked to many different signaling pathways and cell polarity (83, 85, 86). The relationship between pVHL and the primary cilium will be addressed in section 1.3.

Until now, the cell type or types that gives rise to ccRCC remains unclear. There is evidence that ccRCC is most often of proximal tubule origin. This idea is supported by the observation that many ccRCC cases exhibit positive immunoreactivity for proximal tubule specific antigens, including CD10, villin, renal cell carcinoma antigen, ICAM-1, MRP2 and lotus teraglonobulus agglutinin (87-92). Nevertheless, some cases of ccRCC express proteins specific for the distal tubule, including Cytokeratin 19, CD24 and α3-integrin (89, 91). Galectin-3 is also expressed in some ccRCC and is usually expressed in distal tubules and the collecting duct (93). These studies collectively show that ccRCC can express a broad variety of markers of different tubular segments, implying that these tumours can arise from different nephron segments. The implication of these observations for attempts to model ccRCC in mice is that gene deletion should be targeted to as many different nephron segments as possible. For this reason, we have employed the Ksp1.3-Cre^{ERT2} transgene (94), which induces gene deletion specifically in renal epithelial cells of all nephron segments. Since deletion of *Vhl* alone did not result in ccRCC formation in mouse models additional mutations or cellular changes such as those described above are likely to be required to enable *Vhl*-null renal epithelial cells to progress to cyst formation and ultimately ccRCC. In this thesis we focus on combined deletion of *Vhl* and abrogation of the primary cilium whose loss is known to induce kidney cysts.

1.2 The primary cilium

Once neglected by researchers, the primary cilium has become an intensively studied organelle over the past decade. The primary cilium is a microtubule-based organelle present on the vast majority of vertebrate cells (95). There are two types of cilia protruding from the cell, the motile cilia and the generally non-motile cilia (the primary cilium). Motile cilia are composed of 9 microtubule doublets surrounding a central doublet. This structure is known as 9+2 conformation. In contrast, primary cilia lack the central doublet, leading to a 9+0 structure (96). Each cell expresses only a single primary cilium, which originates from the older (mother centriole) of the two centrioles in quiescent cells. Disassembly of the primary

cilium takes place as the cell re-enters the cell cycle (97). Assembly of the primary cilium follows a well-orchestrated formation of different steps (98, 99). First, the basal body migrates to the cell´s plasma membrane and connects to the actin filament and to cytosolic microtubules. During this process the basal body interacts with membrane vesicles that fuse to the membrane to form the ciliary membrane compartment. Secondly, an outgrowth of basal body microtubules protrudes beneath the ciliary membrane to give rise to the cilium. The starting point of this outgrowth is called the transition zone. Microtubule assembly is achieved from the distal tip of the cilium only (100). Even when the cilium reaches its final length this structure is highly dynamic. New tubulin is continually incorporated at the distal part but due to a steady turnover of the tubulin fibre the cilium does not continue to elongate (101-103).

The construction of the primary cilium requires a process called intraflagellar transport (IFT). Because all ciliary proteins are synthesized in the cytoplasm, IFT complexes shuttle all proteins into the cilium and back to the cytoplasm if needed (reviewed in (104)). The transfer of IFT complexes with their cargo proteins to the tip of cilium is called anterograde transport and is mediated by the heterotrimeric kinesin II motor complex (Kif3a, Kif3b and Kap3). After the IFT complex reaches the tip it undergoes a transition resulting in inactivation of the kinesin and the retrograde transport is carried out by dynein (105-108). In this study we have utilized genetic deletion of *Kif3a* to cause genetic ablation of primary cilia. Further analysis of the IFT complexes showed that two subgroups are present, complex A (550kDa) and complex B (710kDa) (109). Mutations affecting IFT complex A (retrograde transport) result in shortened cilia with accumulation of IFT particles similar to dynein mutants whereas mutations in IFT complex B (anterograde) exhibit truncated cilia without IFT particle accumulation phenocopying kinesin mutations (101, 107, 110, 111).

Research of the last decade placed the primary cilium at the center of several important signaling pathways (see chapter 1.2.1) and elucidated its role as a sensory organelle (104, 112). This was achieved by linking different genetic diseases to ciliary dysfunctions, the so-called ciliopathies (113). These ciliopathies include genetic syndromes like Alström syndrome, Bardet-Biedl syndrome (BBS), Joubert syndrome and Meckel-Gruber syndrome (reviewed in (114-116)). It was shown that the primary cilium is important for several sensory functions in the vertebrate animal. It functions as a mechanosensor on renal epithelial cells and it responds to fluid flow by an intracellular calcium signal (117). Dysfunction of IFT is detrimental for the outer segment of photoreceptors and photoreceptor defects are common in many ciliopathies (95, 118, 119). In addition, it was shown that odorant detection is impaired in BBS patients and in mouse cilia mutants (120).

1.2.1 Signaling from the primary cilium and planar cell polarity (PCP)

The primary cilium is involved in a wide variety of signaling cascades including receptor tyrosine kinases, Hedgehog (Hh) and Wnt signaling (112, 121-124).

Hh signaling is involved in developmental processes including growth patterning, cell fate determination, cell proliferation and cell survival (125). In addition, dysregulation of Hh signaling has been described to be involved in several tumor types including medulloblastoma, breast carcinoma, basal cell carcinoma and many more (126). Many publications link Hh signaling to the primary cilium. This relationship was initially discovered when a mouse mutant of *Ift88* showed phenotypic manifestations of dysfunctional Hh signaling including altered digit number and loss of left-right asymmetry (127, 128). It could be shown that the Smo receptor is translocated to the cilium upon Hh binding and that the cilium is required for Smo activity (129, 130). Moreover, Gli1-3 and Sufu also reside in the distal tip and IFT proteins are needed to transmit activator and repressor functions of the Gli proteins into the cell (127, 128, 130, 131). Loss of Gli activator and repressor functions give rise to similar phenotypes to those observed in IFT mutant mice (128).

There is evidence that the primary cilium has an influence on both canonical and non-canonical Wnt signaling and vice versa (132). ß-catenin is associated with adherens junctions at the cell membrane in differentiated cells and is also present freely in the cytoplasm. Stabilization of ß-catenin through mutations or inactivation of APC leads to colorectal cancer (133). Transgenic mice overexpressing ß-catenin develop renal cysts (134). The non-canonical Wnt pathway regulates a pathway called planar cell polarity (PCP) which dictates the cell´s cell division angle and the orientation of the mitotic spindle (135). In the kidney epithelium, tubular flow is sensed by the primary cilium, thus leading to an upregulation of Inversin. Inversin in turn targets Dishevelled (Dsh) for destruction and forces the cell to follow the non-canonical Wnt pathway to prevent cell divisions that are out of the division plane (136). Mutations in *Inversin* also lead to the development of a ciliopathy called nephronophthisis (137).

Taken together, this data implicates a functional connection between Wnt signaling, the primary cilium and control of orientation of cellular division. Indeed, correct mitotic orientation of cells along the tubule axis is crucial for lengthening of renal tubules and it has been shown that in several rodent PKD models there is an increased frequency of pre-cystic epithelial cells that divide with incorrect mitotic orientation (138). Consistent with this finding, a colocalization of Vangl2 and BBS proteins at the basal body was reported (139) leading to the conclusion that the kidney cysts of BBS patients may be caused by misoriented spindle formation due to dysregulated Vangl2 (135, 138). In addition, other ciliary proteins including

Kif3a or Ift20 have also been shown to modulate Wnt signalling (140, 141). Kif3a or Ift20 mutant pups display a severe polycystic phenotype that is preceeded by misorientation of cell division (94, 141). Interestingly, the rapid cystic onset seen after deletion of ciliary proteins during embryogenesis is lost if deletion occurs in quiescent adult kidney cells implying that a certain rate of proliferation, which is still present until P10 or can be induced through kidney damage, is needed for rapid cyst formation (94, 142, 143). Thus, it is believed that a major initiating step in cyst formation is the misorientation of cell division, resulting in initial tubular expansion. Another mechanism of how mitotic spindle orientation is regulated involves pVHL. Depletion of pVHL causes spindle misorientation *in vitro* by decreasing the stability of astral microtubules which function to couple the mitotic spindle to integrin contacts at the cell surface, thereby providing orientation to mitotic cell division (34, 66, 144). Recently, it was shown that *Vhl*-deficient mouse kidneys subjected to ischemic damage to induce epithelial proliferation exhibit spindle misorientation and form cysts and ccRCC precursor lesions (145).

Hence, the loss of the primary cilium may contribute to cyst formation and the initial steps of malignant transformation through alterations in cell proliferation and cell survival (Hh signaling) and loss of polarization and mitotic spindle misorientation (PCP).

1.2.2 Renal ciliopathies

The umbrella name “ciliopathies” is used for a group of disorders associated with genetic mutations which result in malformation or dysfunction of the primary cilium. The first recognized ciliopathy was Bardet-Biedl syndrome (BBS). The first functional evidence of the involvement of the primary cilium came from the observation that BBS8, the protein product of one of the 14 genes that have been identified as being causal to the BBS syndrome, localizes to cilia and was linked to ciliogenesis and intraflagellar transport. The generation of BBS8 null mutants resulted in the classic situs invertus phenotype of cilia deficiency that is also observed in BBS patients (146). Additional analysis confirmed the localization of BBS8 to the centrosomes and the basal body. Several human syndromes are grouped under the term ciliopathies, in these syndromes manifestations can occur in any organ but predominantly affect kidney, liver, eye and brain. Several renal diseases have been described in the context of different ciliopathy syndromes and can be classified i.e. into polycystic (PKD), renal medullary cystic disease (NPHP) and cystic dysplastic kidneys (Meckel-Gruber).

Polycystic kidney disease (PKD) is a family of monogenic disorders with manifestations of multiple cysts primarily in the kidney and the liver (147). The disease is inherited either autosomal dominantly (ADPKD) or in a recessive (ARPKD) fashion. In

general, ADPKD is diagnosed in individuals of 20 to 40 years of age, while ARPKD leads to enlarged kidneys in utero or in the neonatal phase. While ARPKD is a rather rare disease with an incidence of 1:20,000, ADPKD is the most common genetically inherited cystic kidney disease, affecting between 1:400 and 1:1000 individuals (Figure 1.3B). ADPKD is caused by a mutation in either PKD1 or PKD2. These genes code for polycystin-1 (PC-1) and polycystein-2 (PC2), respectively. The majority of patients have mutations in PKD1 (85%) whereas PKD2 is affected in only 15% of the cases (148, 149). PC1 and PC2 form a complex that is partly localized to the membrane of the primary cilium (150). PKHD1 (polycystic kidney and hepatic disease 1) encodes for fibrocystin, a protein that also localizes to the cilium and interacts with the polycystin complex. Mutations in the PKHD1 gene cause ARPKD (Figure 1.3A).

Nephronophthisis (NPHP) is a recessive cystic kidney disorder and the most frequent genetic cause for end-stage renal failure in children and young adults (Figure 1.3C). NPHP is a genetically very heterogeneous disease with at least 13 different identified genes. Surprisingly, these genes account for only 30% of the diagnosed NPHP cases (151). It was shown that the NPHP proteins 1-4 are able to form a complex with each other and that this complex localizes to the transition zone of the primary cilium (137, 152).

Ciliopathies associated with cystic dysplastic kidneys (CDKs) include Meckel-Gruber syndrome (153). CDKs are characterized by poorly differentiated and disorganized nephron segments and a hypoplastic or malformed collecting system (154). CDKs still contain some normal nephrons. In contrast, multicystic dysplastic kidneys (MCDKs) are non-functional and the kidney is composed of cartilage and mesenchymal mantles surrounding undeveloped tubules (154). MCDK can be caused by heterozygous mutation of HNF1B, a transcription factor involved in the regulation of PKHD1 (155). PKHD1 (fibrocystin) is associated with the basal body and the primary cilium and mutations lead to ARPKD (156).

In summary, the identification of the genes that underlie the above-mentioned cystic kidney syndromes led to the realization that all of the protein products of these genes are in some way linked to ciliogenesis or signaling pathways originating from the primary cilium and the dysregulation of these proteins by gene mutation impairs proper cilia function. The primary cilium is therefore a functional suppressor of kidney cyst formation.

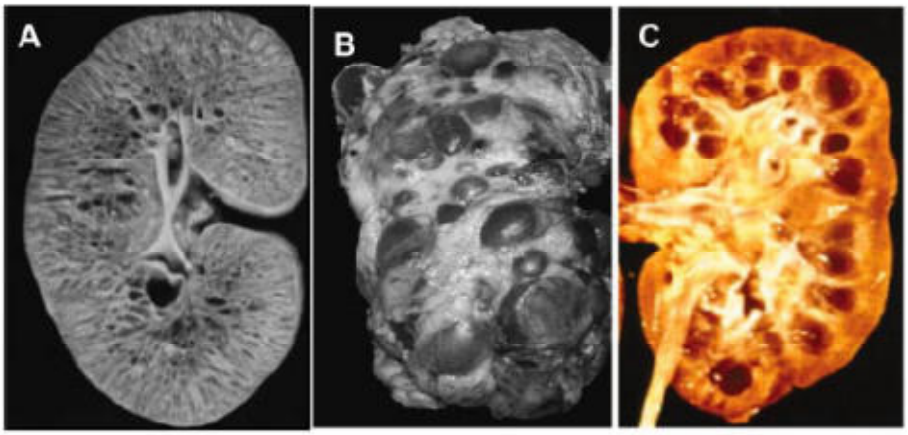

Figure 1.3: Kidneys of different ciliopathy patients. (A) ARPKD kidney of an infant patient. (B) ADPKD kidney of an adult patient. (C) Kidney of a Nephronophtisthis patient. Images (A)+(B) are from Bisceglia *et al.* (157), (C) is from Hildebrant *et al.* (158). Adapted from Gunay-Aygun (159).

1.2.3 Mouse models for renal ciliopathies

In 1994, one of the first observations that cilia are linked to cystic kidney disease came from the Oak ridge polycystic kidney mouse (110, 160). In the following years, more and more mouse models resembling human cystic kidney disease were identified and generated. Some of the most important mouse models are described below.

PKD1: A global homozygous deletion of *Pkd1* is embryonically lethal with observed defects in kidney formation, pancreas and other organs (161, 162). Two different approaches were used to overcome this problem and generate a useful mouse model. On the one hand, the conditional deletion of *Pkd1* after postnatal day 13 leads to a milder progression of the disease (163). On the other hand, a kidney specific deletion of *Pkd1* was achieved by creating a Ksp-Cre;Pkd1$^{fl/-}$ mouse. The offspring were viable and developed cystic kidneys with increased levels of blood urea nitrogen (BUN), cell proliferation and upregulation of components of the MAPK/ERK pathway (164).

Oak ridge polycystic kidney mice (ORPK): The ORPK mouse model provided the first functional link between ciliary defects and the phenotype of polycystic kidneys (110, 165). It was discovered by the Oak Ridge National Laboratory in a large-scale insertion mutagenesis program and resembles the human ARPKD phenotype (160). The animals develop bilateral polycystic kidneys which are enlarged, contain multiple cysts and present destruction of the surrounding parenchyma.

Kif3a knockout mouse: The whole body knockout of *Kif3a*, a kinesin II subunit important for ciliogenesis, during development results in the absence of the primary cilium in the embryonic node, leads to situs inversus and abnormalities of the neural tube and is therefore lethal before renal organogenesis starts (166-168). The specific deletion of *Kif3a* in

renal tubular cells during embryonic development led to the birth of animals with cystic kidneys (166). The epithelial cells lining the cystic regions lost their primary cilium due to inactivation of *Kif3a*. They show an increased proliferation, apoptosis, elevated levels of ß-catenin and c-Myc and decreased p21 (166). Interestingly, the severity of the cystic phenotype can be modulated depending on the time of *Kif3a* deletion. Embryonic kidney-specific deletion leads to a rapid onset of the disease and the animals have to be euthanized around 3-4 weeks of age due to renal failure (94, 166). Deletion of *Kif3a* in neonatal animals resulted in generation of cysts within the first 4 weeks of life and deletion after P11 leads to the development of slowly progressing cysts that first become visible at around 6 months of age (94, 142). We took advantage of these rapid and slow onset models of cyst formation in the studies described in this thesis.

IFT140: Embryonic deletion of *Ift140*, a member of the IFT complex A responsible for retrograde transport, impairs proper ciliary function in collecting ducts (169). These animals develop polycystic kidneys at day 5 with rapid cyst progression while ciliary assembly was not completely abrogated. In addition, increased expression of Wnt pathway genes and Hh mediators was observed. The precystic cells had an increased mitotic index while no effect on spindle orientation was found. Therefore the authors concluded that increased proliferation with dysregulation of Wnt and/or Hh signaling is causative for cyst development in this model.

BBS2 knockout mouse: Bardet-Biedl syndrome is a heterogeneous human disorder presenting with obesity, retinopathy, renal and cardiac malformation. In 2004, a *Bbs2* knockout mouse was generated (170). *Bbs2* is a member of the BBSome which is required for ciliogenesis (171). The function of the BBSome is linked to the Rab8 GDP/GTP exchange factor that is important for the elongation of the ciliary membrane (171). Constitutive deletion of *Bbs2* leads to a resemblance of human BBS in mice (170). Besides obesity, the animals exhibit phenotypes of ciliary dysfunctions including retinopathy, renal cysts and impaired olfaction (170).

1.3 pVHL and the primary cilium

There is evidence that a subset of ccRCC in patients with VHL disease is preceded by premalignant cysts (172). The kidney cysts containing these micro-foci of ccRCC resemble classical ADPKD (63). In general, PKD is linked to mutations affecting the primary cilium or centrosomes. Since VHL disease leads to kidney cysts and ciliary defects are linked to cystic disease this led to the idea that pVHL might also be important for the function of the primary cilium. Indeed, it was shown that pVHL is localized to the primary cilium and it is essential for ciliary assembly (25, 173-175). pVHL interacts with Kif3a and Kap, members of the kinesin-2

family, and co-localizes to the primary cilium (176, 177). pVHL is associated with microtubules and plays a role in microtubule stabilization *in vivo* (34). The microtubule stabilization function of pVHL depends on a specific domain overlapping with a mutational hot spot in VHL disease. The fact that certain naturally occurring mutations exhibit altered microtubule stabilization implies a connection to *VHL*-associated tumor suppressor activity (34). In addition, it was shown that naturally occurring pVHL variants unable to bind Kif3a or Kap were associated with a reduced frequency of primary cilia while HIF1α function was not impaired (178). Furthermore, it was shown that pVHL is involved in mitotic spindle orientation through direct interaction with an atypical protein kinase C complex (Par3-Par6-aPKC) (144, 145, 175, 179, 180). These data link pVHL to cyst formation and cilia function in the kidney, which is known to be dependent on members of the kinesin-2 family (Kif3a, KAP).

An animal model with *Vhl* deletion in proximal tubule cells of the kidney showed cyst formation at a low frequency in old animals (19). The observed low frequency of cyst formation is in line with the data of patients with VHL disease that the majority of *VHL* mutant cells remains quiescent and does not automatically form cysts and leads to the conclusion that additional mutations must occur to lose the primary cilium in a $Vhl^{-/-}$ background. Together, pVHL and GSK3ß were shown to be components of a microtubule regulatory network that is involved in the maintenance of the primary cilium (51). First clues for GSK3ß function in the primary cilium came from the observation that GSK3ß was required for formation and length control of flagella in Chlamydomonas reinhardtii (181). In addition, it could be shown that GSK3ß can inhibit the microtubule stabilizing function of pVHL (182). This led to the discovery that GSK3ß, when active, maintains the primary cilium while inactivating the microtubule stabilizing function of pVHL. If GSK3ß is inactive the inhibition on pVHL is lost and therefore pVHL is able to preserve the primary cilium (51).

In line with these cell culture based observations, cystic regions of VHL disease patients show a hyperactivated PI3K pathway (20). This activation is able to cause inhibitory phosphorylation of GSK3ß through AKT and p70S6K (183, 184). Activation of PI3K signalling is often mediated by loss of its negative regulator Phosphatase and tensin homolog (PTEN) and indeed reduced PTEN levels as well as AKT activation correlate with poor prognostic outcome in sporadic cases of ccRCC (52, 185). Combined deletion of *Vhl* and *Pten* in the mouse resulted in cyst formation in the kidney displaying a reduced frequency of primary cilia and elevated levels of AKT and ERK signaling as well as inhibitory phosphorylation of GSK3ß (20). Taken together, these studies indicate that there is an important role of the primary cilium in VHL disease. Work in this thesis tests the hypothesis that has arisen from these studies, namely that cooperation between loss of the primary cilium and loss of Vhl is able to induce the formation of ccRCC or ccRCC precursor lesions.

1.4 Micro-computed Tomography (µCT)

In this study we have developed a new non-invasive imaging protocol based on computed tomography (CT) that allowed quantitative longitudinal monitoring of cysts in living mice. CT is a 3D x-ray imaging method to obtain x-ray projection images around the axis of an object to generate a stack of thin tomographic images of contiguous slices through the object. CT is a widely used technique for diagnostic and therapeutic purposes in a broad range of medical areas. Micro-computed tomography (µCT) was first developed in the early 1980s (186). There are different levels of small scale CT based on their spatial resolutions: mini-CT, micro-CT and nano-CT (187). The pixel resolution of µCT is usually in the micrometer range. In general, there are two different setups for these devices: a stationary source and detector where a specimen is rotated in the light beam or a stationary specimen where the beam and detector are rotated around it (188). For living animals the latter option is commonly used. In the past, the majority of analysis were performed with *ex vivo* specimen but nowadays µCT imaging can be used to study *in vivo* processes longitudinally in an animal such as metastasis (189), myocardial infarction (190), kidney volume (191) and even embryogenesis (192). In µCT imaging, contrast is produced by the attenuation of X-rays in the examined sample therefore offering a good image quality for elements with a high atomic number such as bones, but very little soft tissue contrast (193). To achieve a good imaging quality in soft tissues the administration of a contrast agent is desirable and often indispensable. Water-soluble, non-ionic iodine-based contrast agents such as Visipaque are commonly used in humans and are quickly eliminated from the blood after intravenous injection through the kidney. In contrast to humans, rodents possess a very short circulation time and the contrast agent is cleared within seconds from the blood (194). This led to the need of continuous injection of a contrast agent during the scanning time (195). Since the new devices have a read out of 30-60 fps and the scanning duration is strongly decreased, for specific indications a single bolus injection of contrast agent is now sufficient to analyze the sample. We show that state of the art µCT imaging is suitable for longitudinal studies of renal cyst formation and progression.

1.5 3D Cell culture of primary kidney epithelial cells

In this study we have developed a 3D culture system for primary renal epithelial cells. Three dimensional (3D) cell culture models provide an approach to study processes like tissue morphogenesis and tumourigenesis and might close the gap between standard 2D cell culture and animal models. Yamada and Cukierman review the advantages and disadvantages of 3D cell cultures and highlight signaling pathways that are differentially regulated in 3D cultures compared to 2D cell cultures including growth factor signaling, cell

survival and cell polarity (196). 3D cell cultures can be used with a single cell type or even with a mixture of different cell types resembling the *in vivo* situation. 3D scaffolds are usually generated from purified collagen I, synthetic biomaterials or Matrigel®. Matrigel® is a heterogeneous composition of different extracellular matrix proteins that is produced and secreted by Engelbreth-Holm-Swarm (EHS) mouse sarcoma cells and sold by Corning Life Science. Different research groups showed that epithelial cell lines are able to form polarized acini with a lumen in 3D cell cultures (197-199). In addition, it was shown that kidney-derived cell lines and even isolated primary rat kidney epithelial cells were able to form structures in a 3D environment (198, 200-202). Furthermore, induced cyst formation in a collecting duct 3D model by elevating cellular cAMP levels was shown (202). Nonmalignant mammary cells form polarized and growth-arrested acini in a 3D assay whereas the malignant cell types form non-polarized, proliferating colonies (203). This indicates that the formation of 3D structures serves as a growth inhibiting signal for non-transformed epithelial cells *in vitro*. This suppressive environment can be overcome by addition of growth factors or intrinsic oncogenic events. The expression of oncogenic Erb2 in a single cell per acini enables the cell to overcome the suppressive influence of the acini (199). These studies argue that 3D culture models are superior to 2D models in reflecting the epithelial environment and studying the initial events involved in tumour formation. For renal derived cells it could be shown that stimulation with HGF (hepatocyte growth factor) leads to tubule formation in 3D assays (200, 202). Several renal kidney epithelial lines are available but so far no primary cell-based 3D assay is available. The ability to utilize primary epithelial kidney cells (pKECs) in a 3D assay would in general be a useful technique allowing researchers to take advantage of all the available genetically modified mouse lines.

1.6 Aims

1. Generation of inducible kidney epithelial cell-specific deletion of *Vhl* and *Kif3a* alone and together to study their potential cooperative effects on cyst formation and ccRCC development.
2. Generation of an inducible kidney epithelial cell-specific combined deletion of *Hif1a* and *Kif3a* to study the role of Hif1α in cystogenesis.
3. Developing a µCT-based non-invasive method for longitudinal quantitative monitoring of cyst formation and progression in mice.
4. Generation of a primary cell-based 3D culture system to study cellular and molecular mechanisms of cyst formation/progression and cell transformation *ex vivo*.

2 Materials and Methods

2.1 Materials

2.1.1 General Chemicals

Reagent	Supplier
30% Acrylamide/Bisacrylamide Solution	Bio-Rad
4′,6-Diamidino-2-phenylindole dihydrochloride (DAPI)	Sigma-Aldrich
Acetic acid (glacial)	Merck
Acetone	Sigma-Aldrich
Agarose, D1 low EEO	Conda
Albumin from bovine serum	Sigma-Aldrich
Ammonium carbonate	Sigma-Aldrich
Ammonium chloride	Fluka
Boric acid	Sigma-Aldrich
Bovine serum albumin (BSA)	Invitrogen
Bromophenol blue	Sigma-Aldrich
Citric acid monohydrate	Sigma-Aldrich
Dimethylsulfoxide (DMSO)	Sigma-Aldrich
di-sodium hydrogen orthophosphate (Na_2HPO_4)	Sigma-Aldrich
Dithiothreitol (DTT)	Sigma-Aldrich
Entellan	Merck
Eosin 1% (aqueous)	BioSystems
Ethanol	AUL
Ethidium bromide	Sigma-Aldrich
Ethylenediamine tetra-acetic acid (EDTA) disodium salt	Sigma-Aldrich
Formalin 10%, neutral buffered	Sigma-Aldrich
Glycerol	Sigma-Aldrich
Haematoxylin (Mayer's)	J.T.Baker
Hydrochloric acid, 32%	Sigma-Aldrich
Hydrogen peroxide	Sigma-Aldrich
Isopropanol	AUL
Magnesium chloride	Sigma-Aldrich
Magnesium sulfate	Sigma-Aldrich
Methanol	AUL
Mineral oil	Sigma-Aldrich
Mowiol	Sigma-Aldrich
N,N,N',N'-Tetramethylethylenediamine (TEMED)	Bio-Rad
N-2-Hydroxyethylpiperazine-N'-2-ethanesulfonic acid	Sigma-Aldrich
NP-40	Sigma-Aldrich
Paraformaldehyde	Sigma-Aldrich
p-coumaric acid	Sigma-Aldrich
Phenyl-methyl-sulphonyl-fluoride (PMSF)	Sigma-Aldrich
Potassium acetate	
Potassium chloride	Sigma-Aldrich
Protease inhibitor cocktail	Sigma-Aldrich
Protein assay Dye Reagent	Bio-Rad
Safflower oil	Migros

Reagent	Supplier
Sodium acetate	Sigma-Aldrich
Sodium azide	Sigma-Aldrich
Sodium chloride	Sigma-Aldrich
Sodium deoxycholate	Sigma-Aldrich
Sodium dihydrogen orthophosphate (NaH_2PO_4)	Sigma-Aldrich
Sodium Dodecyl Sulfate (SDS)	Sigma-Aldrich
Sodium hydroxide	Sigma-Aldrich
Sulforhodamine B sodium salt (SRB)	Sigma-Aldrich
SYBR FAST Universal 2X qPCR Master Mix	KapaBiosystems
Trichloroacetic acid	Sigma-Aldrich
Tris(hydroxymethyl)aminomethane (Tris base)	Sigma-Aldrich
Tris(hydroxymethyl)aminomethane hydrochloride (Tris HCl)	Sigma-Aldrich
Tri-Sodium citrate	Sigma-Aldrich
Triton X-100	Sigma-Aldrich
Tween-20	Sigma-Aldrich
Visipaque® 270	GE Healthcare
Xylene	Thommen-Furler AG

2.1.2 Drugs & tissue culture reagents

Reagent	Supplier
2–Mercaptoethanol	Bio-Rad
2´,7´-dichlorodihydrofluorescein diacetate	Invitrogen
3,3,5 Triiodothyronine (T3)	Sigma-Aldrich
Ampicillin	Sigma-Aldrich
Apo-Transferrin (TF), human	Sigma-Aldrich
Calcium chloride	Sigma-Aldrich
Collagenase Type II	Gibco
D-glucose	Sigma-Aldrich
DMEM/F12	Sigma-Aldrich
Dulbecco's Modified Eagle Medium (DMEM)	Sigma-Aldrich
Epidermal Growth factor (EGF), murine	PeproTech
Fetal Calf Serum (FCS)	Biochrome AG
HBSS	Gibco
Hepatocyte Growth factor (HGF)	PeproTech
HEPES 1M	Sigma-Aldrich
Hydrocortisone (HC)	Sigma-Aldrich
Insulin, human	Sigma-Aldrich
L-Glutamine	Sigma-Aldrich
Matrigel® (growth factor reduced)	Corning
Penicillin/Streptomycin	PAA
Phosphate Buffered Saline (PBS)	Biochrome Ag
Prostagladin E1 (PGE1)	Sigma-Aldrich

Reagent	Supplier
Puromycin	InvivoGen
Sodium bicarbonate	Sigma-Aldrich
Sodium Selenite (SS)	Sigma-Aldrich
Tamoxifen	Sigma-Aldrich
Trypsin EDTA	Gibco
Trypsin inhibitor, soybean	Gibco

2.1.3 Kits

Name	Supplier
ABC Kit (PK6100)	Vectorstain
Avidin/Biotin Blocking Kit (SP 2001)	VectorLaboratories
CellTiter-Glo Luminescent Cell Viability Assay	Promega
CSA detection kit	Dako
DAB Substrate Kit (SK-4100)	VectorLaboratories
Glucose assay Kit II	Biovision
Lactate assay Kit II	Biovision

2.1.4 Antibodies and Lectins

Name	Vendor	Order number	Source	Dilution	Application
β-Actin (AC-74)	Sigma-Aldrich	A2228	Mouse	1:1000	WB
AE1	Gift from Wagner Lab	-	Rabbit	1:250	IF
Alexa-488 Anti-mouse	Life technologies	A11029	Goat	1:1000	IF
Alexa-488 Anti-rabbit	Life technologies	A11008	Goat	1:1000	IF
Alexa-488 Anti-rat	Life technologies	A11006	Goat	1:1000	IF
Alexa-568 Anti-mouse	Life technologies	A11031	Goat	1:1000	IF
Alexa-568 Anti-rabbit	Life technologies	A11036	Goat	1:1000	IF
Alexa-568 Anti-rat	Life technologies	A11077	Goat	1:1000	IF
Aquaporin 2	Gift from Loffing Lab	-	Rabbit	1:3500	IF
ATP V1B1	Gift from Wagner Lab	-	Rabbit	1:250	IF
E-Cadherin	Abcam	Ab11512	Rat	1:200	IF
Fluorescein labeled Dolichos Biflorus Agglutinin (DBA)	Vector Labs	FL-1031	-	1:250	ICC/IF
Fluorescein labeled Lotus Tetragonolobus Lectin (LTA)	Vector Labs	FL-1321	-	1:250	ICC/IF
Glut1	Abcam	Ab14683	Rabbit	1:500	WB/IF
HIF1α (H1α67)	Novus Biotechnologies	NB-100-105	Mouse	1:20000	IHC
phospho-Histone H3 (Ser-10)	Santa Cruz Biotechnologies	sc-8656-R	Rabbit	1:250	IF
HRP anti-mouse	ThermoScientific	31430	Goat	1:1000	IHC
HRP anti-rabbbit	ThermoScientific	31460	Goat	1:1000	IHC
Kif3a	Abcam	Ab11259	Rabbit	1:2000	WB
NaPi2	Gift from Biber Lab	-	Rabbit	1:500	IF
NCC	Millipore	AB3553	Rabbit	1:500	IF
NKCC2	Gift from Loffing Lab	-	Rabbit	1:250	IF
Pendrin	Gift from Wagner Lab	-	Rabbit	1:250	IF
Tamm Horsfall Protein (H-135)	Santa Cruz Biotechnologies	Sc-20631	Rabbit	1:250	IF
Tubulin, acetylated	Sigma-Aldrich	T6793	Mouse	1:1000	IF
Vhl (FL-181)	Santa Cruz Biotechnologies	Sc-5575	Rabbit	1:100	WB

2.1.5 Oligonucleotide sequences

Name	Sequence	Application
IF008 ctrl fwd	ATA ATG CCT TTC CTC AGT AAA CCA G	Genotyping
IF009 ctrl rev	GGA TCC CAT TAC AGA TGG TTG TG	Genotyping
IF054 KspCre fwd	AGG TTC GTG CAC TCA TGG A	Genotyping
IF055 KspCre rev	TCG ACC AGT TTA GTT ACC C	Genotyping
IF77 Vhl fwd1	CTG GTA CCC ACG AAA CTG TC	qPCR
IF78 Vhl fwd2	CTA GGC ACC GAG CTT AGA GGT TTG CG	qPCR
IF79 Vhl rev	CTG ACT TCCACT GAT GCT TGT CAC AG	qPCR
IF163 p53 fwd	GCC CTC TCT TAT CGC CAG AT	Genotyping
IF164 p53 rev	GCT TAT GGG CTT CTC CAA ACT	Genotyping
IF249 HIF1a fwd	GGA GCT ATC TCT CTA GAC C	Genotyping / qPCR
IF250 HIF1a rev	GCA GTT AAG AGC ACT AGT TG	Genotyping / qPCR
IF251 HIF1a fl F	TGG GGA TGA AAA CAT CTG CT	qPCR
IF252 HIF1a fl R	GTT GGG GCA GTA CTG GAA AG	qPCR
IF302 Kif3a P1	AGG GCA GAC GGA AGG GTG G	Genotyping / qPCR
IF303 Kif3a P2	GGC AGA TGG ATC TCT GTG AGT TTG	Genotyping / qPCR
IF419 Vhl fwd	GGA GTA GGA TAA GTC AGC TG	Genotyping
IF420 Vhl rev	GTA CAC CTG AGA GCG GCT TC	Genotyping
IF732 rpS6 promoter rev	AGT CAC TTC CGC CGG CTG TTC	qPCR
IF731 rpS6 promoter fwd	GCG TCA CGA AAA AGA GGC CCG A	qPCR
IF739 Kif3a rec fwd	GCA GAC GGA AGG GTG GTT TA	qPCR
IF740 Ki3a rec rev	CTG CAA GAGGGT GGA AAG GA	qPCR

2.2 Cell culture

2.2.1 Culture of MEFs

MEFs were isolated from embryos of relevant floxed strains at E13.5. After removing the head, internal organs and spinal cord the remaining tissue was minced with a razorblade, incubated for 15 minutes at 37°C in trypsin EDTA, dispersed in growth media (DMEM supplemented with 10% FCS, 2mM glutamine, 1% Pen/Strep and 200 µM β-mercaptoethanol) and plated on a 10cm dish. Cells were split 2-3 days later into two 15cm dishes and after additional 2-3 days they were frozen at passage 2. Cells were cultured in conventional cell culture incubators at 5% oxygen.

2.2.2 Isolation of primary epithelial kidney cells

Kidneys of floxed mice were dissected. After removing the capsule under sterile conditions, kidneys were mashed with a razor blade on ice and digested in a digestion solution (10mg Collagenase Type II, 10mg soybean Trypsin inhibitor in 20ml HBSS with 2% 1M HEPES and 1% Pen/Strep) at 37°C for 30min with frequent agitation. The cell suspension was filtered through a 70µm sieve and washed with HBSS + 5% FCS. After erythrocyte lysis in standard ACK buffer (NH_4Cl 151,4µM, $KHCO_3$ 10µM, EDTA $Na_2 \cdot H_2O$ 12,75µM), the cells were resuspended in K1 medium (DMEM/F12 supplemented with 1% Pen/Strep, 1%L-Glutamin, HEPES 25 mM, Insulin 5 µg/ml, PGE1 1,25 ng/ml, T3 34 pg/ml, Apo-Transferrin 5 µg/ml, sodium selenite 1,73 ng/ml Hydrocortison 18 ng/ml and EGF 25 ng/ml) Cells were seeded at a density of $1x10^6$ cells/10cm dish. The medium was changed after 4 days for the first time and every 3rd day thereafter. If desired, cells were transduced with Adeno-eGFP or Adeno-Cre-GFP after 5-6 days in culture.

2.2.3 Proliferation assays

For proliferation assays for MEFs, cells were seeded at densities of $3x10^5$ cells per 6cm dish in triplicate dishes and counted after 3 days before reseeding at the same density for the next passage. All proliferation assays shown in the figures are representative of at least 3 independent experiments.

For primary kidney cells, a Sulforhodamine B (SRB) colometric assay was performed (204). Cells were cultured in K1 medium containing 10% FCS for 2 days before seeding for the SRB assay. $2x10^3$ cells per well were seeded and fixed in 5% (wt/vol) trichloroacetic acid at the indicated time points. Cells were stained in 0.057% (wt/vol) SRB solution and air dried. SRB was solubilized by incubation in 10 mM Tris base solution (pH 10.5) and OD was

measured at 540 nm in a microplate reader (Anthos Lucy 3). All SRB assays shown in the figures are representative of at least 3 independent experiments.

2.2.4 3D culture

To culture primary epithelial kidney cells in a 3D environment we modified a published protocol by Lee *et al.* (205). A 96-well was coated with 5µl of growth factor-reduced Matrigel® (Matrigel® GR) for 10 min in a cell culture incubator. Primary epithelial kidney cells were grown for ~7 days in K1 medium before starting the 3D culture. $5x10^4$ primary epithelial kidney cells were resuspended in 75µl Matrigel GR and seeded in the coated well. After solidifying of the Matrigel® in an incubator for 30 min 60µl of K1 medium were added to the 3D culture. Medium was changed every 3 days. 3D cultures were treated with Adenoviruses as indicated in the experiments. Every work step involving Matrigel® was carried out on ice. After acini formation the structures were fixed with 4% PFA for 1h at RT followed by three times washing with PBS-Glycine (100mM). Cultures were blocked with 100µl of IF blocking solution (10% goat serum, 1% goat F(ab')2 anti-mouse immunoglobulin G, in IF buffer (0.2% Triton X-100, 0.1% BSA, 0.05% Tween 20 in PBS pH 7.4, sterilized, add 7.7 mM NaN_3 for longterm storage)) for 1.5h at RT. 96-Wells were incubated with the primary antibody diluted in 50µl IF buffer for 2h at RT. After washing three times with 200µl IF buffer for 20 min, the wells were incubated with a secondary antibody diluted in 50µl IF buffer for 45min at RT. 3D cultures were washed once with IF buffer and twice with PBS for 20min each before counterstaining the structures with DAPI (0.5µg/ml in PBS) for 5min at RT. Matrigel® was removed from the well and transferred to a slide for mounting in Mowiol/DABCO.

2.2.5 ATP measurements

Cells were trypsinized, counted (Beckman counter Vi-Cell XR and Z2) and $1.5x10^5$ cells were resuspended in 75µl PBS and 75µl buffer (CellTiter-Glo Luminescent Cell Viability Assay, Promega). Cells were lysed for 10 min at room temperature and distributed as technical triplicates in a 96-well plate. Luminescence signal was detected with a microplate reader (Anthos Lucy 3). Student's t-test was performed for statistical analysis.

2.3 Molecular and biochemical Methods

2.3.1 Genomic DNA qPCR-analysis

FFPE kidney sections were washed 2x1min in Xylol and air dried. Sections were transferred to a 1.5ml Eppendorf tube and genomic DNA was isolated with the Arcturus PicoPure DNA Extraction Kit (life technologies). The real-time PCR analysis of cDNA was performed with SYBR FAST Universal 2X qPCR Master Mix and used primers listed above (2.1.5).

2.3.2 Western blotting

Cells were washed with PBS before lysis. Ice-cold RIPA buffer (50 mM Tris–HCl at pH 7.5, 150 mM sodium chloride, 1% NP-40, 1% sodium deoxycholate, 0.1% SDS, 2mM EDTA, 1 mM sodium fluoride, 1 mM Na_3VO_4, 1 mM PMSF, 1 mM dithiothreitol, 1:100 Protease Inhibitor Cocktail) was added to the wells, the cells were detached using a cell scraper and transferred to a 1.5 ml tube. The cell lysate was centrifuged at 15000 g for 10 min (4℃). The Bradford protein assay was used to determine the protein concentration of the supernatant. The appropriate amount of denaturing 6x Lämmli buffer was added and the samples were boiled at 97℃ for 5 min. Samples were either utilized for SDS-PAGE directly or stored at -20℃ for later use. Proteins were run on 6–15% acrylamide gels, transferred to nitrocellulose membranes and visualized by semi-dry immunoblotting with antibodies described above. The signal was detected using the Fujifilm Luminescent Image Analyzer LAS4000 mini.

2.3.3 Agarose gel electrophoresis

For agarose gel preparation, the desired amount of agarose (between 0.7 and 2%) was boiled in 1x SBA buffer (0.02M NaOH, 0.04M Boric acid in dest. H_2O) and 8µl of ethidium bromide were added for a volume of 100 ml. The liquid was poured into a gel casting device and allowed to set. The gel was placed in an electrophoresis chamber filled with 1x SBA. The DNA samples were mixed with 6x loading buffer (60% 10xSBA, 18% Ficoll type 400, 0.12mM EDTA pH 8.0, 0.15% Bromphenol blue and 0.15% Xylencyanol FF in dest. H_2O) and loaded onto the gel. An electric potential of 100 V was applied for electrophoresis and the DNA bands were visualized using a UV light transilluminator at 366 nm.

2.4 Animal and tissue handling

2.4.1 Mouse strains

Mice expressing a tamoxifen inducible kidney-specific Cre recombinase under the Ksp1.3 promoter (206) were crossed with mice containg loxP sites flanking exon 2 of the *Kif3a* gene (166) and or mice containing loxP sites flanking exon 1 of the *Vhl* gene (207) generating the

following lines: KspCre$^{ERT2\ Tg/+}$;Kif3a$^{fl/fl}$, KspCre$^{ERT2\ Tg/+}$;Vhl$^{fl/fl}$ and KspCre$^{ERT2\ Tg/+}$;Kif3a$^{fl/fl}$;Vhl$^{fl/fl}$. Tamoxifen (TM) treated Cre recombinase expressing mice will be called Kif3a$^{\Delta/\Delta}$, Vhl$^{\Delta/\Delta}$ and Kif3a$^{\Delta/\Delta}$Vhl$^{\Delta/\Delta}$, whereas TM treated Cre negative mice will be referred as Kif3a$^{+/+}$, Vhl$^{+/+}$ and Kif3a$^{+/+}$Vhl$^{+/+}$, respectively. For generation of KspCre$^{ERT2\ Tg/+}$;Kif3a$^{fl/fl}$;Hif1a$^{fl/fl}$ we used a mouse line with loxP sites flanking exon 1 of the Hif1a gene (208). Wild type cells were isolated from C57BL/6 embryos.

2.4.2 Genotyping

Ear biopsies were digested for 15 min at 95°C in lysis buffer (25 mM NaOH, 0.2 mM EDTA, pH 12) and neutralized afterwards with the same amount of neutralisation buffer (40 mM Tris-HCl, pH 5). PCR was carried out according to standard procedures using JumpStart Taq DNA polymerase and primers shown in table 0. The DNA was analyzed on 1.5% agarose gels in SBE buffer (5 mM NaOH bufferd with boric acid, pH 8.5).

2.4.3 Tamoxifen treatment

Tamoxifen was administered to induce Cre/loxP recombination in Ksp1.3-Cre^{ERT2} transgenic mice. Tamoxifen was dissolved in 100% ethanol then diluted 10-fold in corn oil to a final concentration of 20 mg/ml. To induce recombination in newborn mice, nursing dams were injected with tamoxifen (4 mg/40 g body weight) on post-partum days 2–4. Recombination in 6 week old adult animals was achieved by changing the diet to Tamoxifen-containing pellets for 2 weeks. Non-Cre transgenic littermate mice served as controls for all cohorts.

2.4.4 Tissue collection and procedure

Mouse tissues were immersion-fixed in 10% formalin at 4°C overnight and stored in 70% ethanol. After dehydration in serial dilutions (3 h 70% EtOH, 2 h 80% EtOH, 2 h 90% EtOH, 2 h 96% EtOH, 2 h 100% EtOH, 2 h xylene, 3 h paraffin at 65°C), organs were embedded in paraffin and cut into 5 µm sections and fixed on polysine glas slides (VWR).

2.4.5 micro Computed Tomography (µCT)

Animals were anaesthetized and Visipaque® 270 (GE Healthcare) was injected i.v. at 8µl/g bodyweight (191) as contrast agent in a single bolus injection. µCT images were recorded with a Quantum FX microCT (Perkin Elmer) and the following settings: 100µA, 90kV, respiratory gating and fine scanning. µCT data were exported as DICOM images to be analyzed manually with the Myrian® software (intrasense®) for volumetric measurements and 3D reconstruction and in the Quantum FX data format for overview X-ray pictures.

2.4.6 Blood collection and analysis

Animals were anaesthetized and blood was terminally collected by puncture of the heart and treated with sodium-heparin. Blood plasma was stored at – 80°C for further analysis. Creatinine and blood urea nitrogen (BUN) were determined using the UniCel® DxC 800 Synchron® Clinical System in cooperation with the ZIRP (University of Zürich).

2.5 Histological analysis

2.5.1 Haematoxylin and Eosin (H&E) staining

Tissue sections were dewaxed for 3 min in xylene and hydrated for 2 min each in serial dilutions of ethanol washes (100%, 95%, 70%). Nuclei were stained for 4 min in haematoxylin and dipped 3 times in 0.3% acid alcohol for differentiation. Proteins were stained for 8 min in 1% eosin solution. Finally, specimen were dehydrated for 2 min in serial ethanol dilutions (70%, 95%, 100%) and xylene (3 min) and mounted in entellan.

2.5.2 Immunohistochemistry

Tissue sections were dewaxed in xylene and hydrated in series of ethanol washes (10 min xylene, 10 min 100 % EtOH, 10 min 95% EtOH, 5 min in 70% EtOH) and washed for 5 min in PBS-T (137 mM NaCl, 2.7 mM KCl, 19 mM Na_2HPO_4, 1.7 mM KH_2PO_4, pH 7.4, 0.3% Triton x-100). For antigen retrieval, slides were cooked for 5 min at 110°C in 0.1 M citrate buffer (pH 6) using a standardized pressure cooker (HistosPro, Milestone). Immunohistochemistry targeting Hif1α protein was performed using the Dako Catalyzed Signal Amplification (CSA) kit according to the manufacturer's instruction. The following changes were included in the protocol: After peroxidase block, specimen were incubated for 15 min in avadin solution (TBS, supplemented with 1% BSA, 0.1% Tween, 2 drops avadin solution per 250 µl solution), followed by 15 min biotin solution (TBS, containing 1% BSA, 0.1% Tween 20 and 2 drops biotin solution per 250 µl solution). For washing, standard TBS-T (50 mM Tris, 150 mM NaCl, 0.1% Tween 20) was used before primary antibody incubation, whereas high salt TBS-T (0.05 M Tris-HCl pH 7.6 containing 0.3 M NaCl and 0.1 % Tween 20) was used afterwards. Rehydration of sections and counterstaining was performed as described in 2.5.1.

2.5.3 Immunofluorescence (Tissues)

For immunofluorescence, specimen were processed as described above (2.7.2), however, the avadin/biotin block was not performed. After primary antibody incubation, sections were incubated with fluorophor-labelled secondary antibodies for 1 h. Subsequently, slides were washed with PBS and nuclei were stained for 10 min with DAPI (0.5 ng/ml in PBS containing

10% goat serum). After washing in PBS and ddH_2O, sections were mounted in Mowiol/DABCO.

2.5.4 Immunocytochemistry

Cells were cultured on round glass cover slips in a 6-well plate to perform immunofluorescence on cells grown *in vitro.* After washing with PBS the cells were fixed in 4% PFA for 1 h at room temperature. Removal of PFA is followed by a washing step. The cover slips were incubated with blocking solution (see 10% goat serum/0.3% Triton/PBS) for 1 h at room temperature. Incubation with subsequent antibodies was carried out as described in 2.5.3.

2.5.5 Image acquisition and procession

Brightfield and fluorescence microscopy was performed on either a Zeiss Scope A1 microscope or an Axiovert 40 CRC microscope. Images were obtained with an Axiocam MRc5 camera using the Axiovision LE64 software and processed with Adobe Photoshop. Confocal microscopy was performed on a Leica SP5 at the ZMB of the University of Zurich

3 Results

3.1 Simple and atypical kidney cyst formation results from the cooperative effects of deletion of *Vhl* and loss of the primary cilium

Manuscript in preparation

Combined deletion of *Vhl* and loss of the primary cilium affects planar cell division and causes simple and atypical renal cysts

Holger Lehmann[a], Daniele Vicari[a] and Ian J. Frew[a,b]

[a] Institute of Physiology, University of Zurich, Zurich, Switzerland

[b] Zurich Center for Integrative Human Physiology, University of Zurich, Zurich, Switzerland

Running title: Cooperative cyst suppression by Vhl and primary cilia

Key words: kidney, cyst, ccRCC, mouse model, planar cell division

Corresponding author:

Ian Frew

Institute of Physiology

University of Zurich

Winterthurerstrasse 190

CH-8057 Zurich

Switzerland

Phone: +41 44 635 5004

Fax: +41 44 635 6814

Email: ian.frew@access.uzh.ch

Abstract

A subset of familial and sporadic clear cell renal cell carcinomas (ccRCC) is believed to develop from cystic precursor lesions. Loss of function of the von Hippel-Lindau (*VHL*) tumor suppressor gene sensitizes renal epithelial cells to lose the primary cilium in response to specific signals. Since the primary cilium suppresses renal cyst formation, loss of the cilium may represent an initiating event in the formation of ccRCC. To test this idea, we analyzed the consequences of inducible renal epithelial-specific deletion of *Vhl* together with ablation of the primary cilium via deletion of *Kif3a*. We developed a micro-CT-based imaging approach to allow quantitative longitudinal monitoring of cystic burden in living animals, revealing that loss of *Vhl* and loss of *Kif3a* cooperatively shortened the latency of cyst initiation, increased the number of cysts per kidney and increased the total cystic burden. In contrast to findings in other cystic models, cysts in *Kif3a* mutant mice did not display accumulation of HIF1α and deletion of *Hif1a* together with *Kif3a* did not affect cyst development or progression, arguing against an involvement of HIF1α in promoting renal cyst growth in general. *Vhl/Kif3a* double mutation also increased the frequency of cysts that displayed multilayered epithelial growth, which correlated with an increased frequency of misoriented cystic epithelial cell divisions. Thus, loss of *Vhl* and loss of primary cilia cooperatively induce the formation of simple and atypical cysts that resemble ccRCC precursor lesions but these cysts do not progress to form tumors.

Significance statement

The sequence of molecular and cellular alterations that lead to clear cell renal cell carcinoma (ccRCC) are unclear. Using mouse genetics, we show that deletion of the von Hippel-Lindau tumor suppressor gene, which is inactivated in 90% of cases of human ccRCC, in combination with loss of the primary cilium, a structure that functions as a cellular antenna to suppress uncontrolled kidney cell proliferation, causes the formation of kidney cysts that resemble suspected precursor lesions of ccRCC. These findings shed light on the first steps of formation of the most frequent form of kidney cancer. Our development of a method allowing quantitative monitoring of kidney cysts in living mice will facilitate future studies of cystic kidney diseases.

Introduction

von Hippel-Lindau (VHL) disease is an autosomal-dominant genetic disorder caused by inheritance of a mutant allele of the *VHL* gene. Amongst other disease manifestations, VHL patients have an increased risk of developing renal cysts and bilateral, multifocal solid or cystic clear cell renal cell carcinomas (ccRCC), in which the wild type *VHL* allele is invariably lost due to somatic mutation or gene silencing (1). Kidneys of VHL patients typically develop a spectrum of lesions harboring biallelic *VHL* inactivation that likely represent precursor lesions of solid and cystic ccRCC, including small foci of micro-ccRCC with a solid appearance, simple cysts that are lined by a single layer of proliferating epithelial cells and atypical cysts that contain regions of multilayered or disorganized epithelial growth resembling foci of ccRCC (2). These findings have suggested a disease progression model whereby ccRCC can form via cyst-dependent and cyst-independent pathways in VHL patients (3). The *VHL* gene is also biallelically inactivated in more than 90% of sporadic ccRCC cases (4). While most *VHL* mutant ccRCCs have a solid morphology, approximately 5% are termed multilocular cystic renal cell carcinomas that contain cysts with small nodular aggregates of clear cell tumor cells within and between the walls of the cysts (5, 6). This observation suggests that sporadic ccRCC might also arise via cyst-dependent and cyst-independent pathways. Acquired cystic kidney disease caused by long-term renal dialysis results in an approximately 100-fold increased risk of developing different forms of renal cell carcinoma, further emphasizing that renal cysts can be precursors of carcinomas (7).

The protein product of the *VHL* gene, pVHL, mediates numerous biological activities, including targeting the α-subunits of the hypoxia-inducible transcription factors (HIF1α, HIF2α, HIF3α) for proteolytic degradation (8) and stabilizing the microtubule network (9). This latter function of pVHL appears to be important in the context of the cyst-dependent pathway of disease progression through a role of pVHL in regulating the primary cilium. The primary cilium is a specialized microtubule-based structure that functions as a sensory organelle for numerous chemical and mechanical stimuli (10). Genetic mutations that compromise the signaling functions or the structure of primary cilia cause polycystic kidney diseases, the most frequent class of genetically-inherited renal diseases, demonstrating that the primary cilium acts to suppress uncontrolled proliferation of renal epithelial cells and cyst formation (11). Several studies have shown that loss of pVHL function increases the propensity of cells to lose their primary cilia (12-15). pVHL localizes to the primary cilium and acts cooperatively with GSK3β activity to stabilize the axoneme, the microtubule scaffold of the primary cilium (15). Hyperactivation of the PI3K signaling pathway and inactivation of GSK3β in *VHL* mutant cystic lesions in VHL patient kidneys results in loss of maintenance of the primary cilium (15).

We previously demonstrated that these cooperative genetic and signaling alterations cause loss of the primary cilium and hypothesized that the absence of the cilium is the trigger for initiation of cyst formation (3, 15). This concept was supported by mouse studies showing that combined kidney epithelial cell-specific deletion of *Vhl* and *Pten* together, but not of either gene alone, caused renal epithelial cysts that displayed reduced frequencies of ciliated epithelial cells (16). A limitation of the conclusions that could be drawn from this study was that it was not possible to determine whether cyst formation resulted solely from loss of the cilium, from the cooperative effects of loss of the cilium plus loss of *Vhl* or from cooperative effects of loss of the cilium plus loss of *Vhl* plus activation of the PI3K pathway. Additionally, since these mice developed diverse benign malignancies in the genital tract that necessitated early euthanasia (17), it was also not possible to age the mice to determine if cystic lesions could progress to form ccRCCs. In the current study we address these limitations by generating an inducible model of *Vhl* deletion together with genetic ablation of primary cilia through deletion of *Kif3a*, a component of the kinesin-II microtubule motor complex that is necessary for the formation of primary cilia (18). Renal epithelium-specific deletion of *Kif3a* causes a polycystic phenotype, the severity of which depends on the time point of deletion. Deletion during embryogenesis or postnatally before day 10 causes rapid-onset polycystic kidney disease requiring early euthanasia of the animals, while *Kif3a* deletion in animals after P11 results in a slow-onset cystic phenotype emerging at 6 months of age (11, 18, 19). We took advantage of a system of inducible gene deletion in adult renal epithelia using the *Ksp1.3-Cre*^{ERT2} transgene (19) to allow long-term follow-up of cyst progression in kidneys mutant for *Vhl* and lacking primary cilia.

Loss of pVHL function causes stabilization of HIF1α in cystic lesions in VHL patients (2). Recent studies have argued that HIF1α might also play a more general role in cystic lesions that arise in genetic conditions other than VHL disease. HIF1α is stabilized in cystic epithelial cells due to microenvironmental hypoxia in a rat model of polycystic kidney disease and in human polycystic kidney disease tissues (20). Based on studies using two in vitro models of cyst formation, it was proposed that HIF1α activation promotes cyst formation (21). However, the hypothesis that HIF1α activation may contribute to the formation or progression of cystic lesions has not been tested in a physiologically relevant cystic model. In this study we tested this idea by deleting *Hif1a* in the *Kif3a*-deletion model of kidney cyst formation.

Results

To investigate potential cooperative effects of *Kif3a*, *Vhl* and *Hif1a* deletion on cyst formation and malignant transformation we generated mouse lines allowing inducible kidney epithelium-specific deletion of *Kif3a* (Ksp1.3-Cre$^{ERT2\ Tg/+}$;Kif3a$^{fl/fl}$), *Kif3a/Vhl* (Ksp1.3-Cre$^{ERT2\ Tg/+}$;Kif3a$^{fl/fl}$;Vhl$^{fl/fl}$) and *Kif3a/Hif1a* (Ksp1.3-Cre$^{ERT2\ Tg/+}$;Kif3a$^{fl/fl}$;Hif1a$^{fl/fl}$). Non-transgenic (Ksp1.3-Cre$^{ERT2\ +/+}$) littermates were used as control animals. 6 week-old mice were fed tamoxifen-containing food for 2 weeks to induce activation of Cre recombinase. Treated animals are hereafter referred to as Kif3a$^{\Delta/\Delta}$, Kif3a$^{\Delta/\Delta}$;Vhl$^{\Delta/\Delta}$ or Kif3a$^{\Delta/\Delta}$;Hif1a$^{\Delta/\Delta}$ and controls as Kif3a$^{fl/fl}$, Kif3a$^{fl/fl}$;Vhl$^{fl/fl}$ or Kif3a$^{fl/fl}$;Hif1a$^{fl/fl}$, respectively. Recombination-specific PCR of genomic DNA isolated from kidneys revealed that all genes were deleted as expected (Fig. 1A) and quantitative real-time PCR analysis of recombination at the *Kif3a* locus revealed a similar frequency of recombination in Kif3a$^{\Delta/\Delta}$, Kif3a$^{\Delta/\Delta}$;Vhl$^{\Delta/\Delta}$ and Kif3a$^{\Delta/\Delta}$;Hif1a$^{\Delta/\Delta}$ mice (Fig. 1B). Renal cysts formed in all genotypes and anti-acetylated tubulin staining of kidneys harvested 9 months after tamoxifen feeding showed that epithelial cells lining cysts in Kif3a$^{\Delta/\Delta}$, Kif3a$^{\Delta/\Delta}$;Vhl$^{\Delta/\Delta}$ or Kif3a$^{\Delta/\Delta}$;Hif1a$^{\Delta/\Delta}$ mice lacked primary cilia (Fig. 1C), confirming the functional effect of *Kif3a* deletion. Immunohistochemistry using an antibody against HIF1α showed nuclear staining in cystic epithelial cells in Kif3a$^{\Delta/\Delta}$;Vhl$^{\Delta/\Delta}$ but not in Kif3a$^{\Delta/\Delta}$ mutant mice (Fig. 1C), confirming the efficiency of *Vhl* deletion. The absence of HIF1α nuclear accumulation in cysts in Kif3a$^{\Delta/\Delta}$ mice showed that these lesions are not hypoxic, in contrast to results obtained in a rat polycystic kidney model (20). Tubules in Kif3a$^{\Delta/\Delta}$;Vhl$^{\Delta/\Delta}$ mutant kidneys in which single or multiple epithelial cells were positive for HIF1α staining (Fig. S1B) were observed at a frequency approximately 10-fold higher than the number of cysts. Similarly, tubular cells were frequently seen that displayed elevated staining for Glut-1, a HIF1α-inducible protein, and concomitant loss of primary cilia, demonstrating deletion of *Vhl* and *Kif3a* in these cells (Fig. S1H). These tubules harboring *Vhl* and *Kif3a* mutant cells exhibited no apparent morphological abnormalities, meaning that these cells had not initiated cyst formation within 9 months after *Vhl* and *Kif3a* were deleted. We conclude that the frequency of gene deletion is not the limiting factor in determining the extent of cyst formation in these mouse models. Staining with markers of different nephron segments revealed that cysts develop from proximal tubules (NaPi), thick ascending loops of Henle (THP), distal convoluted tubules (NCC and ATPV1B1), collecting ducts (Aqp2 and ATPV1B1), as well as the epithelium at the urinary pole of the glomerulus (Fig. S2), consistent with the expression pattern of the Ksp1.3-Cre^{ERT2} transgene (19).

To quantitatively monitor cyst formation and progression we adapted a µCT-based imaging technique involving intravascular injection of a contrast agent that is concentrated via the renal tubular system, allowing visualization of the kidney structure (22). We discovered that cysts either do not receive the contrast agent or fail to concentrate it and therefore appear as dark regions in µCT imaging. All mice were imaged at 8, 16, 20, 24, 28, 32 and 36 weeks after administration of tamoxifen food (Fig. 2). Kidneys were isolated and blood plasma was taken after the last time point. Visual inspection of the µCT images revealed no cyst formation in control animals but that the Δ/Δ genotypes developed kidney cysts over time. Kif3a$^{\Delta/\Delta}$ and Kif3a$^{\Delta/\Delta}$;Hif1a$^{\Delta/\Delta}$ animals exhibited a moderate cystic phenotype characterized by the development of 2-20 small to medium cysts per kidney. While some Kif3a$^{\Delta/\Delta}$;Vhl$^{\Delta/\Delta}$ mice also exhibited an apparent moderate cystic phenotype, many developed a severe phenotype and displayed many more larger cysts. Visual comparison of µCT images with histological sections of the same kidneys suggested that the µCT imaging approach accurately reflects the cystic burden (Fig. 2). A major advantage of this longitudinal imaging approach is that total cystic burden can be quantified by 3D reconstruction of the volumes of all of the cystic lesions in the entire kidney (Fig. 3A). Compared to Kif3a$^{\Delta/\Delta}$ and Kif3a$^{\Delta/\Delta}$;Hif1a$^{\Delta/\Delta}$ mice, which behaved almost identically to one another, Kif3a$^{\Delta/\Delta}$;Vhl$^{\Delta/\Delta}$ mice developed cysts earlier and with higher penetrance at all timepoints (Fig. 3B), showed a dramatically increased total cystic burden (Fig. 3C) and histological analysis revealed that there were four times the number of cysts per kidney section (Fig. 3D). Determination of total kidney volumes using µCT demonstrated an excellent correlation with determination of kidney weights (Fig. S3A-C) further validating the accuracy of the µCT approach. Analyses of creatinine (Fig. S3D) and urea (Fig. S3E) levels in blood plasma revealed that kidney function was only marginally impaired in Kif3a$^{\Delta/\Delta}$;Vhl$^{\Delta/\Delta}$ mice with non-significant trends towards increased creatinine and urea levels, implying that the µCT imaging approach is able to detect and quantify cystic lesions in otherwise fully functioning kidneys. Since the creatinine and urea values for all control animals were in the normal ranges, we conclude that monthly rounds of µCT imaging over the life of the animal does not compromise kidney function. Moreover, Kif3a$^{\Delta/\Delta}$;Hif1a$^{\Delta/\Delta}$ and Kif3a$^{\Delta/\Delta}$;Vhl$^{\Delta/\Delta}$ mice that were fed tamoxifen but not subjected to monthly imaging developed cysts similarly to those that were repeatedly imaged (Fig. S4), showing that the repeated injection of the contrast agent and µCT imaging does not contribute to the cystic phenotype.

To compare the proliferative status of epithelial cells in cystic lesions from the different genotypes we selected cohorts of mice that displayed a comparable moderate cystic phenotype. Ki67 staining was used to label proliferating cells. Some cysts contained proliferating cells while others did not (Fig. 4A). Quantifications revealed no differences between Kif3a$^{\Delta/\Delta}$, Kif3a$^{\Delta/\Delta}$;Hif1a$^{\Delta/\Delta}$ and Kif3a$^{\Delta/\Delta}$;Vhl$^{\Delta/\Delta}$ mice in terms of the frequency of cysts that contained proliferating cells (Fig. 4B) or the frequency of Ki67 positive cells within the proliferating cysts (Fig. 4C). The increased cystic number and total cystic burden in Kif3a$^{\Delta/\Delta}$;Vhl$^{\Delta/\Delta}$ mice appears to result from an increased frequency of cyst initiation at earlier timepoints, rather than an absolute increased rate of growth of cysts.

Since VHL patients develop simple cysts, atypical cysts and ccRCCs, we analysed the histological appearance of the cystic lesions in our models. The vast majority of cysts in all genotypes were simple cysts lined by a single epithelial layer (Fig. 5A-C). In Kif3a$^{\Delta/\Delta}$ and Kif3a$^{\Delta/\Delta}$;Hif1a$^{\Delta/\Delta}$ mutant mice, 1.9% (n=204) and 2.1% (n=282) of cysts, respectively, displayed small foci of multilayered or disorganized epithelial growth that projected into the lumen of the cyst (Fig. 5A and C). In contrast, in Kif3a$^{\Delta/\Delta}$;Vhl$^{\Delta/\Delta}$ mice the frequency of these atypical cysts was 8.0% (n=914) (Fig. 5B). No tumors were observed in these mice.

Several studies have shown that deletion of cyst-suppressing genes early in postnatal development while the kidney is actively proliferating induces a more severe and rapid-onset cystic phenotype than gene deletion in adult kidneys (11, 19, 23). To achieve early cyst formation in a manner that does not compromise overall kidney function, we injected nursing dams with a dose of tamoxifen that induced a low level of recombination in the kidneys of feeding pups, to induce a limited number of cysts in all genotypes which could be followed using µCT imaging for 9 months (Fig. S5). As an additional control, deletion of *Vhl* alone in P2 mice did not cause the development of cysts (Fig. S5), consistent with our previous findings using the non-inducible version of the *Ksp1.3-Cre* transgene, which is expressed during embryogenesis and throughout adulthood (16). Staining for HIF1α and anti-acetylated tubulin confirmed the functional effects of deletion of *Kif3a* and *Vhl* in the relevant genotypes (Fig. S6). This method of deletion gave considerable variation within and between litters in terms of the extent of cyst formation, precluding meaningful quantitative comparisons of cystic burden between the genotypes. Morphological analyses of kidneys 9 months after gene deletion revealed very similar phenotypes to adult gene deletion with respect to the formation of simple and atypical cysts and absence of tumors. In Kif3a$^{\Delta/\Delta}$ and Kif3a$^{\Delta/\Delta}$;Hif1a$^{\Delta/\Delta}$ mutant mice 3.3% (n=333) and 3.5% (n=692) of cysts, respectively, contained regions of

atypical epithelial growth (Fig. S7) while 9.3% (n=647) of cysts in Kif3a$^{\Delta/\Delta}$;Vhl$^{\Delta/\Delta}$ mice exhibited atypical morphology (Fig. S7). These results collectively show that combined mutation of *Vhl* and *Kif3a* not only increases the initiation of cystogenesis but also increases the frequency of transition to atypical cysts, mimicking the ccRCC precursor lesions that arise in VHL patient kidneys.

Cyst initiation in several animal models of loss of function of primary cilia is preceded by misorientation of tubular epithelial cell divisions, resulting in cell divisions across the plane of the tubule (24). This causes tubular expansion, which is believed to contribute to cyst initiation. pVHL regulates the stability of mitotic astral microtubules and is thereby also necessary for achieving planar cell division (25). Tubular damage-induced epithelial cell proliferation in *Vhl* mutant kidney tubules leads to an enhanced rate of misoriented cell division and correlates with the formation of microcysts in these animals (26). We tested the idea that the combined effects of loss of two different mechanisms that normally act to ensure oriented cell division could account for the increases in the frequencies of cyst initiation and transition to atypical cysts observed in Kif3a$^{\Delta/\Delta}$;Vhl$^{\Delta/\Delta}$ mice. Anaphase cells in cystic epithelia of Kif3a$^{\Delta/\Delta}$ and Kif3a$^{\Delta/\Delta}$;Vhl$^{\Delta/\Delta}$ mice were identified by staining for the mitotic marker phospho-histone H3 and the plane of cell division was determined by measuring the angle between the plane of the cystic epithelium and a line parallel to the midline of the separating mitotic chromosome arrays (Fig. 5D). Anaphases in Kif3a$^{\Delta/\Delta}$;Vhl$^{\Delta/\Delta}$ cysts displayed a significantly greater spread of angles than anaphases in Kif3a$^{\Delta/\Delta}$ cysts (Fig. 5E). Notably, approximately one third of Kif3a$^{\Delta/\Delta}$;Vhl$^{\Delta/\Delta}$ anaphases were oriented more out of the plane of the epithelium than within the plane of the epithelium (angle less than 45^{o}) whereas about one eighth of Kif3a$^{\Delta/\Delta}$ displayed this phenotype. This increase in frequency of misoriented cell division correlates closely with the approximate 3-4 fold increases in cyst number and frequency of atypical cysts in Kif3a$^{\Delta/\Delta}$;Vhl$^{\Delta/\Delta}$ compared to Kif3a$^{\Delta/\Delta}$ mice.

Discussion

Despite intensive study, the molecular and cellular mechanisms that underlie the formation of ccRCC remain unclear and an autochthonous mouse model of this disease has yet to be developed. We previously proposed a model of disease initiation in which loss of the microtubule stabilizing function of pVHL in combination with signaling alterations in the PI3K and ERK pathways results in failure of epithelial cells to maintain the primary cilium. We suggested that loss of this organelle causes pre-neoplastic cyst formation in VHL patients (3, 15, 16). Our current studies validate this hypothesis but also suggest that a modification of the initial primary cilium-centric model of cyst formation is necessary. The observations that deletion of *Vhl* together with deletion of *Kif3a* shortens the latency of cyst initiation, increases the total number of cysts and total cystic burden compared to deletion of *Kif3a* alone, argue that loss of the primary cilium represents a secondary event in *VHL* mutant cells that cooperates with other cellular changes that arise due to loss of pVHL function and that together these alterations induce cyst formation.

A second important conclusion of this study is that *Vhl/Kif3a*-deficient cystic lesions can persist for at least 6-9 months in mice without progressing to form tumors. Nonetheless, a 3- to 4-fold increase in the frequency of cysts that displayed regions of multilayered epithelial growth projecting into the cystic lumen was observed in Kif3a$^{\Delta/\Delta}$;Vhl$^{\Delta/\Delta}$ mice compared to Kif3a$^{\Delta/\Delta}$ and Kif3a$^{\Delta/\Delta}$;Hif1a$^{\Delta/\Delta}$ mice. Since simple cysts are believed to progress to atypical cysts in the cyst-dependent pathway of ccRCC formation, Kif3a$^{\Delta/\Delta}$;Vhl$^{\Delta/\Delta}$ mice appear to accurately mimic ccRCC precursor lesions. It should be noted that while the frequency of cyst formation in Kif3a$^{\Delta/\Delta}$;Vhl$^{\Delta/\Delta}$ mice is much higher than that seen in Vhl$^{\Delta/\Delta}$;Trp53$^{\Delta/\Delta}$ mice, the degree of atypical growth in the Kif3a$^{\Delta/\Delta}$;Vhl$^{\Delta/\Delta}$ model is much less than that observed in Vhl$^{\Delta/\Delta}$;Trp53$^{\Delta/\Delta}$ mice, which displayed atypical cysts characterized by extensive epithelial proliferation into the lumen as well as the presence of solid neoplasms that had apparently filled the lumen of the cyst (39). This argues that combined loss of the primary cilium plus loss of pVHL function represents an initial trigger for the onset of cyst formation and for the transition to disorganized epithelial proliferation but that these molecular and cellular changes alone are insufficient for sustained neoplastic growth. Additional mutations that occur frequently in ccRCC such as *PBRM1*, *BAP1*, *SETD2* or *TP53* or *PI3K* pathway alterations (4, 27) might allow tumor formation from these atypical cystic precursors.

Given the diversity of the molecular and cellular processes that are regulated by pVHL (28) and by primary cilia (10), it appears likely that multiple mechanisms functioning together might underlie the cooperative phenotypes that arise due to *Vhl* and *Kif3a* deletion. Interestingly, since many normal tubules harboring deletion of *Vhl* and *Kif3a* do not form cysts within 9 months of gene deletion, it is evident that loss of *Vhl* together with loss of primary cilia does not automatically lead to cyst formation. Rather, it is likely that these mutant cells are sensitized to form cysts in response to as-yet-unidentified cues in the kidney microenvironment. For example, cellular proliferation following damage to nephrons has been shown to trigger cyst formation in adult kidneys that lack a variety of cyst-predisposing genes (11, 19, 23). We speculate that the continuous cell turnover that occurs in the adult kidney (29) may represent the proliferative events that allow cyst formation by *Kif3a*- or *Vhl*/*Kif3a*-deficient cells, with the latter genotype being more sensitized than the former to initiate cyst formation. One likely contributing factor to this sensitization is dysregulation of planar epithelial cell division. During development, or during repair of a damaged adult kidney tubule, cellular divisions normally orient along the length of the tubule, ensuring that the tubule lengthens. Misoriented cellular divisions across the plane of the tubule increase the diameter of the tubule and this is believed to represent an initial step in cyst formation (24). Numerous studies have linked the primary cilium to control of oriented cell division via control of non-canonical Wnt and planar cell polarity signaling pathways. Loss of cilia, or of several important signaling components of cilia, causes misorientation of cellular division in normal tubules before cysts form (reviewed in (24)). In this context, it is interesting that pVHL controls the plane of cell division via a different mechanism. pVHL regulates the stability of the astral microtubule network that links the mitotic spindle poles to integrin contacts on the cell surface, thereby controlling the orientation of the mitotic spindle (25). Genetic deletion of *Vhl* in kidney tubules subjected to ischemic damage to induce cellular proliferation caused an increase in the frequency of misoriented epithelial cell divisions, correlating with the formation of microcysts in these animals (26). Consistent with the idea that *Vhl* and *Kif3a* double deletion leads to the loss of two different mechanisms that normally act to ensure oriented cell division, anaphases in cystic epithelia of $Kif3a^{\Delta/\Delta}$;$Vhl^{\Delta/\Delta}$ mice were more frequently misoriented out of the plane of the cystic epithelium than those in $Kif3a^{\Delta/\Delta}$ mice. The expansion of a simple cyst and maintenance of a single epithelial layer requires that cells continue to divide within the plane of the cystic epithelium. We propose that the transition to multilayered epithelial growth in atypical cysts may occur if cell divisions occur perpendicularly to the plane of the epithelial cells that line the cysts, resulting in a daughter cell that could grow on top of the existing cystic epithelium. The higher frequency (33%) of misaligned anaphases relative to the frequency of atypical cysts (8-9%) in $Kif3a^{\Delta/\Delta}$;$Vhl^{\Delta/\Delta}$ mice may potentially be reconciled by the likely failure of a certain fraction of daughter cells

to survive if they divide away from contacts with the basement membrane. It may be speculated that additional genetic alterations might increase the probability of successfully establishing an epithelial outgrowth into the cystic lumen. Misorientation of cellular division may also account for the increased frequency of cyst initiation in $Kif3a^{\Delta/\Delta};Vhl^{\Delta/\Delta}$ mice. While we were unfortunately unable to test the orientation of cellular division in normal tubules prior to cyst initiation due to the relatively low frequency of Cre-mediated recombination and lack of a method of detecting the *Kif3a* and *Vhl/Kif3a* mutant mitotic cells, it seems plausible to suggest that an increased rate of misoriented cell division by $Kif3a^{\Delta/\Delta};Vhl^{\Delta/\Delta}$ tubular epithelial cells might result in a more frequent expansion of the diameters of tubules and increased cyst initiation.

Another potential mechanism that may contribute to cyst formation is HIFα activation. *Vhl* deletion in mouse proximal tubular epithelial cells using the *Pepck-Cre* transgene caused cyst formation in a small fraction of older mice (30). Since this phenotype could be rescued by co-deletion of *Arnt*, encoding HIF1α, the dimerization partner of HIF1α and HIF2α that is necessary for transcriptional activation, but not by co-deletion of *Hif1a* (30), it is possible that the combined activities of HIF1α and HIF2α may promote cyst formation in the *Vhl/Kif3a* deletion model. Indeed, a more general role for HIF1α stabilization in cyst progression has been recently proposed (20, 21). In this study however, we find that cystic lesions induced by *Kif3a* deletion are not characterized by HIF1α stabilization nor does the deletion of *Hif1a* have any effect on the formation of cysts in this model. It may be that HIF1α stabilization is limited to more severe polycystic kidneys than achieved in this model, or that cellular signaling changes induced by mutation of the *PKD1/PKD2* genes in autosomal dominant polycystic kidney disease contribute to HIF1α activation in cysts in a manner that is not reproduced by complete loss of the primary cilium, for example through constitutive mTOR activation (31-33), which causes enhanced translation of HIF1α (34, 35).

Finally, these studies have developed and validated a non-invasive method of quantification of cystic burden in mice that should prove useful for future studies investigating polycystic kidney diseases. Typical experimental approaches currently depend on end-point measurements of large cohorts of mice that are sacrificed for analyses at different timepoints. Quantification of cystic burdens requires analyses of histological sections and therefore represents only a fractional sampling of the cysts in the kidney. The ability to longitudinally and quantitatively monitor cystic burdens in entire intact kidneys of cohorts of

mice over time will facilitate ongoing efforts to understand the genetic basis of different polycystic kidney diseases and to develop effective therapies against these diseases.

Materials and Methods

Animals

Mice expressing a tamoxifen-inducible kidney-specific Cre recombinase under the Ksp1.3 promoter (36) were crossed with *Kif3a*$^{fl/fl}$ (18), *Vhl*$^{fl/fl}$ (37) and/or *Hif1a*$^{fl/fl}$ (38) animals. Gene deletion in 6 week-old animals was achieved by feeding with tamoxifen food (400 ppm) from Harlan Laboratories for 2 weeks. For gene deletion in P2 animals nursing dams were injected intraperitoneally with tamoxifen (0.1 mg/g body weight) from days P2-P4. Mouse experiments were conducted under experimental license 131/2012 from the Veterinary Office of the Canton of Zurich. Sequences of genotyping primers are given in table S1.

micro Computed Tomography (µCT)

Visipaque® 270 (GE Healthcare) was injected intraveneously at 8 µl/g body weight as described in (22). µCT images were obtained with a Quantum FX microCT (Perkin Elmer) with the following settings: 100 µA, 90 kV, respiratory gating and fine scanning. µCT data were exported as DICOM images to be analyzed manually with the Myrian® software (intrasense®) for volumetric measurements and 3D reconstruction and in the Quantum FX data format for overview X-ray pictures.

Immunohistochemistry

Immunohistochemistry and immunofluorescence of formalin-fixed paraffin-embedded kidneys was performed as described (39) with the following antibodies: α-ATPV1B1 (gift from C. Wagner), α-Aqp2 (gift from J. Loffing), α-Glut1 (Abcam), α-HIF1α (Novus Biotechnologies), α-THP (Santa Cruz Biotechnology), α-NaPi (gift from J. Biber), α-NCC (Millipore) and α-acetylated Tubulin (Sigma-Aldrich). Secondary Alexa-488 or Alexa-568 coupled antibodies were from Life Technologies. HRP-coupled α-mouse secondary antibody was from ThermoScientific.

Genomic DNA qPCR analysis

Paraffin embedded kidney sections were washed 2 x 1 min in Xylol and air dried. Genomic DNA was isolated with the Arcturus PicoPure DNA Extraction Kit (Life Technologies). Real-time PCR analysis was performed with SYBR FAST Universal 2X qPCR Master Mix and the primers are listed in Table S1.

Blood plasma analysis

Animals were anaesthetized and blood was collected by puncture of the heart and treated with sodium-heparin. Creatinine and blood urea nitrogen (BUN) were determined using the UniCel® DxC 800 Synchron® Clinical System.

Acknowledgements

We are grateful to Peter Igarashi for providing mice, to Nadine Nägele for assistance with plasma measurements, to Thi Dan Linh Nguyen-Kim and Olivio Donati for assistance with quantifications of µCT images and to Jürg Bieber, Carsten Wagner and Johannes Loffing for providing antibodies. This study was supported by SNF Förderungsprofessur (PP00P3_128257) and by ERC Starting Grant (260316).

Figure Legends

Figure 1: Generation of mice allowing inducible deletion of *Kif3a, Kif3a/Vhl or Kif3a/Hif1a*. (A) PCR of genomic DNA from kidneys of $Kif3a^{\Delta/\Delta}$ and $Kif3a^{fl/fl}$ (top), $Kif3a^{\Delta/\Delta}$;$Vhl^{\Delta/\Delta}$ and $Kif3a^{fl/fl}$;$Vhl^{fl/fl}$ (middle) and $Kif3a^{\Delta/\Delta}$; $Hif1a^{\Delta/\Delta}$ and $Kif3a^{fl/fl}$;$Hif1a^{fl/fl}$ (bottom) mice. PCR reactions using primers specific for the floxed (fl) and recombined (Δ) alleles were performed (indicated on top) and the positions of the expected products are shown on the side. The promoter region of ribosomal protein S6 (S6) served as internal control. (B) Quantitative real time PCR analyses of the ratio of the Kif3a recombined (Δ) and floxed (fl) alleles in kidneys from the indicated genotypes. Mean ± St. Dev. (n=3-7). (C) Representative H&E, anti-Hif1α and anti-acetylated tubulin staining of histologically normal and cystic (Cy) regions of $Kif3a^{\Delta/\Delta}$, $Kif3a^{\Delta/\Delta}$;$Vhl^{\Delta/\Delta}$ and $Kif3a^{\Delta/\Delta}$; $Hif1a^{\Delta/\Delta}$ kidneys. Scale bars = 20 µM.

Figure 2: Longitudinal imaging of cyst progression. Representative µCT images of wild type (A), $Kif3a^{\Delta/\Delta}$ (B), $Kif3a^{\Delta/\Delta}$;$Vhl^{\Delta/\Delta}$ (C) and $Kif3a^{\Delta/\Delta}$; $Hif1a^{\Delta/\Delta}$ (D) mice taken at 8, 16, 28 and 36 weeks after treatment and corresponding histological section of one kidney (36 weeks) from each of the imaged mice. Mice were scored visually as having a moderate or severe cystic phenotype and the number of animals of each genotype with each score is shown. Scale bar in H&E images = 1 mm.

Figure 3: Quantitative assessment of cystic burden reveals increased cyst formation in $Kif3a^{\Delta/\Delta}$;$Vhl^{\Delta/\Delta}$ kidneys. (A) Coronal µCT image and 3D reconstruction of representative $Kif3a^{\Delta/\Delta}$, $Kif3a^{\Delta/\Delta}$;$Vhl^{\Delta/\Delta}$ and $Kif3a^{\Delta/\Delta}$;$Hif1a^{\Delta/\Delta}$ kidneys at 36 weeks after treatment. Kidneys (yellow) and cysts (red) are shown on top of the x-ray image. (B) Percentage of animals displaying kidney cysts in µCT images at different timepoints after gene deletion. $Kif3a^{\Delta/\Delta}$ (n=10), $Kif3a^{\Delta/\Delta}$;$Vhl^{\Delta/\Delta}$ (n=16), $Kif3a^{\Delta/\Delta}$;$Hif1a^{\Delta/\Delta}$ (n=9). (C) Quantification of total cystic volume per kidney. Mean ± SEM, $Kif3a^{\Delta/\Delta}$ (n=14), $Kif3a^{\Delta/\Delta}$;$Vhl^{\Delta/\Delta}$ (n=30) and $Kif3a^{\Delta/\Delta}$;$Hif1a^{\Delta/\Delta}$ (n=16). (D) Number of cysts per kidney section determined by analyses of histological sections through the longitudinal midline of kidneys. Mean ± SEM, $Kif3a^{\Delta/\Delta}$ (n=24), $Kif3a^{\Delta/\Delta}$;$Vhl^{\Delta/\Delta}$ (n=27) and $Kif3a^{\Delta/\Delta}$;$Hif1a^{\Delta/\Delta}$ (n=17). * $p<0.05$ and *** $p<0.005$, Student's unpaired T-test.

Figure 4: Ki67 staining reveals no differences between genotypes in rate of proliferation of cystic cells. (A) Examples of cysts from each genotype that either display no cells that stain for Ki67 ($Ki67^-$) or that contain Ki67 labelled cells ($Ki67^+$). (B) Percentage of cysts that display Ki67 labelled cells, Mean ± SEM, $Kif3a^{\Delta/\Delta}$ (n=54), $Kif3a^{\Delta/\Delta}$;$Vhl^{\Delta/\Delta}$ (n=56), $Kif3a^{\Delta/\Delta}$;$Hif1a^{\Delta/\Delta}$ (n=62). (C) Percentage of Ki67 positive cells per Ki67 positive cyst, Mean ± SEM, $Kif3a^{\Delta/\Delta}$ (n=36), $Kif3a^{\Delta/\Delta}$;$Vhl^{\Delta/\Delta}$ (n=37), $Kif3a^{\Delta/\Delta}$;$Hif1a^{\Delta/\Delta}$ (n=36).

Figure 5: Examples of the histological appearances of cystic lesions. Representative H&E stained sections of simple cysts (left) and atypical cysts (right) from $Kif3a^{\Delta/\Delta}$ (A), $Kif3a^{\Delta/\Delta}$;$Vhl^{\Delta/\Delta}$ (B) and $Kif3a^{\Delta/\Delta}$; $Hif1a^{\Delta/\Delta}$ (C) mice 36 weeks after gene deletion was induced in adult mice. Scale bar = 20 µm. (D) anti-phospho Histone H3 (red) and DAPI (blue) staining of normal (left) and misoriented (right) anaphases. Scale bar = 10 µm. The local plane of the cystic epithelium was determined by drawing a line through the two adjacent nuclei and the anaphase plane was determined by drawing a line parallel to the midline of the dividing chromosomes to calculate the anaphase angle α. (E) Quantification of the angle α of anaphases in $Kif3a^{\Delta/\Delta}$ (n=23), $Kif3a^{\Delta/\Delta}$;$Vhl^{\Delta/\Delta}$ (n=42) cystic epithelia.

Supplementary Figure 1: Deletion of *Vhl* and *Kif3a* does not automatically initiate cyst formation. (A-C) Anti-HIF1α immunohistochemistry and (D-I) anti-Glut1 (green) and anti-acetylated tubulin (red) co-staining of non-cystic (A-C,G-I) and cystic (D-F) regions of $Kif3a^{\Delta/\Delta}$ (A,D,G), $Kif3a^{\Delta/\Delta}$;$Vhl^{\Delta/\Delta}$ (B,E,H) and $Kif3a^{\Delta/\Delta}$;$Hif1a^{\Delta/\Delta}$ (C,F,I) kidneys harvested 36 weeks after tamoxifen feeding. Scale bars = 50 µm (A-C) and 20 µm (D-I). In H the cells in the bottom half of the tubule show strong staining for Glut-1, indicating *Vhl* deletion, and lack primary cilia, indicating deletion of *Kif3a*, while the cells in the top half of the tubule do not stain for Glut-1 but do display primary cilia.

Supplementary Figure 2: Cysts arise from multiple nephron segments. Examples of cysts that stain positively for the following tubular segment markers: (A) Tamm-Horsfall protein (THP, thick ascending loop of Henle), (B) sodium-chloride symporter (NCC, distal convoluted tubule), (C) sodium/phosphate cotransporter (NaPi, proximal tubule), (D) ATPase V1B1 subunit (ATPV1B1, distal tubule and collecting duct), (E) Aquaporin2 (Aqp2, collecting duct). (F) A cyst originating from the epithelium at the urinary pole of the glomerulus. Scale bars = 20 µm.

Supplementary Figure 3: Kidney parameters. (A) Two kidney volume (measured from µCT data) to bodyweight (2KV/BW) ratio and (B) two kidneyweight to body weight ratio (2KW/BW), Mean ± SEM, $Kif3a^{fl/fl}$ (n=8), $Kif3a^{\Delta/\Delta}$ (n=7), $Kif3a^{fl/fl}$;$Vhl^{fl/fl}$ (n=8), $Kif3a^{\Delta/\Delta}$;$Vhl^{\Delta/\Delta}$ (n=14), $Kif3a^{fl/fl}$;$Hif1a^{fl/fl}$ (n=11), $Kif3a^{\Delta/\Delta}$;$Hif1a^{\Delta/\Delta}$ (n=9). (C) Correlation between µCT measurement of volume of kidneys with weight of kidneys. r^2 reflects Spearman's rank correlation coefficient with associated p-value. (D) Creatinine and (E) Urea levels were measured in blood plasma. Mean ± SEM, $Kif3a^{fl/fl}$ (n=8), $Kif3a^{\Delta/\Delta}$ (n=6), $Kif3a^{fl/fl}$;$Vhl^{fl/fl}$ (n=6), $Kif3a^{\Delta/\Delta}$;$Vhl^{\Delta/\Delta}$ (n=9), $Kif3a^{fl/fl}$;$Hif1a^{fl/fl}$ (n=11), $Kif3a^{\Delta/\Delta}$;$Hif1a^{\Delta/\Delta}$ (n=9). Student's unpaired T-test was performed and no significant differences were observed.

Supplementary Figure 4: Repeated µCT imaging does not influence the cystic phenotype. Representative µCT images and H&E stained sections of (A) $Kif3a^{\Delta/\Delta}$;$Hif1a^{\Delta/\Delta}$ (n=4) and (B) $Kif3a^{\Delta/\Delta}$;$Vhl^{\Delta/\Delta}$ (n=10) mice 36 weeks after tamoxifen feeding. These mice were not subjected to monthly imaging and developed cysts similarly to mice that were repeatedly imaged.

Supplementary Figure 5: Longitudinal imaging of cyst formation following gene deletion in P2 animals. Representative µCT images of (A) wild type, (B) $Kif3a^{\Delta/\Delta}$, (C) $Kif3a^{\Delta/\Delta}$;$Vhl^{\Delta/\Delta}$, (D) $Kif3a^{\Delta/\Delta}$; $Hif1a^{\Delta/\Delta}$ and (E) $Vhl^{\Delta/\Delta}$ mice taken at 8, 16, 28 and 36 weeks after gene deletion at P2 and corresponding histological section of one kidney (36 weeks) from each of the imaged mice. Mice were scored visually as having a moderate or severe cystic phenotype and the number of animals of each genotype with each score is shown. Scale bar in H&E images = 1 mm.

Supplementary Figure 6: Verification of functional consequences of gene deletion in P2 animals. Representative H&E, anti-Hif1α and anti-acetylated tubulin staining of $Kif3a^{\Delta/\Delta}$, $Kif3a^{\Delta/\Delta}$;$Vhl^{\Delta/\Delta}$, $Kif3a^{\Delta/\Delta}$; $Hif1a^{\Delta/\Delta}$ and $Vhl^{\Delta/\Delta}$ kidneys. Scale bars = 20 µM.

Supplementary Figure 7: Examples of the histological appearances of cystic lesions in P2 animals. Representative H&E stained sections of simple cysts (left) and atypical cysts (right) from $Kif3a^{\Delta/\Delta}$ (A), $Kif3a^{\Delta/\Delta}$;$Vhl^{\Delta/\Delta}$ (B) and $Kif3a^{\Delta/\Delta}$; $Hif1a^{\Delta/\Delta}$ (C) mice 36 weeks after gene deletion was induced in P2 mice. Scale bar = 20 µm.

Name	Sequence 5'-3'	Application
Hif1a fwd	GGA GCT ATC TCT CTA GAC C	Genotyping / qPCR
Hif1a rev	GCA GTT AAG AGC ACT AGT TG	Genotyping / qPCR
Hif1a fl fwd	TGG GGA TGA AAA CAT CTG CT	qPCR
Hif1a fl rev	GTT GGG GCA GTA CTG GAA AG	qPCR
Kif3a P1	AGG GCA GAC GGA AGG GTG G	Genotyping / qPCR
Kif3a P2	GGC AGA TGG ATC TCT GTG AGT TTG	Genotyping / qPCR
Kif3a rec fwd	GCA GAC GGA AGG GTG GTT TA	qPCR
Kif3a rec rev	CTG CAA GAGGGT GGA AAG GA	qPCR
Ksp1.3-Cre fwd	AGG TTC GTG CAC TCA TGG A	Genotyping
Ksp1.3-Cre rev	TCG ACC AGT TTA GTT ACC C	Genotyping
rpS6 promoter rev	AGT CAC TTC CGC CGG CTG TTC	qPCR
rpS6 promoter fwd	GCG TCA CGA AAA AGA GGC CCG A	qPCR
Vhl fwd	GGA GTA GGA TAA GTC AGC TG	Genotyping
Vhl rev	GTA CAC CTG AGA GCG GCT TC	Genotyping
Vhl fwd1	CTG GTA CCC ACG AAA CTG TC	qPCR
Vhl fwd2	CTA GGC ACC GAG CTT AGA GGT TTG CG	qPCR
Vhl rev	CTG ACT TCCACT GAT GCT TGT CAC AG	qPCR

Table S1: Primer sequences.

References

1. Maher ER & Kaelin WG, Jr. (1997) von Hippel-Lindau disease. *Medicine (Baltimore)* 76(6):381-391.
2. Mandriota SJ*, et al.* (2002) HIF activation identifies early lesions in VHL kidneys: evidence for site-specific tumor suppressor function in the nephron. *Cancer Cell* 1(5):459-468.
3. Thoma CR, Frew IJ, & Krek W (2007) The VHL tumor suppressor: riding tandem with GSK3beta in primary cilium maintenance. *Cell Cycle* 6(15):1809-1813.
4. Sato Y*, et al.* (2013) Integrated molecular analysis of clear-cell renal cell carcinoma. *Nat Genet* 45(8):860-867.
5. Moch H (2010) Cystic renal tumors: new entities and novel concepts. *Adv Anat Pathol* 17(3):209-214.
6. von Teichman A*, et al.* (2011) VHL mutations and dysregulation of pVHL- and PTEN-controlled pathways in multilocular cystic renal cell carcinoma. *Mod Pathol* 24(4):571-578.
7. Chen YB & Tickoo SK (2012) Spectrum of preneoplastic and neoplastic cystic lesions of the kidney. *Arch Pathol Lab Med* 136(4):400-409.
8. Maxwell PH*, et al.* (1999) The tumour suppressor protein VHL targets hypoxia-inducible factors for oxygen-dependent proteolysis. *Nature* 399(6733):271-275.
9. Hergovich A, Lisztwan J, Barry R, Ballschmieter P, & Krek W (2003) Regulation of microtubule stability by the von Hippel-Lindau tumour suppressor protein pVHL. *Nat Cell Biol* 5(1):64-70.
10. Berbari NF, O'Connor AK, Haycraft CJ, & Yoder BK (2009) The primary cilium as a complex signaling center. *Curr Biol* 19(13):R526-535.
11. Davenport JR*, et al.* (2007) Disruption of intraflagellar transport in adult mice leads to obesity and slow-onset cystic kidney disease. *Curr Biol* 17(18):1586-1594.
12. Esteban MA, Harten SK, Tran MG, & Maxwell PH (2006) Formation of primary cilia in the renal epithelium is regulated by the von Hippel-Lindau tumor suppressor protein. *J Am Soc Nephrol* 17(7):1801-1806.
13. Lutz MS & Burk RD (2006) Primary cilium formation requires von hippel-lindau gene function in renal-derived cells. *Cancer Res* 66(14):6903-6907.
14. Mans DA*, et al.* (2008) Mobility of the von Hippel-Lindau tumour suppressor protein is regulated by kinesin-2. *Exp Cell Res* 314(6):1229-1236.
15. Thoma CR*, et al.* (2007) pVHL and GSK3beta are components of a primary cilium-maintenance signalling network. *Nat Cell Biol* 9(5):588-595.
16. Frew IJ*, et al.* (2008) pVHL and PTEN tumour suppressor proteins cooperatively suppress kidney cyst formation. *EMBO J* 27(12):1747-1757.
17. Frew IJ*, et al.* (2008) Combined VHLH and PTEN mutation causes genital tract cystadenoma and squamous metaplasia. *Mol Cell Biol* 28(14):4536-4548.
18. Lin F*, et al.* (2003) Kidney-specific inactivation of the KIF3A subunit of kinesin-II inhibits renal ciliogenesis and produces polycystic kidney disease. *Proc Natl Acad Sci U S A* 100(9):5286-5291.
19. Patel V*, et al.* (2008) Acute kidney injury and aberrant planar cell polarity induce cyst formation in mice lacking renal cilia. *Hum Mol Genet* 17(11):1578-1590.
20. Bernhardt WM*, et al.* (2007) Involvement of hypoxia-inducible transcription factors in polycystic kidney disease. *Am J Pathol* 170(3):830-842.
21. Buchholz B*, et al.* (2014) Hypoxia-inducible factor-1alpha causes renal cyst expansion through calcium-activated chloride secretion. *J Am Soc Nephrol* 25(3):465-474.
22. Almajdub M, Magnier L, Juillard L, & Janier M (2008) Kidney volume quantification using contrast-enhanced in vivo X-ray micro-CT in mice. *Contrast Media Mol Imaging* 3(3):120-126.

23. Piontek K, Menezes LF, Garcia-Gonzalez MA, Huso DL, & Germino GG (2007) A critical developmental switch defines the kinetics of kidney cyst formation after loss of Pkd1. *Nat Med* 13(12):1490-1495.
24. Fischer E & Pontoglio M (2009) Planar cell polarity and cilia. *Semin Cell Dev Biol* 20(8):998-1005.
25. Thoma CR*, et al.* (2009) VHL loss causes spindle misorientation and chromosome instability. *Nat Cell Biol* 11(8):994-1001.
26. Hell MP, Duda M, Weber TC, Moch H, & Krek W (2014) Tumor Suppressor VHL Functions in the Control of Mitotic Fidelity. *Cancer Res*.
27. TCGA (2013) Comprehensive molecular characterization of clear cell renal cell carcinoma. *Nature* 499(7456):43-49.
28. Frew IJ & Krek W (2008) pVHL: a multipurpose adaptor protein. *Sci Signal* 1(24):pe30.
29. Rinkevich Y*, et al.* (2014) In Vivo clonal analysis reveals lineage-restricted progenitor characteristics in Mammalian kidney development, maintenance, and regeneration. *Cell Rep* 7(4):1270-1283.
30. Rankin EB, Tomaszewski JE, & Haase VH (2006) Renal cyst development in mice with conditional inactivation of the von Hippel-Lindau tumor suppressor. *Cancer Res* 66(5):2576-2583.
31. Boehlke C*, et al.* (2010) Primary cilia regulate mTORC1 activity and cell size through Lkb1. *Nat Cell Biol* 12(11):1115-1122.
32. Deere JD*, et al.* (2010) Viral decay kinetics in the highly active antiretroviral therapy-treated rhesus macaque model of AIDS. *PLoS One* 5(7):e11640.
33. Shillingford JM*, et al.* (2006) The mTOR pathway is regulated by polycystin-1, and its inhibition reverses renal cystogenesis in polycystic kidney disease. *Proc Natl Acad Sci U S A* 103(14):5466-5471.
34. Rowe I*, et al.* (2013) Defective glucose metabolism in polycystic kidney disease identifies a new therapeutic strategy. *Nat Med* 19(4):488-493.
35. Toschi A, Lee E, Gadir N, Ohh M, & Foster DA (2008) Differential dependence of hypoxia-inducible factors 1 alpha and 2 alpha on mTORC1 and mTORC2. *J Biol Chem* 283(50):34495-34499.
36. Shao X, Johnson JE, Richardson JA, Hiesberger T, & Igarashi P (2002) A minimal Ksp-cadherin promoter linked to a green fluorescent protein reporter gene exhibits tissue-specific expression in the developing kidney and genitourinary tract. *J Am Soc Nephrol* 13(7):1824-1836.
37. Haase VH, Glickman JN, Socolovsky M, & Jaenisch R (2001) Vascular tumors in livers with targeted inactivation of the von Hippel-Lindau tumor suppressor. *Proc Natl Acad Sci U S A* 98(4):1583-1588.
38. Ryan HE*, et al.* (2000) Hypoxia-inducible factor-1alpha is a positive factor in solid tumor growth. *Cancer Res* 60(15):4010-4015.
39. Albers J*, et al.* (2013) Combined mutation of Vhl and Trp53 causes renal cysts and tumours in mice. *EMBO Mol Med* 5(6):949-964.

Figure 1

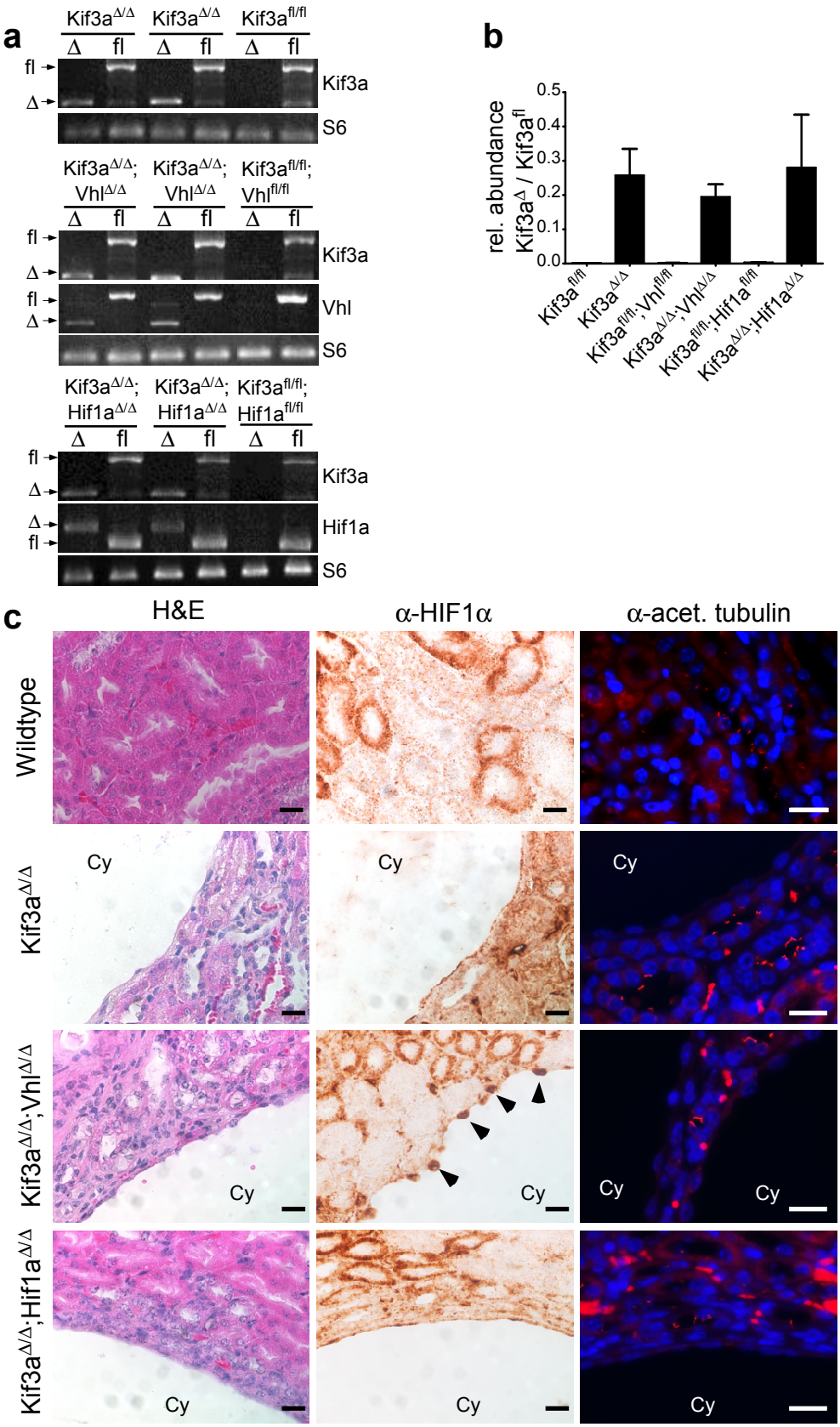
a
Kif3a Δ/Δ
Kif3a Δ/Δ
Kif3a fl/fl
Δ fl Δ fl Δ fl
fl
Δ
Kif3a
S6
Kif3a Δ/Δ; Vhl Δ/Δ
Kif3a Δ/Δ; Vhl Δ/Δ
Kif3a fl/fl; Vhl fl/fl
Vhl
Kif3a Δ/Δ; Hif1a Δ/Δ
Kif3a Δ/Δ; Hif1a Δ/Δ
Kif3a fl/fl; Hif1a fl/fl
Hif1a
b
rel. abundance Kif3a Δ / Kif3a fl
0.5
0.4
0.3
0.2
0.1
0.0
Kif3a fl/fl
Kif3a Δ/Δ
Kif3a fl/fl;Vhl fl/fl
Kif3a Δ/Δ;Vhl Δ/Δ
Kif3a fl/fl;Hif1a fl/fl
Kif3a Δ/Δ;Hif1a Δ/Δ
c
H&E
α-HIF1α
α-acet. tubulin
Wildtype
Kif3a Δ/Δ
Kif3a Δ/Δ;Vhl Δ/Δ
Kif3a Δ/Δ;Hif1a Δ/Δ
Cy

Figure 2

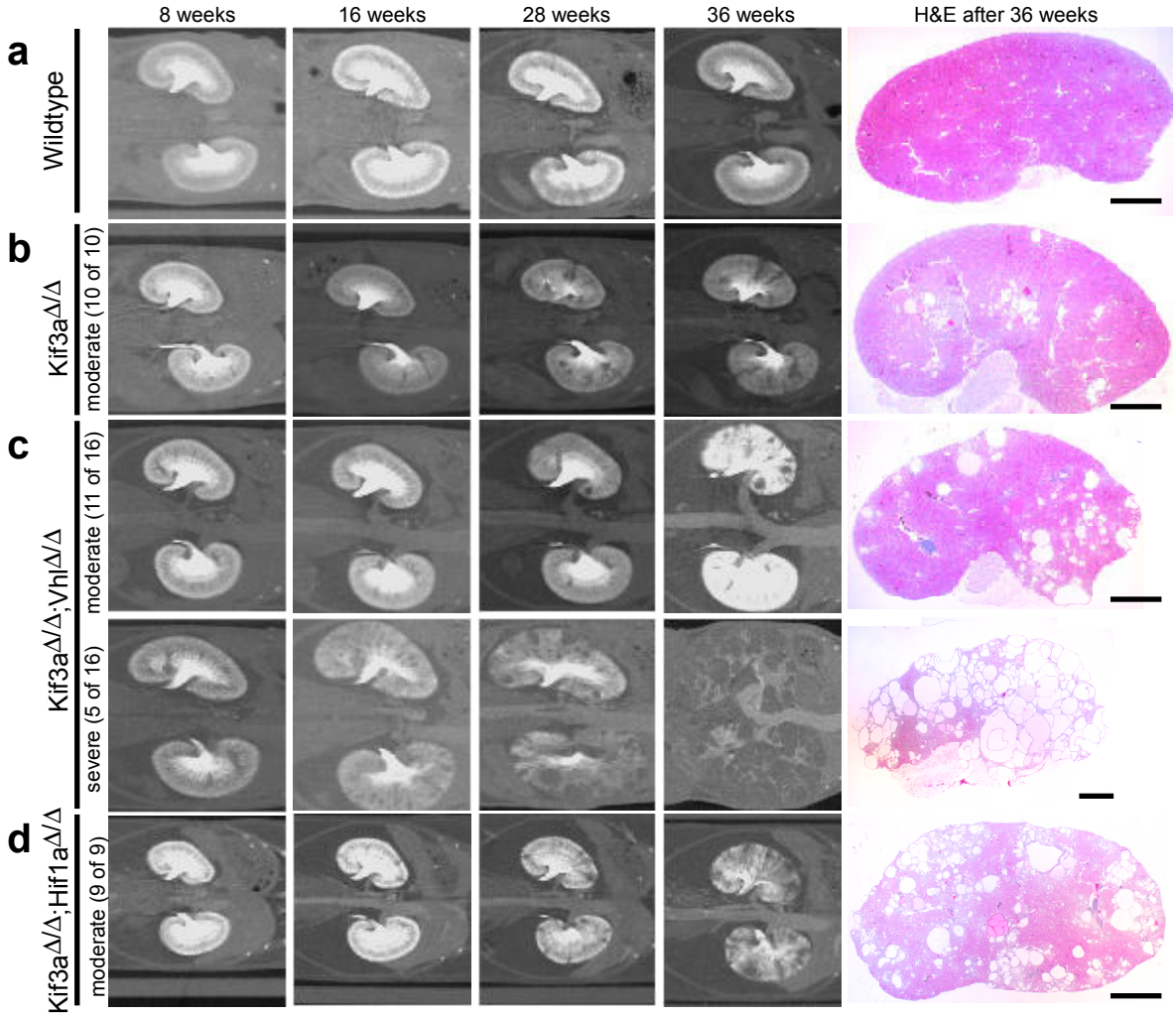
8 weeks
16 weeks
28 weeks
36 weeks
H&E after 36 weeks
a
Wildtype
b
Kif3aΔ/Δ
moderate (10 of 10)
c
Kif3aΔ/Δ;VhlΔ/Δ
moderate (11 of 16)
severe (5 of 16)
d
Kif3aΔ/Δ;Hif1aΔ/Δ
moderate (9 of 9)

Figure 3

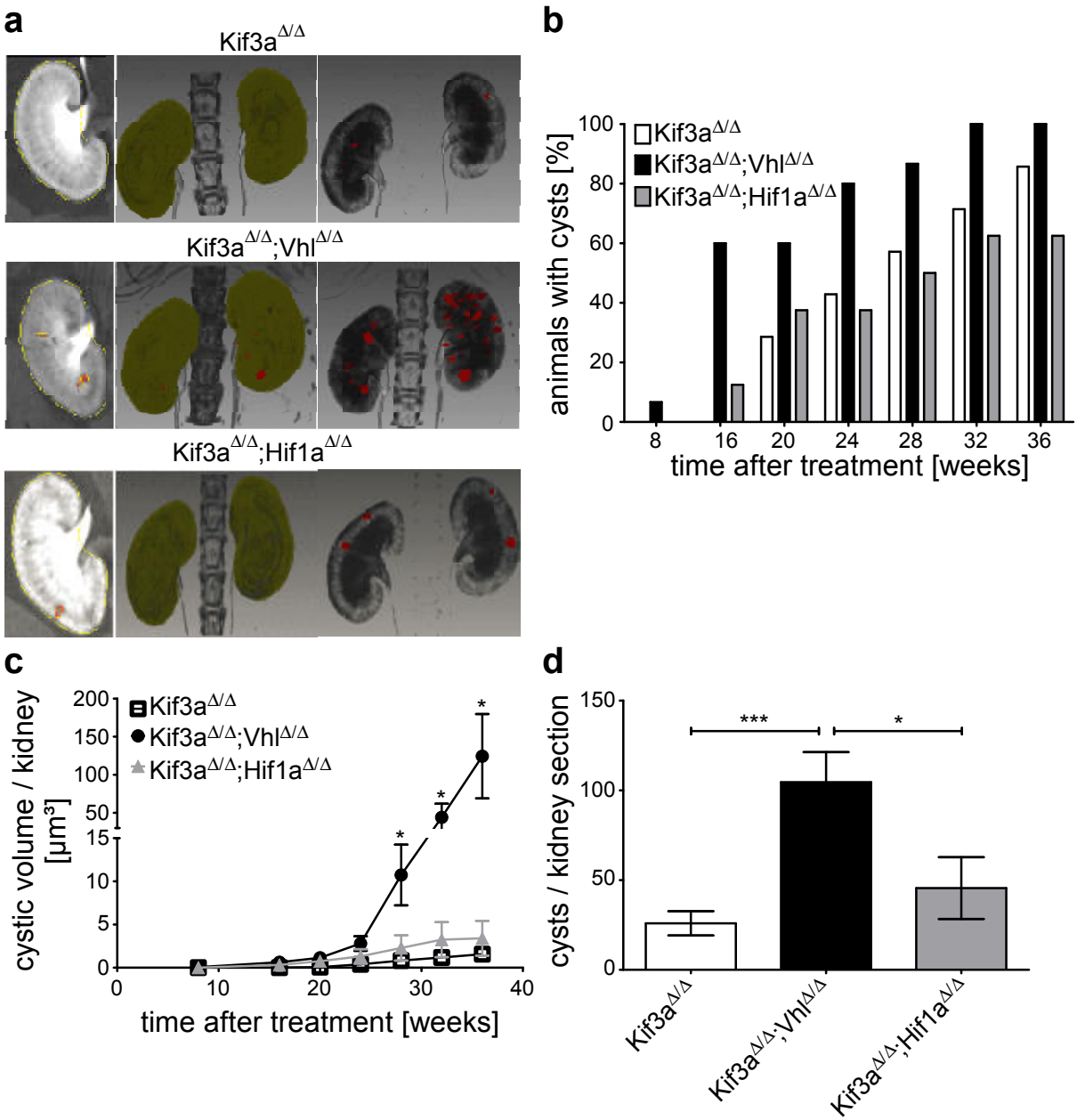
a
Kif3a$^{\Delta/\Delta}$
Kif3a$^{\Delta/\Delta}$;Vhl$^{\Delta/\Delta}$
Kif3a$^{\Delta/\Delta}$;Hif1a$^{\Delta/\Delta}$
b
Kif3a$^{\Delta/\Delta}$
Kif3a$^{\Delta/\Delta}$;Vhl$^{\Delta/\Delta}$
Kif3a$^{\Delta/\Delta}$;Hif1a$^{\Delta/\Delta}$
animals with cysts [%]
0
20
40
60
80
100
8
16
20
24
28
32
36
time after treatment [weeks]
c
Kif3a$^{\Delta/\Delta}$
Kif3a$^{\Delta/\Delta}$;Vhl$^{\Delta/\Delta}$
Kif3a$^{\Delta/\Delta}$;Hif1a$^{\Delta/\Delta}$
cystic volume / kidney [µm³]
0
5
10
15
50
100
150
200
0
10
20
30
40
time after treatment [weeks]
*
*
*
d
cysts / kidney section
0
50
100
150
***
*
Kif3a$^{\Delta/\Delta}$
Kif3a$^{\Delta/\Delta}$;Vhl$^{\Delta/\Delta}$
Kif3a$^{\Delta/\Delta}$;Hif1a$^{\Delta/\Delta}$

Figure 4

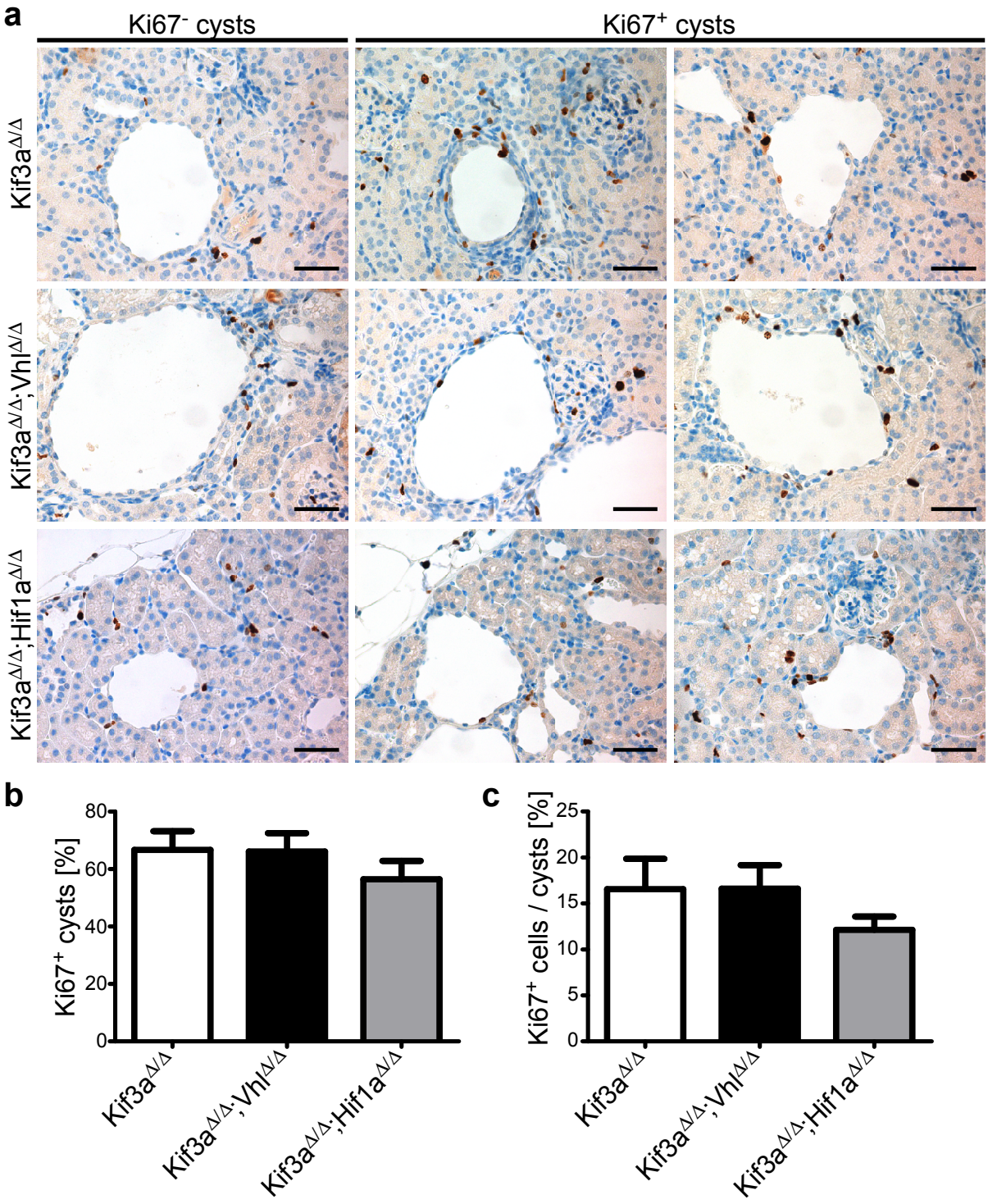
a
Ki67- cysts
Ki67+ cysts
Kif3a Δ/Δ
Kif3a Δ/Δ;Vhl Δ/Δ
Kif3a Δ/Δ;Hif1a Δ/Δ
b
Ki67+ cysts [%]
0
20
40
60
80
Kif3a Δ/Δ
Kif3a Δ/Δ;Vhl Δ/Δ
Kif3a Δ/Δ;Hif1a Δ/Δ
c
Ki67+ cells / cysts [%]
0
5
10
15
20
25
Kif3a Δ/Δ
Kif3a Δ/Δ;Vhl Δ/Δ
Kif3a Δ/Δ;Hif1a Δ/Δ

Figure 5

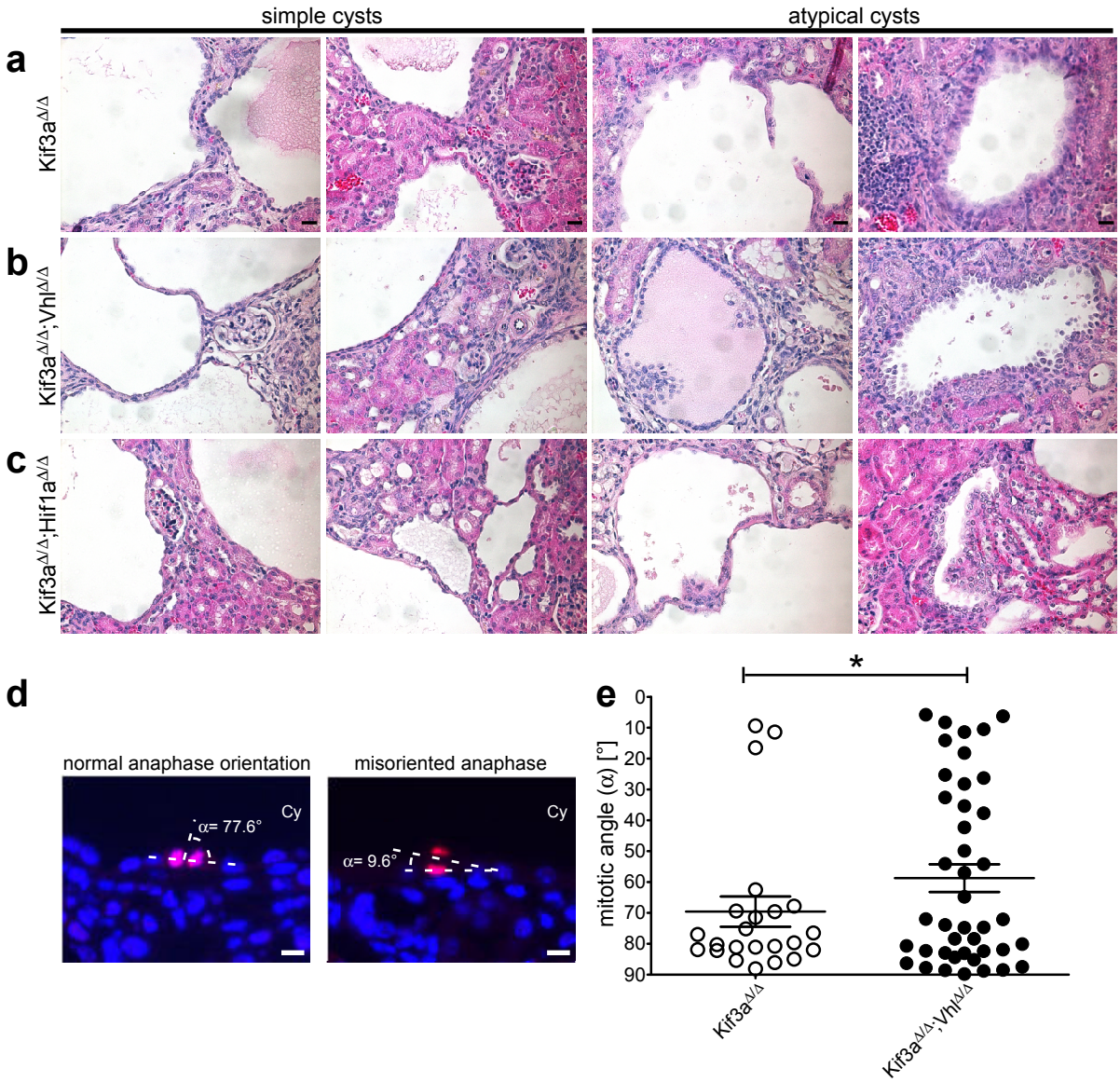
simple cysts
atypical cysts
a
Kif3a$^{\Delta/\Delta}$
b
Kif3a$^{\Delta/\Delta}$;Vhl$^{\Delta/\Delta}$
c
Kif3a$^{\Delta/\Delta}$;Hif1a$^{\Delta/\Delta}$
d
normal anaphase orientation
misoriented anaphase
Cy
α= 77.6°
α= 9.6°
e
*
mitotic angle (α) [°]
0
10
20
30
40
50
60
70
80
90
Kif3a$^{\Delta/\Delta}$
Kif3a$^{\Delta/\Delta}$;Vhl$^{\Delta/\Delta}$

Supplementary Figure S1

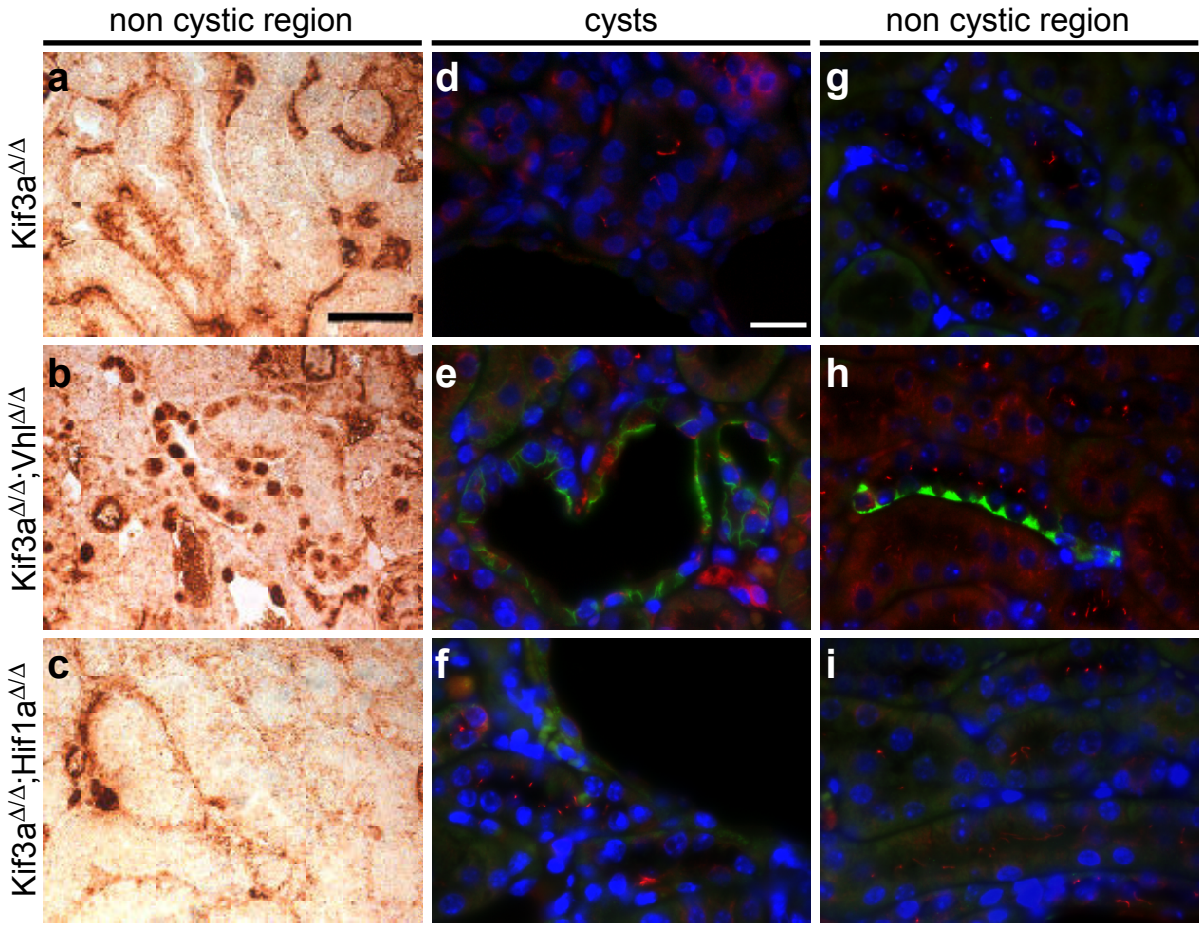

Supplementary Figure S2

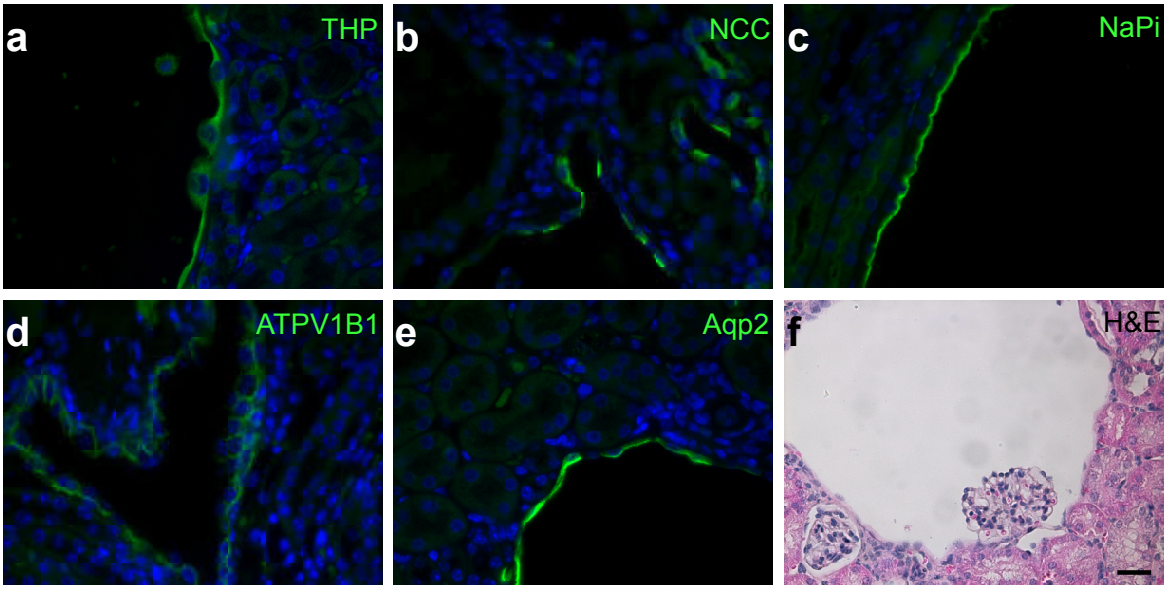

Supplementary Figure S3

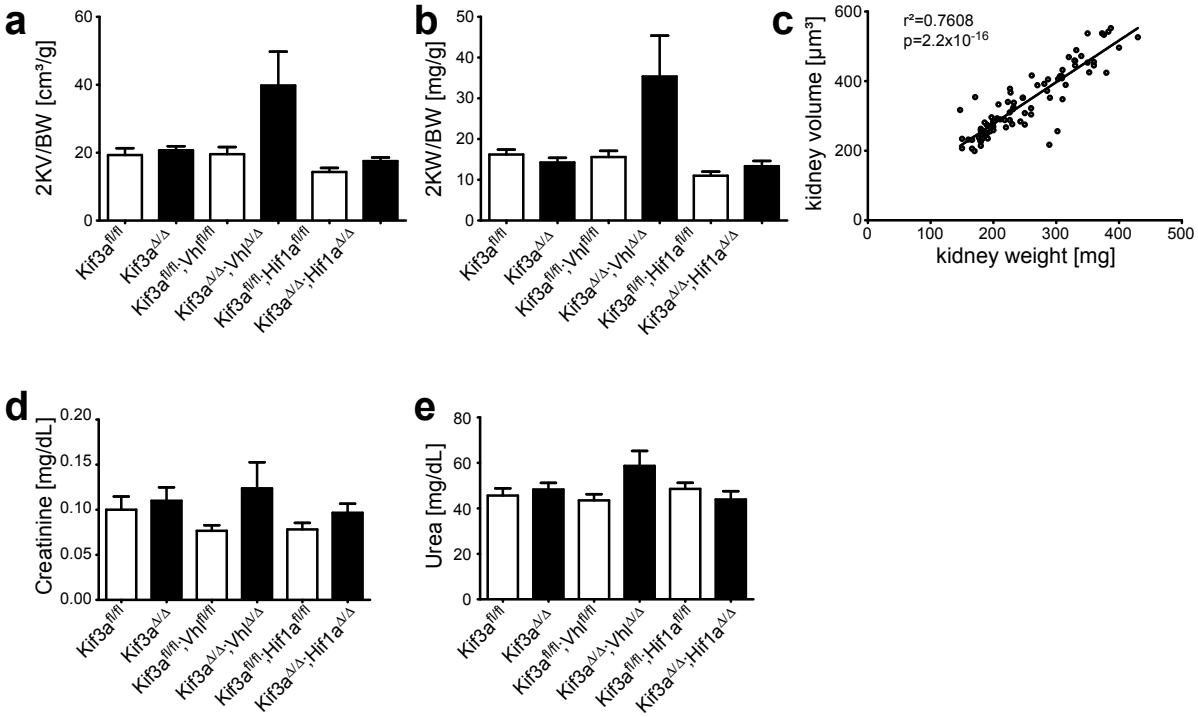

Supplementary Figure S4

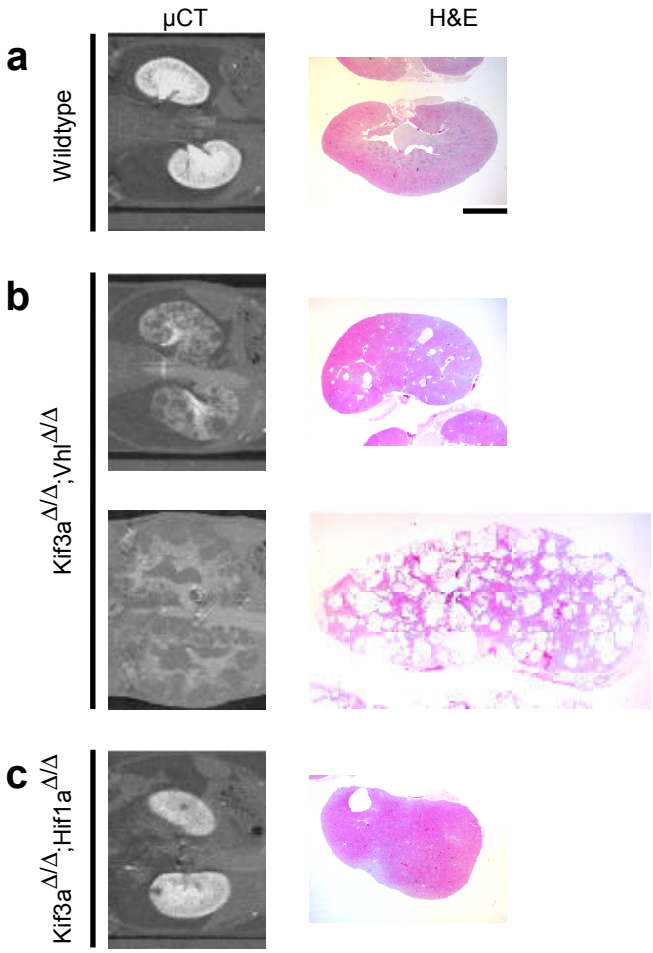

Supplementary Figure S5

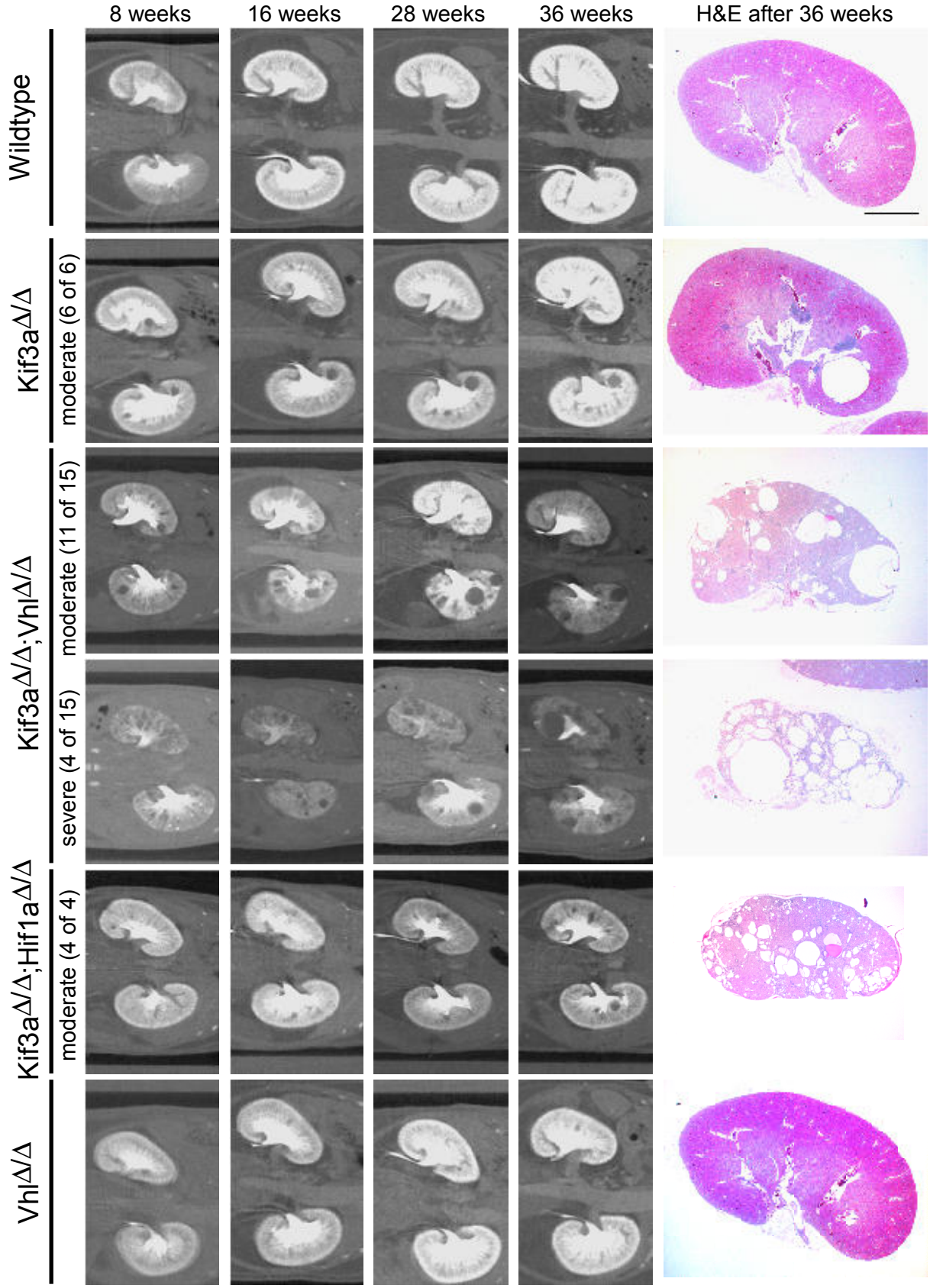

Supplementary Figure S6

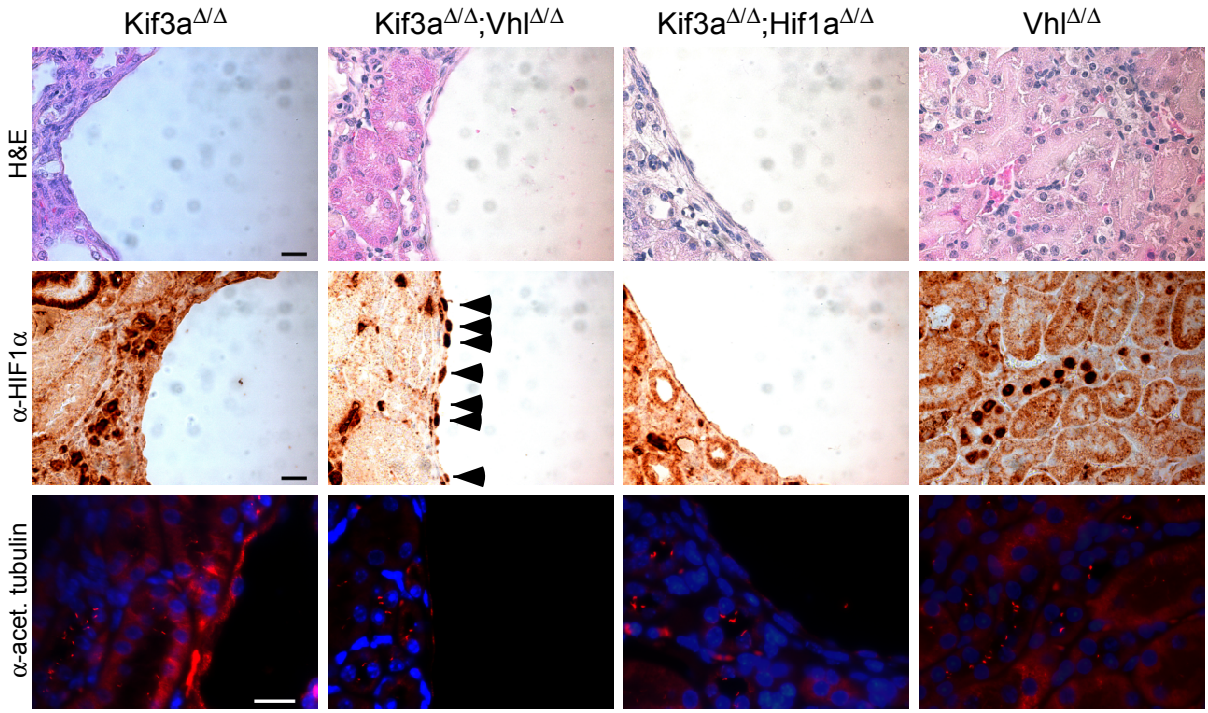

Supplementary Figure S7

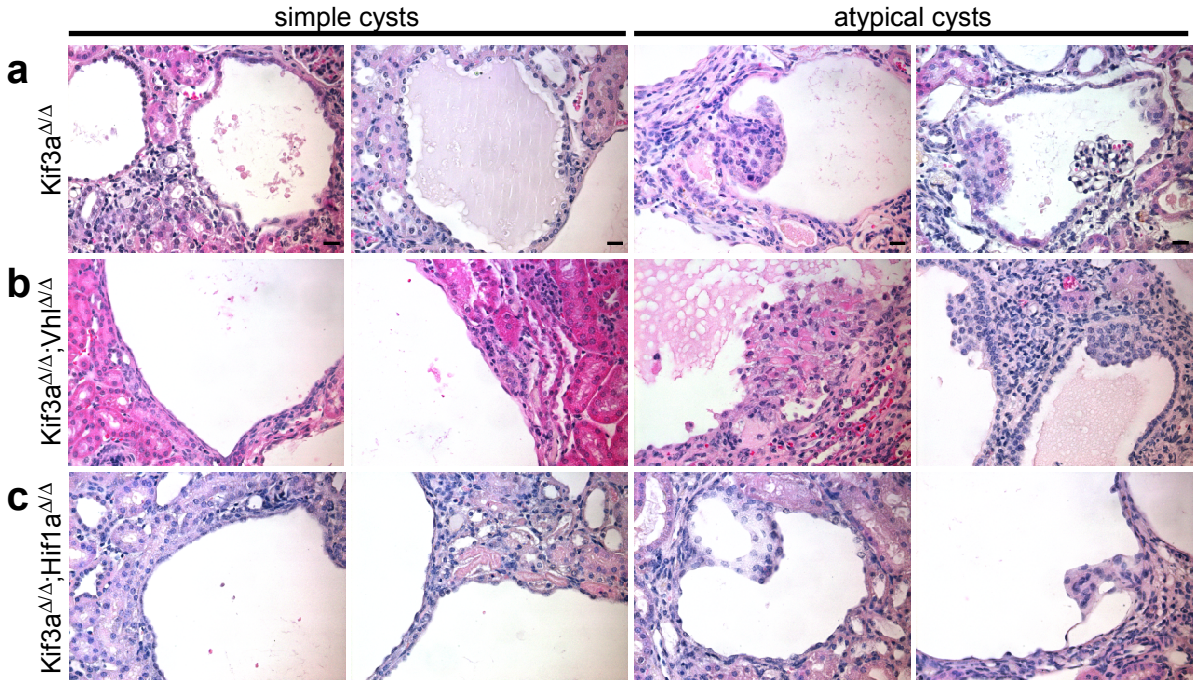

3.2 Additional animal studies performed

In addition to the data given in the manuscript we further analyzed the P2 animals. Representative coronal µCT images and 3D reconstructions at 36 weeks after treatment are shown for Kif3a$^{\Delta/\Delta}$, Kif3a$^{\Delta/\Delta}$;Vhl$^{\Delta/\Delta}$, Kif3a$^{\Delta/\Delta}$;Hif1a$^{\Delta/\Delta}$ and Vhl$^{\Delta/\Delta}$ animals (Figure 3.2.1 A). We determined blood plasma creatinine (Figure 3.2.1 B) and Urea (Figure 3.2.1 C) levels of these animals. No significant differences between Δ/Δ genotypes and/or controls were observed (Figure 3.2.1 B+C). These results are similar to the data obtained from the adult animals. In the P2 animals we did not observe such severe polycystic kidney phenotypes probably due to the low dose of tamoxifen that we administered to the nursing dam. The variability between the litters is probably responsible for the great variances we measured for creatinine levels (Figure 3.21. B). Nevertheless, this data further supports the idea that µCT imaging is a suitable tool to detect and follow cyst formation *in vivo* and appears to be more sensitive than analysis of blood plasma creatinine and urea levels.

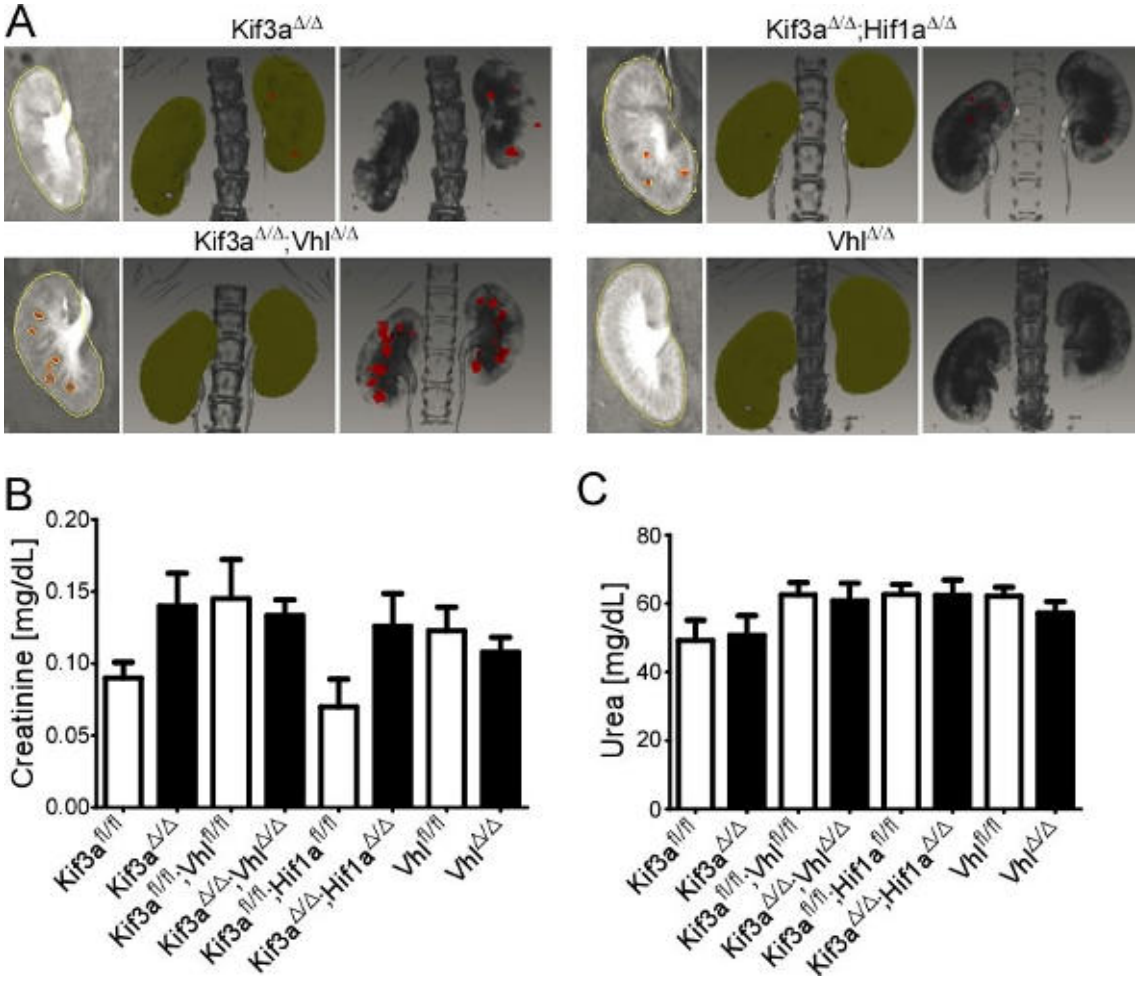

Figure 3.2.1: Cyst analysis of gene deletion in P2 animals. µCT images at 36 weeks after treatment and 3D reconstructions of Kif3a$^{\Delta/\Delta}$, Kif3a$^{\Delta/\Delta}$;Vhl$^{\Delta/\Delta}$, Kif3a$^{\Delta/\Delta}$;Hif1a$^{\Delta/\Delta}$ and Vhl$^{\Delta/\Delta}$ animals (A) with kidneys (yellow) and cysts (red). Blood plasma levels of creatinine (B) and Urea (C) were measured 36 weeks after treatment.

3.3 Influence of *Kif3a* and *Vhl* co-deletion on proliferation, ATP levels and Glucose metabolism

Having established that kidney specific co-deletion of *Kif3a* and *Vhl* leads to increased cystic burden *in vivo* we conducted a series of experiments to investigate potential underlying molecular mechanisms using culture of primary mouse embryo fibroblasts (pMEFs) and primary kidney epithelial cells (pKECs). Based on the fact that deletion of VHL leads to the accumulation of HIF1α which is able to mediate the Warburg effect in ccRCC and that recently the primary cilium was linked to the regulation of energy metabolism through mTORC1 (209-211), we investigated if the basic energy metabolism (ATP and Glucose) was changed upon loss of *Vhl* and/or *Kif3a*. We further speculated that possible deregulation of these metabolites may cause proliferative differences.

pMEFs derived from E13.5 embryos from $Kif3a^{fl/fl}$, $Kif3a^{fl/fl};Vhl^{fl/fl}$, $Vhl^{fl/fl}$ and wild type (wt) animals were cultured under 5% O_2 cell culture conditions. Gene deletion was mediated by adenoviral delivery of Cre recombinase (or GFP as control) and the knockout efficiency was confirmed by western blot (Figure 3.3.1 A). Intracellular ATP levels were measured with the CellTiter-Glo Luminescent Cell Viability Assay but no difference was observed either between Cre-treated (Δ/Δ) and GFP control cells of the same genotype nor between genotypes (Figure 3.3.1 B left). Glucose utilization was measured by determining the levels of lactate and glucose in the medium of Δ/Δ and control cells. Only $Kif3a^{\Delta/\Delta};Vhl^{\Delta/\Delta}$ cells exhibited increased levels of lactate in the medium (Figure 3.3.1 B middle). However, surprisingly these cells also used less glucose which is reflected in the higher amount of glucose in the medium after a 48 hour culture period (Figure 3.3.1 B right). Deletion of *Kif3a* and *Vhl* together or alone did not result in increased proliferation in pMEFs rather a slight reduction in all Δ/Δ pMEFs was observed (Figure 3.3.1 C). The results that we obtained from the analysis of our pMEFs are consistent with the data observed in our *in vivo* model and clearly show that the pMEFs are neither immortalized nor transformed.

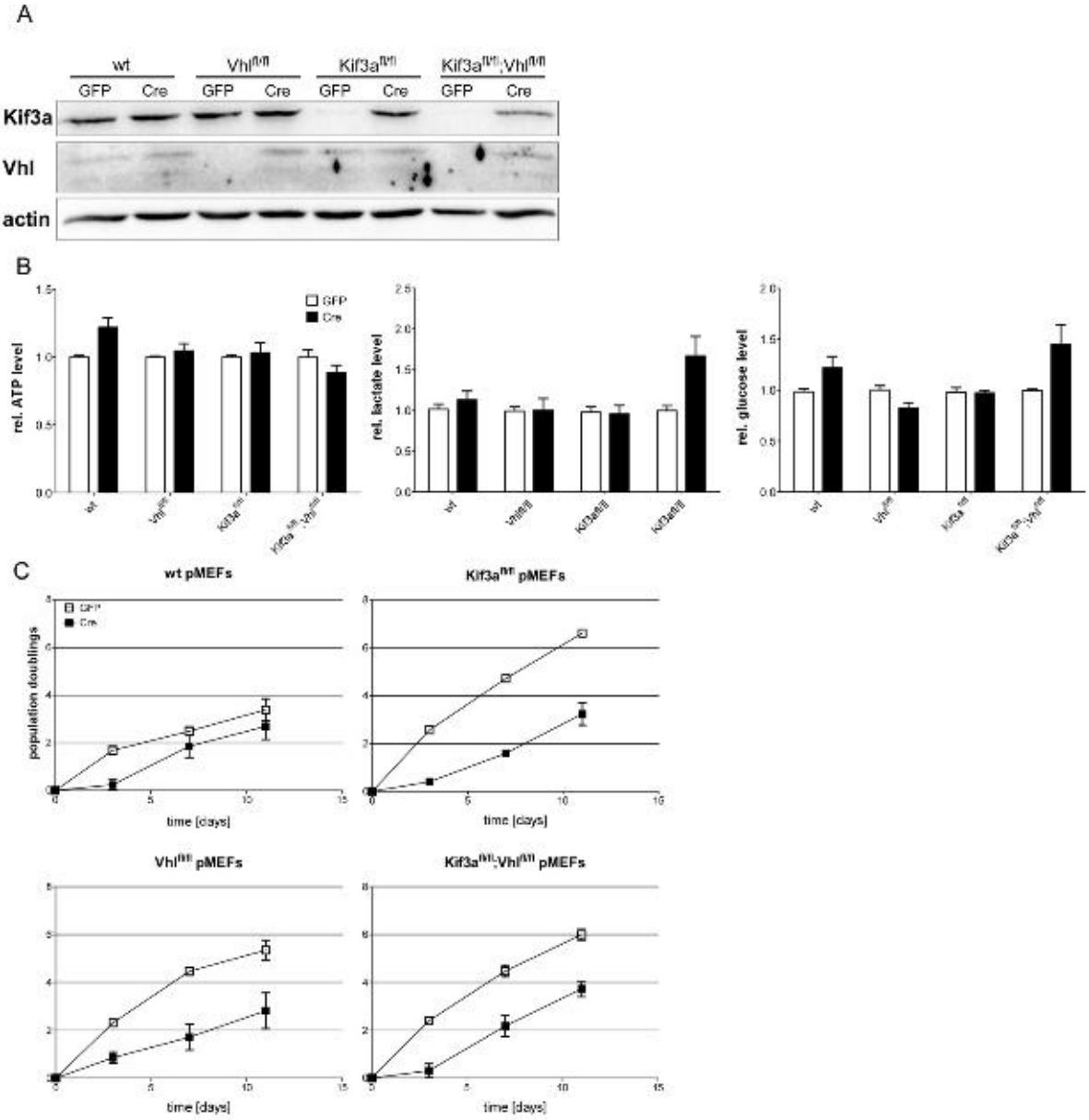

Figure 3.3.1: Effects of Kif3a and Vhl deletion on basic metabolism and proliferation in pMEFs. (A) Representative western blot of Kif3a, Vhl and actin of Cre-treated and GFP control protein lysates from wt, Vhl$^{fl/fl}$, Kif3a$^{fl/fl}$ and Kif3a$^{fl/fl}$Vhl$^{fl/fl}$ pMEFs. (B) Relative levels of cellular ATP (left), lactate (middle) and glucose (right) in the medium of treated and control pMEFs. N=3. (C) Proliferation curves of pMEFs, representative graphs of three independent experiments given. Labels on the middle panel of B need to have the fl/fl in superscript and the Vhlfl/fl is missing from the Kif Vhl genotype (last label, middle graph).

While pMEFs are a cell type that is easy to work with experimentally, we sought to better reproduce the animal models by isolating pKECs from the various fl/fl mice and performing proliferation assays and basic metabolism assays following administration of adenoviruses expressing GFP or Cre. Culturing of pKECs was achieved by digestion of 4-6 week old mouse kidneys and culturing in defined medium containing growth factors that allow epithelial cell proliferation but prevent stromal cell proliferation. This culture system was validated by showing that pKECs express an epithelial cell marker (E-Cadherin) and tubular markers (NaPi and NKCC2) (Figure 3.3.2 A) and form an epithelial layer in 5% O_2 standard cell culture (Figure 3.3.2 B). However, after 2-3 weeks in culture, pKECs lose their epithelial properties and adapt the shape of mesenchymal cells (Figure 3.3.2 C).

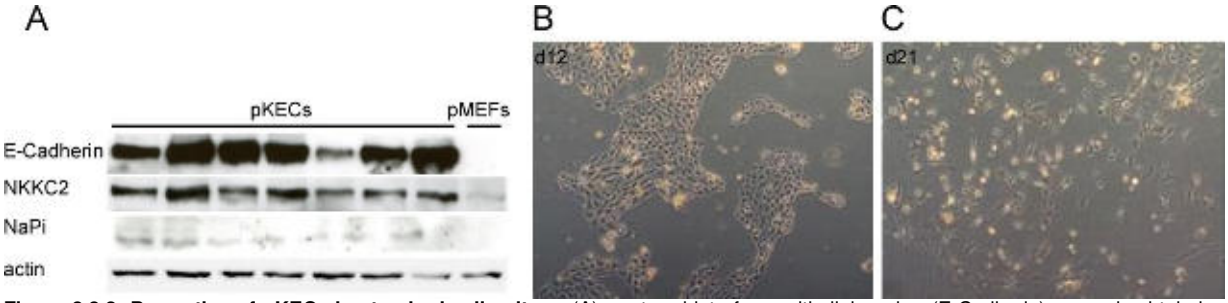

Figure 3.3.2: Properties of pKECs in standard cell culture. (A) western blot of an epithelial marker (E-Cadherin), a proximal tubule marker (NaPi) and a collecting duct marker (NKCC2), β-actin was used as loading control. Brightfield microscopy of pKECs after 12 (B) and 21 (C) days in cell culture.

We confirmed the gene knockout on protein level by western blotting on pKECs used for the experiments and the targeted genes were completely abrogated as intended (Figure 3.3.3 A). Cre treatment led to a small decrease of intracellular ATP levels in all genotypes (Figure 3.3.3 B top left). A slight decrease in uptake of 2-deoxyglucose (2-DOG), a marker for glucose uptake, was measured but was only significant between $Vhl^{\Delta/\Delta}$ and $Vhl^{fl/fl}$ cells (Figure 3.3.3 B top right). 2-DOG is transported with the same kinetics as glucose but once inside the cell it cannot be phosphorylated and eventually completely inhibits glucose metabolism. Therefore, 2-DOG uptake is actually not the best way to study glucose metabolism. No significant changes in glucose utilization and lactate production were measured in the conditioned medium of pKECs (Figure 3.3.3 B lower panels). We also performed short term growth curves for all the genotypes since pKECs do not permit repeated splitting and long culture conditions. Cells were seeded and after initial cell growth gene deletion was facilitated by adeno-Cre or adeno-GFP as control. Cells were fixed on five consecutive days and protein content was determined by SRB staining. No difference between Δ/Δ and control cells was observed during this period (Figure 3.3.3 C). In fact, the overall proliferation of the pKECs during cell culture is very low as can be seen by the relative proliferation depicted in Figure 3.3.3 C. The relative strong increase in $Kif3^{fl/fl}$ pKECs

might also be due to the fact that the number of cells per well is in part dependent on the amount of cells which initially attach after seeding. We concluded that the low rates of proliferation and tendency of the cells to undergo dedifferentiation in culture mean that this assay is not a reliable or meaningful one. Nonetheless, it is clear that the *Kif3a/Vhl* double mutant renal epithelial cells are neither immortalized nor transformed, consistent with the data from *in vivo* gene deletion.

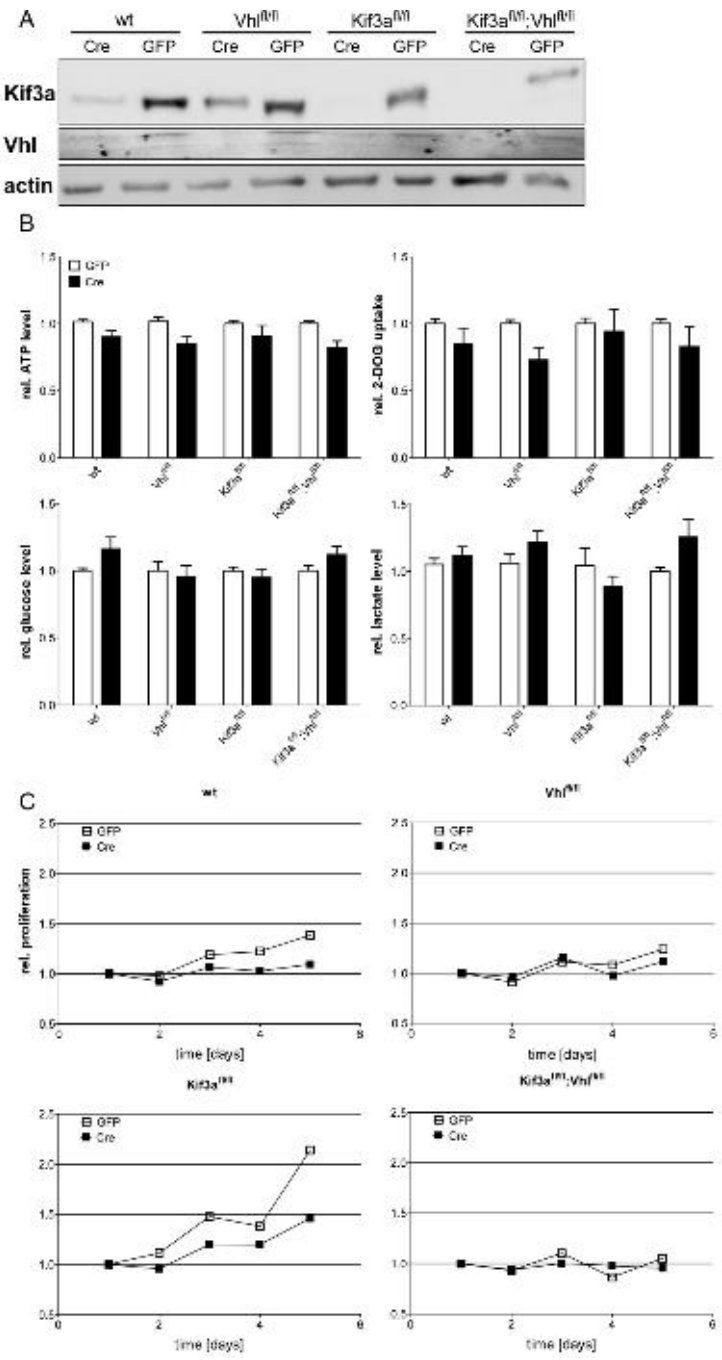

Figure 3.3.3: Effects of Kif3a and Vhl deletion on basic metabolism and proliferation in pKECs. (A) Representative western blot of Kif3a, Vhl and actin of Cre-treated and GFP control protein lysates from wt, Vhl$^{fl/fl}$, Kif3a$^{fl/fl}$ and Kif3a$^{fl/fl}$Vhl$^{fl/fl}$ pKECs. (B) Relative levels of cellular ATP (left), 2-DOG uptake (middle left) lactate (middle) and glucose (right) in the medium of treated and control pKECs. N=4. (C) SRB curves of pKECs, representative graphs of three independent experiments given.

3.4 Primary kidney epithelial cells form polarized acini in a matrigel-based 3D cell culture assay

Since growth of cells on standard cell culture plastic does not reflect the epithelial cell-cell interactions that occur in the context of renal tubules we sought to study the role of *Kif3a* and *Vhl* in cyst formation *in vitro* by establishing a new 3D renal epithelial cell culture model. To do so we used mouse primary kidney epithelial cells (pKECs) for two reasons. First, we wanted to study the deletion of *Kif3a* and/or *Vhl* in otherwise unaltered cells, which is not possible if cultured immortalized cell lines were used. Secondly, the use of pKECs gave us the possibility to use our previously generated mouse strains to delete the gene combinations we want. We tested several different protocols. Initially, we started our 3D cell cultures with a protocol (202) that uses a murine cortical collecting duct (mCCD) cell line in a 3D model. Figure 3.4.1 A+B show the tube formation capacity of the mCCD cells whereas our pKECs did not exhibit this function in the kind of 3D structure (Figure 3.4.1 C+D). This may be due to the fact that we used freshly isolated cells and not an established clone of a cell line.

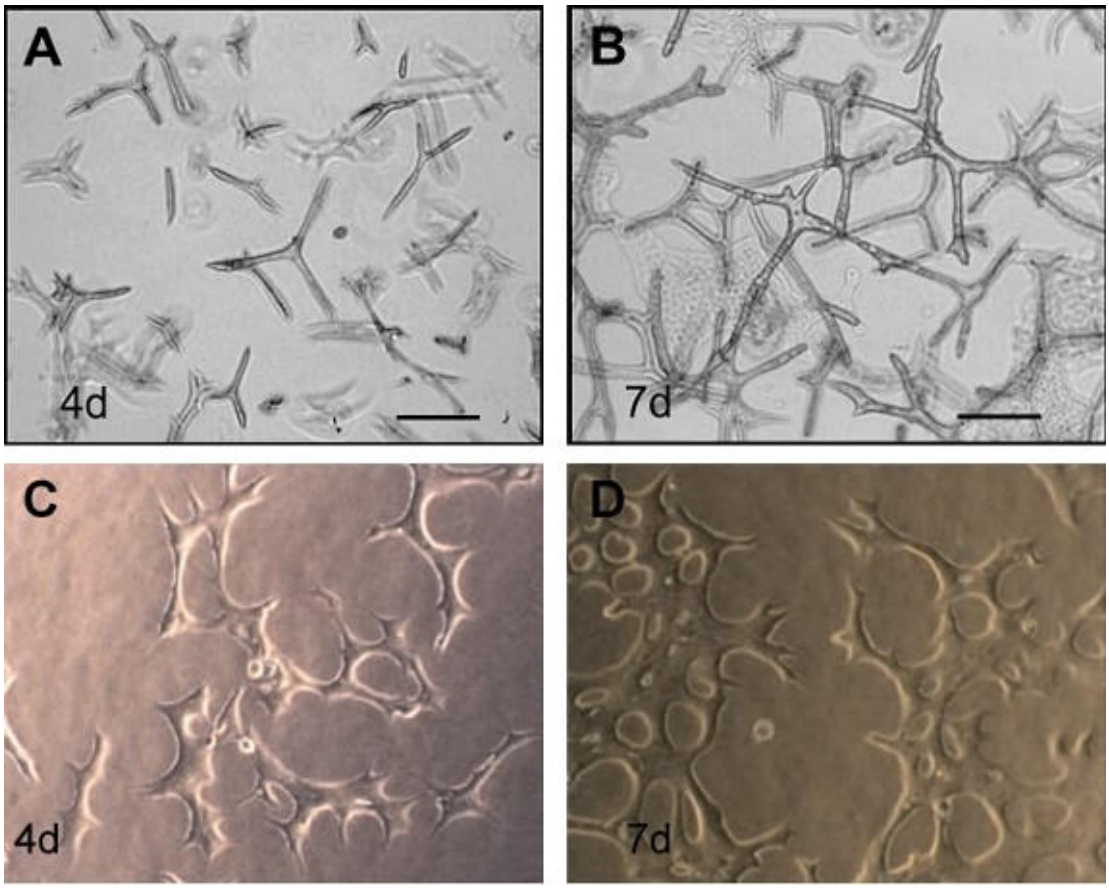

Figure 3.4.1: Tube formation capacity of mCCD and pkECS. mCCD cells after 4 days (A) and 7 days (B) in 3D culture show tube formation. pKECs after 4 days (C) and 7 days (D) do not exhibit this feature. Scale bars are 200µm. Pictures A+B taken from Montesano *et al.* (202).

To continue with the 3D cell culture we experimented with different published protocols for 3D cell culture systems and used renal tubule segments or isolated pKECs in these systems (205, 212, 213). Figure 3.4.2 shows the comparison of the protocols. The protocol from Lee *et al.* published in Nature Protocols in combination with our pKECs leads to the formation of acini-like structures as shown in the literature for epithelial cells (197-199). Unfortunately, the addition of HGF did not lead to the outgrowth of cells from the acini-like structures or enhanced tube formation in any of the tested conditions (Figure 3.4.2 lower panel).

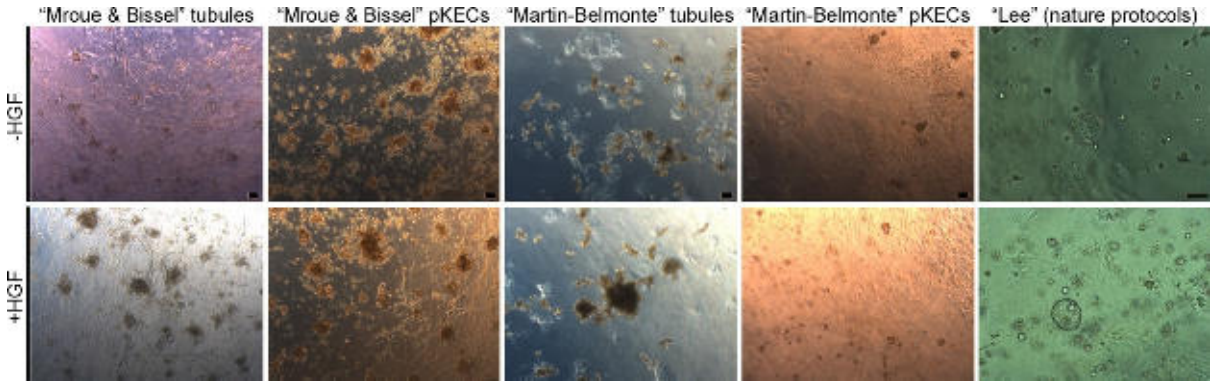

Figure 3.4.2: Overview of different 3D cell culture protocols. Scale bar 20µm

With this protocol our pKECs were able to form acini-like structures in the 3D assay and a clear lumen is visible in higher magnification brightfield pictures (Figure 3.4.3A+B). To confirm that our acini-like structures truly derive from epithelial cells we performed immunofluorescence stainings. We could detect that all cells forming the 3D structure stain positively for E-Cadherin, a marker of epithelial cells (Figure 3.4.4). Co-staining for ß-Catenin was used as an alternative way to visualize the cell border between single cells (figure 3.4.4 A) and validated the epithelial nature of the cells. In addition, we observed that some of the cells comprising an acinus bind either LTA or DBA, marker for proximal tubule or collecting duct, respectively (Figure 3.4.4 A). Taken together these results indicate that our acini are derived from epithelial cells and they maintain tubule segment specific features in the 3D system. Secondly, it also shows that acini are not always formed by a single cell but may originate from two or more aggregated cells from different nephron segments. Furthermore, we investigated if the cells in our acini-like structures maintain their polarization which is usually lost in standard 2D cell culture. For this purpose we stained for acetylated tubulin, a protein highly abundant in the primary cilium of polarized renal epithelial cells. The primary cilium is only visible in non-proliferating cells and cilia of cells in an epithelial layer all point to same direction, into the lumen of the renal tubule. Polarization towards the lumen of the structure was observed in our pKECs 3D cell culture system (Figure 3.4.4 B).

Having validated that this culture system allows maintenance of epithelial characteristics of primary cells in culture, we next sought to study the effect of loss of *Vhl* and *Kif3a*. We transduced acini with adenoviral vectors to induce gene deletion. We used a relatively low titer of adenovirus to prevent toxic side effects which were observed if high titer adenoviral vectors were used in standard cell culture. The low titer resulted mainly in partial and sometimes in complete transduction of acini (Figure 3.4.3 A). Unfortunately, the protein amount we obtained from the 3D cell culture was too low to confirm the knockout by immunoblot. Recombination of the *Kif3a* gene locus results in loss of the primary cilium. We observed that some of the cells in $Kif3a^{\Delta/\Delta}$;$Vhl^{\Delta/\Delta}$ acini indeed did not form the primary cilium (Figure 3.4.4 C). One reason that we did not observe acini in which all cells lacked the primary cilium may be due to the low adenoviral titer we used in our experiments. Another reason may be the time point of *Kif3a* inactivation. A recent publication showed that reabsorption of the primary cilium may take up to 15 days after deletion of *Kif3a* (214). Unfortunately, acini without deletion of *Kif3a* also contained cells that lacked a primary cilium (Figure 3.4.4 C) indicating that some of the cells in the acini are still proliferating. This made it impossible for us to distinguish the treated from the untreated 3D cultures using the presence or absence of the primary cilium as a marker. Nonetheless, we assumed that gene deletion had occurred successfully and screened multiple acini. We observed no obvious morphological changes in $Kif3a^{\Delta/\Delta}$;$Vhl^{\Delta/\Delta}$ acini compared to $Kif3a^{fl/fl}$;$Vhl^{fl/fl}$ controls. We measured the diameter of acini formed by $Kif3a^{\Delta/\Delta}$;$Vhl^{\Delta/\Delta}$ and $Kif3a^{fl/fl}$;$Vhl^{fl/fl}$ pKECs but saw no significant differences (Figure 3.4.3 C). The partial gene deletion may induce very subtle changes, which we could not measure with our experimental system. We conclude that additional mutations may be necessary to overcome the repressive environment exerted by epithelial cell-cell contact within the acini or that this cell culture system does not accurately reproduce factors that are necessary *in vivo* for cyst formation, such as urinary flow, growth factor signalling or interactions with basement membranes or stromal cells.

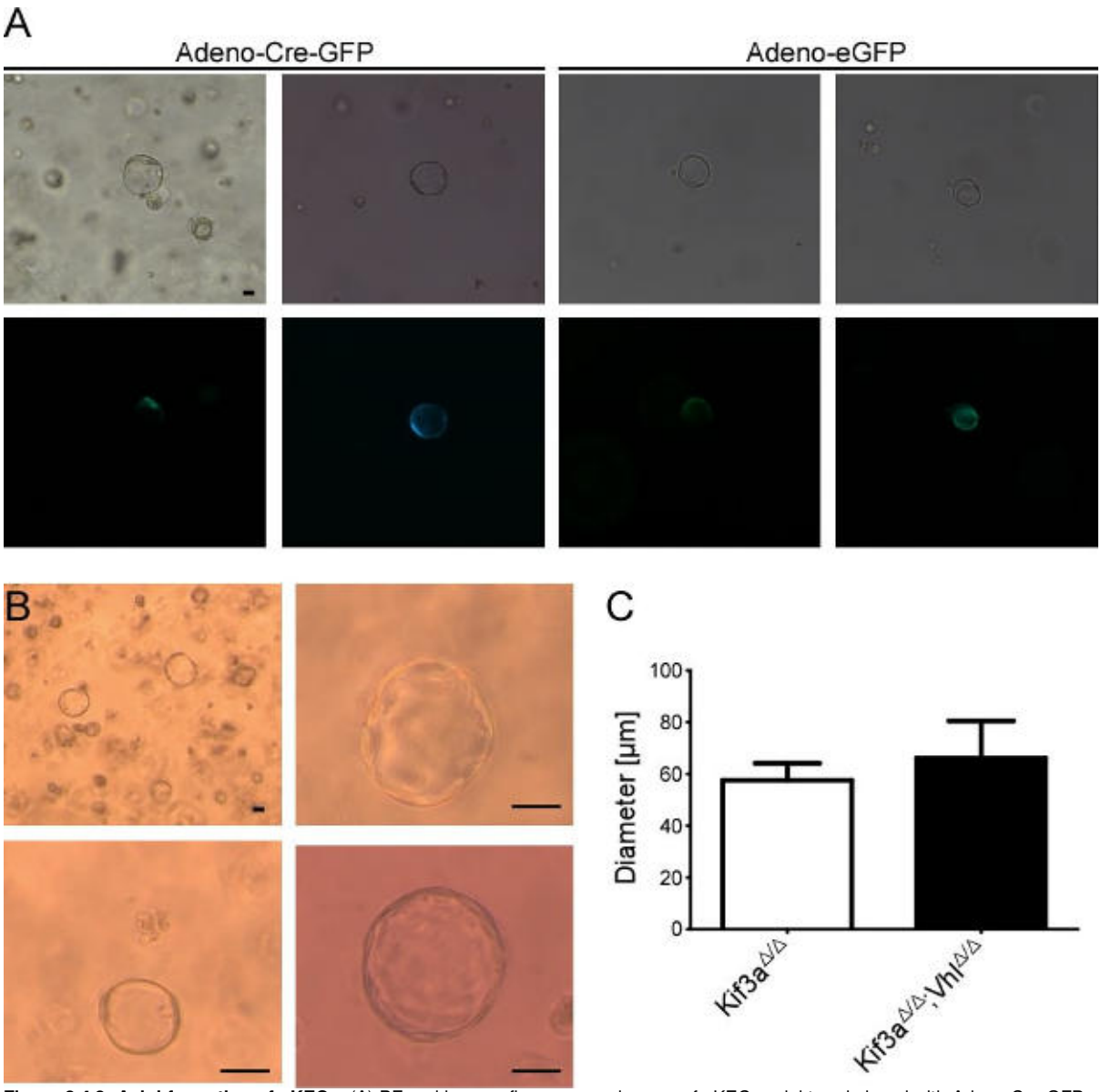

Figure 3.4.3: Acini formation of pKECs. (A) BF and immunofluorescence images of pKECs acini trandsduced with Adeno-Cre-GFP or Adeno-eGFP 3 days after seeding. (B) Bright field microscopy of Kif3a$^{\Delta/\Delta}$;Vhl$^{\Delta/\Delta}$ pKECs acini. (C) Diameters of Kif3a$^{fl/fl}$;Vhl$^{fl/fl}$ and Kif3a$^{\Delta/\Delta}$;Vhl$^{\Delta/\Delta}$ pKECs are 57.5±24.8 and 66.1±29.6, respectively; N=16. Pictures are taken 10 days after seeding. All bars represent 20µm.

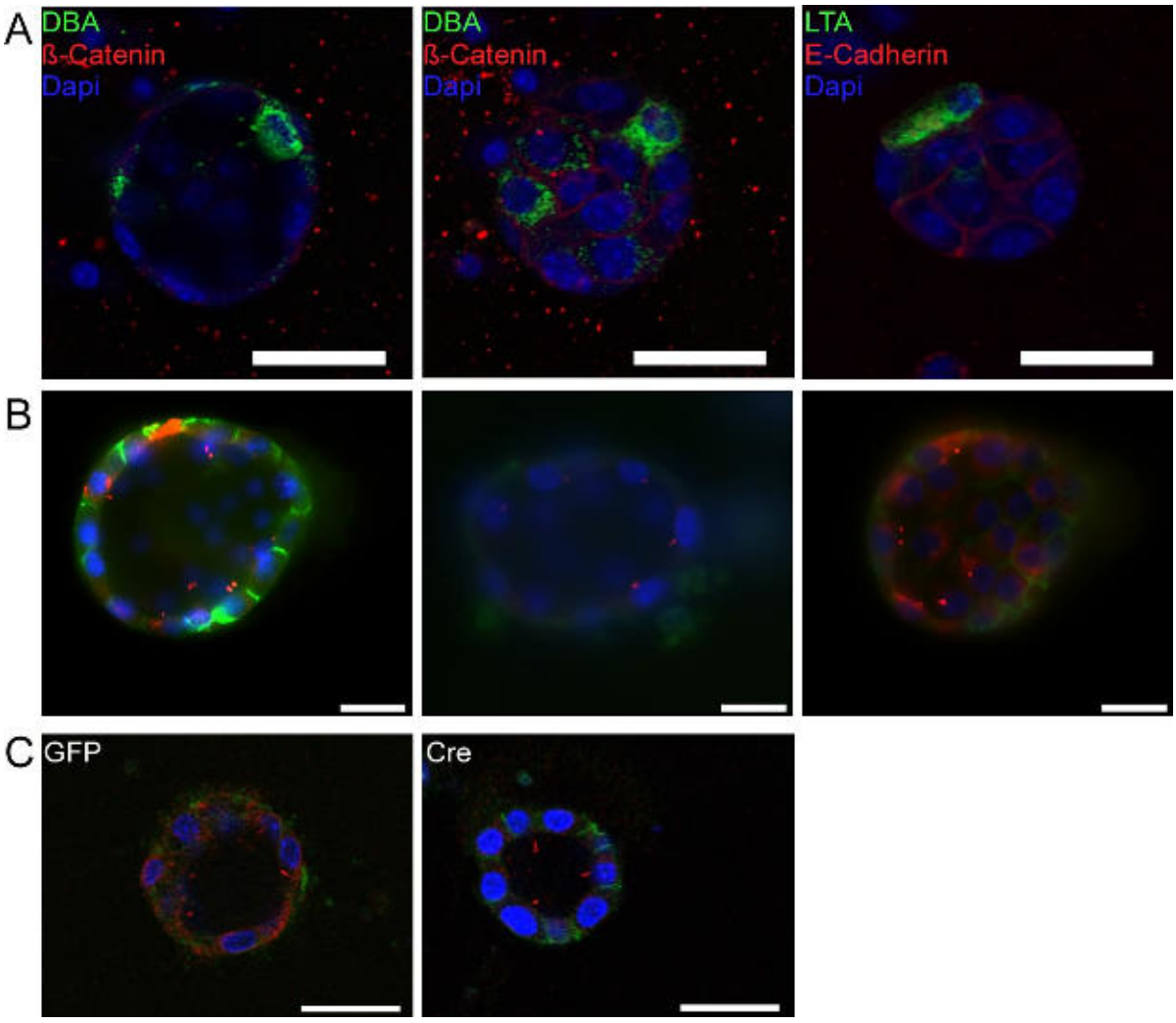

Figure 3.4.4: pKEC acini exhibit a polarized orientation epithelial origin. (A) Co-staining of DBA (collecting duct) with ß-Catenin (cell junction) or LTA (proximal tubues) with E-Cadherin (epithelial marker), bars equal 30µm. (B) anti-acetylated Tubulin staining (red) and anti-E-Cadherin (green) in pKECs acini, bars equal 20µm. (C) anti-acetylated Tubulin staining (red) and anti-E-Cadherin (green) in *Kif3a*$^{fl/fl}$;*Vhl*$^{fl/fl}$ acini treated with Cre (left) or GFP (right), bars equal 30µm. Pictures in A+C were taken with an SP5 confocal microscope.

4 Discussion

Despite intensive research, the molecular and cellular mechanisms underlying the generation of ccRCC remain unknown and no autochthonous mouse model for this disease has been developed yet. The results presented in this study complement previous studies and generate ideas for future experiments. A proposed model of ccRCC initiation in which loss of the microtubule stabilizing function of pVHL in combination with altered PI3K and ERK signaling causing failure to maintain the primary cilium suggested that loss of this organelle is the trigger for pre-neopastic cyst formation in VHL patients can now be further adjusted (20, 51, 66). We observed a drastic increase in the frequency of cyst initiation, enhanced cyst progression and a shortened latency if *Vhl* was deleted together with *Kif3a* compared to *Kif3a* deletion alone. This serves as evidence that loss of the primary cilium is a secondary event in *VHL* mutant cells that in turn cooperates with other cellular changes which arise due to loss of pVHL function and that all these effects together induce cyst formation. Multiple mechanisms may underlie this cooperation due to the diversity of molecular and cellular processes which are regulated by pVHL and by the primary cilium itself (215, 216).

Our mouse model of combined *Vhl* and *Kif3a* deletion shows a high frequency of cyst formation in 100% of mice at nine months after Tamoxifen treatment. This is a huge increase compared to the small fraction (~20%) of older (>1year) mice that develop cysts if *Vhl* is deleted in proximal tubular epithelial cells using the Pepck-Cre transgene (19). Since the effect of *Vhl* deletion alone under the control of the Pepck-promoter could be rescued by co-deletion of *Arnt*, encoding HIF1β, but not by co-deletion of *Hif1a*, it is possible that cyst formation in our *Kif3a/Vhl* mouse model is promoted by combined activation of HIF1α and HIF2α (19). A more general role for HIF1α in cyst formation was recently proposed (43, 217). However, in our study we found no HIF1α stabilization or increase in expression of the HIF1α induced protein Glut-1 in cysts in *Kif3a* mutant mice. There were no phenotypic consequences of *Hif1a* deletion on loss of *Kif3a*-induced cyst formation. Since our *Kif3a* deletion model results only in a mild cystic phenotype it may be that HIF1α stabilization is only limited to more severe polycystic kidneys. On the other hand, altered signaling pathways induced by PKD1/PKD2 mutations in autosomal dominant kidney disease may contribute to HIF1α stabilization in cysts, for example constitutive mTOR activation causes enhanced translation of HIF1α in a way that cannot be phenocopied by loss of the primary cilium (82, 209, 218-220). To test the effect of HIF1α in a more severe mouse model we would propose the deletion of *Hif1a* in an ADPKD model or study the effect of developmental *Hif1a*/*Kif3a* deletion which results in a stronger cystic phenotype than observed in adult mice.

Another conclusion that can be drawn from our *in vivo* studies is that *Vhl*-deficient cystic lesions can persist for at least nine months in mice without neoplastic progression.

This suggests that additional mutations are necessary to result in malignant transformation. Nevertheless, we observed a 3-4 fold increase in the frequency of atypical cyst formation in Kif3a$^{\Delta/\Delta}$;Vhl$^{\Delta/\Delta}$ mice compared to Kif3a$^{\Delta/\Delta}$ and Kif3a$^{\Delta/\Delta}$;Hif1a$^{\Delta/\Delta}$ mice. These cysts displayed a multilayered epithelial growth projecting into the lumen of cystic lesion. Since simple cysts are believed to progress into atypical cysts and ultimately into ccRCC in the cyst-dependent ccRCC progression model (Figure 1.3) (63-66), we believe that Kif3a$^{\Delta/\Delta}$;Vhl$^{\Delta/\Delta}$ mice accurately mimic ccRCC precursor lesions. While Kif3a$^{\Delta/\Delta}$;Vhl$^{\Delta/\Delta}$ mice exhibited numerous simple cysts, the frequency and extent of atypical growth in this model is much less than that seen in *Vhl*/*Trp53* mutant mice. The combined deletion of *Vhl* and *Trp53* resulted a much lower rate of cyst formation but frequent appearance of atypical cysts characterized by extensive epithelial proliferation into the lumen of cystic lesions and solid neoplasms that apparently filled the lumen (24). This data leads to the conclusion that loss of the primary cilium in combination with loss of pVHL functions as an initial cause for the onset of cyst formation and for the transition to disorganized epithelial proliferation but that it is not sufficient for persistent neoplastic growth. The deletion of a tumour suppressor like *Trp53*, *Rb* or *Cdkn2a* in Kif3a$^{\Delta/\Delta}$;Vhl$^{\Delta/\Delta}$ mice might enhance the transition of the frequent simple and the rare atypical cystic lesions to the next stage of ccRCC progression model. In this context we have recently generated mice allowing inducible renal epithelial-specific triple deletion of *Kif3a/Vhl/Trp53*. These mice will be analysed in the coming months.

One cellular process that may explain the observed phenotypes may be the dysregulation of a process called planar cell polarity (PCP) which ensures the correct orientation of the mitotic spindle and correct planar cell division. Normally, renal epithelial cell division occurs along the length axis of the tubule to ensure lengthening during development or repair after kidney injury. It was also shown that the orientation of the mitotic spindle was distorted in rodent PKD models (138). Disturbance of the PCP pathway and therefore misoriented mitotic spindle formation might lead to the transition of normal tubules to cystic enlargements. Multiple studies have linked the loss of the primary cilium to misorientation of cell division that precedes cyst formation (reviewd in (221)). Rapid and dramatic cyst formation is seen upon perinatal loss of the primary cilium but is not observed when the primary cilium is deleted in quiescent renal epithelial cells of adult animals, rather slow onset cyst formation results (94, 141). Kidney damage-induced proliferation leads to rapid cyst formation in adult animals that have genetic ciliary defects, implying a synergistic interaction between proliferation and misoriented mitotic spindle formation. Interestingly, pVHL regulates the stability of the astral microtubule network that links the mitotic spindle to the cell surface, thereby controlling the correct orientation of cell division (144). Recently, a mouse model of *Vhl* deletion that was subjected to ischemic damage causing cellular proliferation showed misoriented mitotic spindle formation and these mice developed microcysts (145). Taken

together, this data leads to the plausible conclusion that the disturbance of two independent pathways that ensure cell division in the correct plane may enhance the rate of misorented cell division which could result in a more frequent tubule expansion and cyst initiation (Figure 4.1 A). The transition from simple cysts into atypical cysts may be based on the same mechanism. The expansion of a simple cyst requires that cells divide within the plane of the cystic epithelium. We propose that the transition to multilayered/atypical cysts may occur if cell divisions occur perpendicularly to the plane of the epithelial cells that line the cysts, resulting in daughter cells that are growing on top of the existing cystic epithelium (Figure 4.1 B). We found that approximately one third of anaphases of Kif3a$^{\Delta/\Delta}$;Vhl$^{\Delta/\Delta}$ mice show an altered mitotic spindle orientation compared to roughly one eighth of anaphases in Kif3a$^{\Delta/\Delta}$ animals. This result supports our hypothesis (Figure 4.1) that one possible mechanism contributing to the cooperative effect from loss of *Vhl* and loss of the primary cilium is based upon loss of correct mitotic spindle orientation. It is noteworthy that the frequency of misoriented anaphases is higher than the incidence of atypical cyst formation. We speculate that not all cell divisions that occur perpendicularly to the plane of the cyst result in daughter cells attaching to the cyst wall as these cells would lack contacts with the extracellular matrix of the basement membrane. It is possible that some or many of the recently divided cells may detach from the cyst wall and enter the cystic space where they may undergo apoptosis. It is also possible that additional mutations need to occur that further increase proliferation and enable neoplastic growth are required to induce renal cancers.

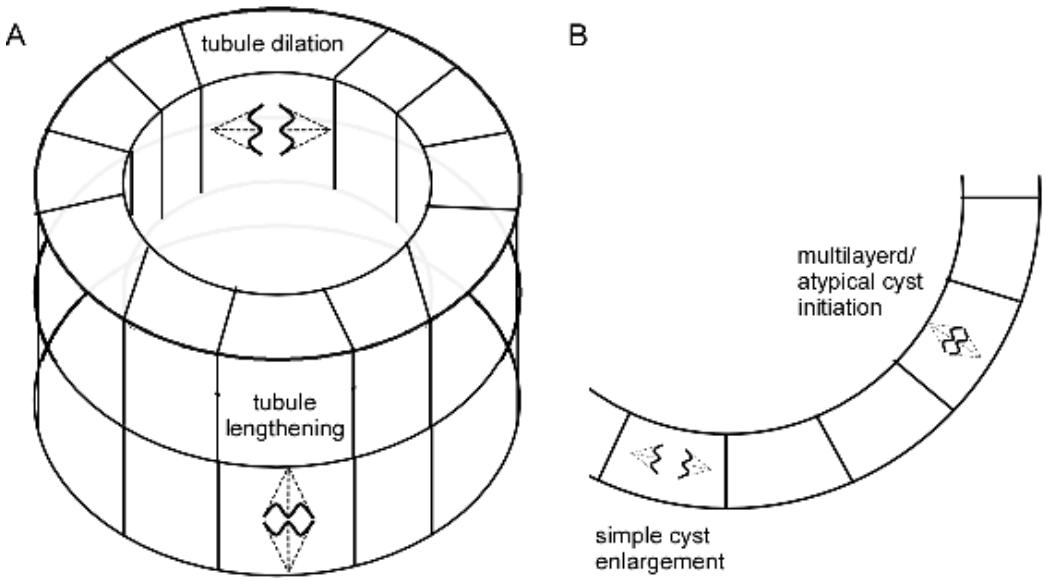

Figure 4.1: Influence of mitotic spindle orientation on cyst initiation and progression. (A) Mitotic spindle orientation along the length axis of a renal tubule leads to lengthening during development and after kidney injury. Orientation of the mitotic spindle perpendicular to the tubule axis may result in tubule enlargement, which initiates simple cyst formation. (B) Continuous division along the plane of the cyst wall leads to enlargement of simple cysts whereas division perpendicular to the axis of the cyst wall might initiate multilayered and atypical cystic phenotypes.

In vitro experiments were performed to investigate molecular and cellular changes that were induced through the co-deletion of *Kif3a* and *Vhl*. We used pMEFs and pKECs derived from our mouse lines. We investigated the effect of *Kif3a* and *Vhl* co-deletion on proliferation and metabolic changes. In pMEFs we measured intracellular ATP levels, glucose utilization and lactate production. These metabolic properties are frequently altered in malignant transformed cells and contribute to the Warburg effect. We could not detect any significant differences based on these assays indicating that the pMEFs did not undergo malignant transformation. Proliferation curves were performed to assess differences in proliferation between all genotypes. The proliferation of Δ/Δ cells was slightly but not significantly decreased compared to their respective control cells concluding that loss of *Kif3a* and *Vhl* does not result in enhanced proliferation rates. We reasoned that pKECs might be better suited to reproduce the animal models and therefore performed proliferation assays and basic metabolism assays after treatment with adeno-Cre-GFP or adeno-eGFP as control. While pMEFs are easy to handle pKECs are more difficult to work with experimentally because they have a low proliferation rate, tend to undergo dedifferentiation and do not permit passaging. To test the proliferation rate of pKECs we performed a SRB assay on five consecutive days but the proliferation rate was in general low and no difference between Δ/Δ and control cells was observed. The analysis of basic metabolism also did not show a difference in intracellular ATP levels, glucose utilization, lactate production and 2-DOG uptake. Taken together our *in vitro* data is consistent with the animal models and clearly shows that loss of the primary cilium and loss of *Vhl* is not sufficient to induce either immortalization or malignant transformation.

We developed a non-invasive technique that allows quantitative longitudinal monitoring of cyst progression in the same living animal based on computed tomography (µCT). µCT imaging is usually deployed for the analysis of fixed tissues *ex vivo.* In 2008, the first description of µCT imaging of mice kidney in living animals was reported (191). So far renal cysts were only analyzed *ex vivo* in a rat model (222). Here we described for the first time µCT *in vivo* imaging of mouse renal cysts. We performed µCT scans of anaesthetized animals. Since the µCT is based on X-ray images we used iodine containing contrast agent (Visipaque®) to be able to visualize the kidney. Intraveneous administration of the contrast agent leads to renal filtration and accumulation of the contrast agent in the kidney tubules but is not concentrated in the cystic regions due to either impaired filtration or concentration. Our µCT approach generated similar results to CT imaging of patients with cystic kidney disease. Our data shows that this technique is suitable to visualize and follow cyst formation over time in the same animals. We believe that µCT imaging to monitor cyst formation is superior to measurements of standard kidney function parameters like blood urea and creatinine levels

as this imaging technique is able to detect cystic lesions in transgenic animals that do not differ in blood urea and creatinine levels from wild type animals. The analysis of kidney parameters showed that only those transgenic animals with very severe cystic phenotypes displayed increases in blood urea nitrogen and creatine, whereas µCT imaging was able to quantitatively assess renal cysts also in transgenic animals with a very few cystic lesions. The data we obtained from µCT imaging was confirmed by histological analysis, further supporting the evidence that µCT imaging is more sensitive than analysis of blood urea and creatinine levels. In addition, our technique might help to reduce the number of animals needed to perform such experiments since one can conduct multiple quantitative measurements within the same animal. We believe that this technique might be of great use especially for clinical researchers testing treatment options for cystic diseases. It is now possible to determine the cystic volume of the exact same animal before, during and after treatment. We also analyzed transgenic animals only at nine months after tamoxifen treatment to rule out any side effects of repeated anaesthesia and Visipaque® administration and indeed we observed the same cystic phenotype. Our research on µCT *in vivo* imaging may generally prove to be beneficial for all future studies that aim to investigate polycystic kidney disease in rodent.

To study molecular and cellular processes of cyst initiation/progression *ex vivo* we developed a Matrigel®-based 3D culture system. Several kidney-derived cell lines were available for 3D systems (198, 200-202) but since we wanted to study the process of cyst initiation of physiologically normal kidney epithelial cells we utilized pKECs in our 3D culture system. The use of pKECs also provides the advantage of being able to induce genetic changes through viral delivery of Cre in pKECs from *Kif3a*$^{fl/fl}$, *Kif3a*$^{fl/fl}$;*Vhl*$^{fl/fl}$ and *Vhl*$^{fl/fl}$ mice. The modification of a recent 3D culture protocol (Lee et al Nature) allowed the growth of polarized pKECs as acini in a Matrigel®-based 3D culture system. These acini resemble the 3D structures that arise from the 3D culturing of other epithelioid cell lines (197-199). Furthermore, marker stainings showed that the pKECs are indeed derived from renal epithelial tubule cells therefore allowing researchers in general to take advantage of all available genetically modified mouse strains for renal epithelial 3D systems. Cre-mediated recombination can be performed at different time points during pKECs isolation and most likely with inducible Cre lines if the promoter is active in the respective cell type. Our data shows that we can generate polarized acini with a primary cilium facing the lumen resembling the *in vivo* situation of renal epithelial tubule cells and hence may be used to study cyst initiation *ex vivo*. Unfortunately, we could not observe cyst formation in *Kif3a*$^{\Delta/\Delta}$;*Vhl*$^{\Delta/\Delta}$ or *Kif3a*$^{\Delta/\Delta}$ acini. This is probably due to the low concentration of Adeno-Cre-GFP we used because we

observed a strong Adeno-Cre-GFP toxicity on 2D cultured pKECs. The use of lentiviral vectors expressing Cre may help to overcome this problem. Another way would be the use of tamoxifen-induced Cre translocation with the KspCre^{ERT2} transgenic lines. Taken together, this new cell culture model system allows the formation of polarized acini resembling the *in vivo* orientation of renal epithelial cells but deletion of *Kif3a* and *Vhl* was so far not sufficient to overcome the suppressive environment of the 3D structure on uncontrolled proliferation and cyst formation. In an *ex vivo* screening approach to identify genetic cooperation partners that may promote neoplastic transformation of cysts, it would be interesting in future experiments to utilize this 3D culture system with pKECs derived from *Kif3a/Vhl* floxed animals and introduce additional genetic changes that are found in human ccRCCs. Those combinations that allow transformation may permit proliferation of cells into the lumen of acini or outgrowths of acini to form solid or invasive structures. Candidate genes could then potentially be considered to introduce into the inducible *Kif3a/Vhl* deletion mouse model to attempt to generate a model of cystic ccRCC.

References

1. Maher ER*, et al.* (1991) Von Hippel-Lindau disease: a genetic study. *J Med Genet* 28(7):443-447.
2. Neumann HP & Wiestler OD (1991) Clustering of features of von Hippel-Lindau syndrome: evidence for a complex genetic locus. *Lancet* 337(8749):1052-1054.
3. Maher ER & Kaelin WG, Jr. (1997) von Hippel-Lindau disease. *Medicine (Baltimore)* 76(6):381-391.
4. Latif F*, et al.* (1993) Identification of the von Hippel-Lindau disease tumor suppressor gene. *Science* 260(5112):1317-1320.
5. Seizinger BR*, et al.* (1988) Von Hippel-Lindau disease maps to the region of chromosome 3 associated with renal cell carcinoma. *Nature* 332(6161):268-269.
6. Duan DR*, et al.* (1995) Inhibition of transcription elongation by the VHL tumor suppressor protein. *Science* 269(5229):1402-1406.
7. Gnarra JR*, et al.* (1994) Mutations of the VHL tumour suppressor gene in renal carcinoma. *Nat Genet* 7(1):85-90.
8. Kibel A, Iliopoulos O, DeCaprio JA, & Kaelin WG, Jr. (1995) Binding of the von Hippel-Lindau tumor suppressor protein to Elongin B and C. *Science* 269(5229):1444-1446.
9. Nickerson ML*, et al.* (2008) Improved identification of von Hippel-Lindau gene alterations in clear cell renal tumors. *Clin Cancer Res* 14(15):4726-4734.
10. Pause A*, et al.* (1997) The von Hippel-Lindau tumor-suppressor gene product forms a stable complex with human CUL-2, a member of the Cdc53 family of proteins. *Proc Natl Acad Sci U S A* 94(6):2156-2161.
11. Shuin T*, et al.* (1994) Frequent somatic mutations and loss of heterozygosity of the von Hippel-Lindau tumor suppressor gene in primary human renal cell carcinomas. *Cancer Res* 54(11):2852-2855.
12. Lonser RR*, et al.* (2003) von Hippel-Lindau disease. *Lancet* 361(9374):2059-2067.
13. Maher ER*, et al.* (1990) Clinical features and natural history of von Hippel-Lindau disease. *Q J Med* 77(283):1151-1163.
14. Hes F*, et al.* (2000) Genotype-phenotype correlations in families with deletions in the von Hippel-Lindau (VHL) gene. *Hum Genet* 106(4):425-431.
15. Kaelin WG, Jr. (2002) Molecular basis of the VHL hereditary cancer syndrome. *Nat Rev Cancer* 2(9):673-682.
16. Zbar B*, et al.* (1996) Germline mutations in the Von Hippel-Lindau disease (VHL) gene in families from North America, Europe, and Japan. *Hum Mutat* 8(4):348-357.
17. Gnarra JR*, et al.* (1997) Defective placental vasculogenesis causes embryonic lethality in VHL-deficient mice. *Proc Natl Acad Sci U S A* 94(17):9102-9107.
18. Ma W*, et al.* (2003) Hepatic vascular tumors, angiectasis in multiple organs, and impaired spermatogenesis in mice with conditional inactivation of the VHL gene. *Cancer Res* 63(17):5320-5328.
19. Rankin EB, Tomaszewski JE, & Haase VH (2006) Renal cyst development in mice with conditional inactivation of the von Hippel-Lindau tumor suppressor. *Cancer Res* 66(5):2576-2583.
20. Frew IJ*, et al.* (2008) pVHL and PTEN tumour suppressor proteins cooperatively suppress kidney cyst formation. *EMBO J* 27(12):1747-1757.
21. Mathia S*, et al.* (2013) Action of hypoxia-inducible factor in liver and kidney from mice with Pax8-rtTA-based deletion of von Hippel-Lindau protein. *Acta Physiol (Oxf)* 207(3):565-576.
22. Schietke RE*, et al.* (2012) Renal tubular HIF-2alpha expression requires VHL inactivation and causes fibrosis and cysts. *PLoS One* 7(1):e31034.
23. Schley G*, et al.* (2011) Hypoxia-inducible transcription factors stabilization in the thick ascending limb protects against ischemic acute kidney injury. *J Am Soc Nephrol* 22(11):2004-2015.

24. Albers J*, et al.* (2013) Combined mutation of Vhl and Trp53 causes renal cysts and tumours in mice. *EMBO Mol Med* 5(6):949-964.
25. Blankenship C, Naglich JG, Whaley JM, Seizinger B, & Kley N (1999) Alternate choice of initiation codon produces a biologically active product of the von Hippel Lindau gene with tumor suppressor activity. *Oncogene* 18(8):1529-1535.
26. Iliopoulos O, Kibel A, Gray S, & Kaelin WG, Jr. (1995) Tumour suppression by the human von Hippel-Lindau gene product. *Nat Med* 1(8):822-826.
27. Iliopoulos O, Ohh M, & Kaelin WG, Jr. (1998) pVHL19 is a biologically active product of the von Hippel-Lindau gene arising from internal translation initiation. *Proc Natl Acad Sci U S A* 95(20):11661-11666.
28. Schoenfeld A, Davidowitz EJ, & Burk RD (1998) A second major native von Hippel-Lindau gene product, initiated from an internal translation start site, functions as a tumor suppressor. *Proc Natl Acad Sci U S A* 95(15):8817-8822.
29. Stebbins CE, Kaelin WG, Jr., & Pavletich NP (1999) Structure of the VHL-ElonginC-ElonginB complex: implications for VHL tumor suppressor function. *Science* 284(5413):455-461.
30. Kamura T*, et al.* (1999) Rbx1, a component of the VHL tumor suppressor complex and SCF ubiquitin ligase. *Science* 284(5414):657-661.
31. Lisztwan J, Imbert G, Wirbelauer C, Gstaiger M, & Krek W (1999) The von Hippel-Lindau tumor suppressor protein is a component of an E3 ubiquitin-protein ligase activity. *Genes Dev* 13(14):1822-1833.
32. Lonergan KM*, et al.* (1998) Regulation of hypoxia-inducible mRNAs by the von Hippel-Lindau tumor suppressor protein requires binding to complexes containing elongins B/C and Cul2. *Mol Cell Biol* 18(2):732-741.
33. Maxwell PH*, et al.* (1999) The tumour suppressor protein VHL targets hypoxia-inducible factors for oxygen-dependent proteolysis. *Nature* 399(6733):271-275.
34. Hergovich A, Lisztwan J, Barry R, Ballschmieter P, & Krek W (2003) Regulation of microtubule stability by the von Hippel-Lindau tumour suppressor protein pVHL. *Nat Cell Biol* 5(1):64-70.
35. Ivan M*, et al.* (2001) HIFalpha targeted for VHL-mediated destruction by proline hydroxylation: implications for O2 sensing. *Science* 292(5516):464-468.
36. Ohh M*, et al.* (2000) Ubiquitination of hypoxia-inducible factor requires direct binding to the beta-domain of the von Hippel-Lindau protein. *Nat Cell Biol* 2(7):423-427.
37. Epstein AC*, et al.* (2001) C. elegans EGL-9 and mammalian homologs define a family of dioxygenases that regulate HIF by prolyl hydroxylation. *Cell* 107(1):43-54.
38. Tanimoto K, Makino Y, Pereira T, & Poellinger L (2000) Mechanism of regulation of the hypoxia-inducible factor-1 alpha by the von Hippel-Lindau tumor suppressor protein. *EMBO J* 19(16):4298-4309.
39. Dayan F, Roux D, Brahimi-Horn MC, Pouyssegur J, & Mazure NM (2006) The oxygen sensor factor-inhibiting hypoxia-inducible factor-1 controls expression of distinct genes through the bifunctional transcriptional character of hypoxia-inducible factor-1alpha. *Cancer Res* 66(7):3688-3698.
40. Arany Z*, et al.* (1996) An essential role for p300/CBP in the cellular response to hypoxia. *Proc Natl Acad Sci U S A* 93(23):12969-12973.
41. Wenger RH, Stiehl DP, & Camenisch G (2005) Integration of oxygen signaling at the consensus HRE. *Sci STKE* 2005(306):re12.
42. Belibi F*, et al.* (2011) Hypoxia-inducible factor-1alpha (HIF-1alpha) and autophagy in polycystic kidney disease (PKD). *Am J Physiol Renal Physiol* 300(5):F1235-1243.
43. Buchholz B*, et al.* (2014) Hypoxia-inducible factor-1alpha causes renal cyst expansion through calcium-activated chloride secretion. *J Am Soc Nephrol* 25(3):465-474.
44. McCormick F (1999) Signalling networks that cause cancer. *Trends Cell Biol* 9(12):M53-56.
45. Luo J, Manning BD, & Cantley LC (2003) Targeting the PI3K-Akt pathway in human cancer: rationale and promise. *Cancer Cell* 4(4):257-262.

46. Cantley LC & Neel BG (1999) New insights into tumor suppression: PTEN suppresses tumor formation by restraining the phosphoinositide 3-kinase/AKT pathway. *Proc Natl Acad Sci U S A* 96(8):4240-4245.
47. Gustafson S, Zbuk KM, Scacheri C, & Eng C (2007) Cowden syndrome. *Semin Oncol* 34(5):428-434.
48. Fresno Vara JA*, et al.* (2004) PI3K/Akt signalling pathway and cancer. *Cancer Treat Rev* 30(2):193-204.
49. Fruman DA, Meyers RE, & Cantley LC (1998) Phosphoinositide kinases. *Annu Rev Biochem* 67:481-507.
50. Testa JR & Bellacosa A (2001) AKT plays a central role in tumorigenesis. *Proc Natl Acad Sci U S A* 98(20):10983-10985.
51. Thoma CR*, et al.* (2007) pVHL and GSK3beta are components of a primary cilium-maintenance signalling network. *Nat Cell Biol* 9(5):588-595.
52. Pantuck AJ*, et al.* (2007) Prognostic relevance of the mTOR pathway in renal cell carcinoma: implications for molecular patient selection for targeted therapy. *Cancer* 109(11):2257-2267.
53. Robb VA, Karbowniczek M, Klein-Szanto AJ, & Henske EP (2007) Activation of the mTOR signaling pathway in renal clear cell carcinoma. *J Urol* 177(1):346-352.
54. Huang J & Manning BD (2008) The TSC1-TSC2 complex: a molecular switchboard controlling cell growth. *Biochem J* 412(2):179-190.
55. Inoki K, Zhu T, & Guan KL (2003) TSC2 mediates cellular energy response to control cell growth and survival. *Cell* 115(5):577-590.
56. Zoncu R, Efeyan A, & Sabatini DM (2011) mTOR: from growth signal integration to cancer, diabetes and ageing. *Nat Rev Mol Cell Biol* 12(1):21-35.
57. Blagosklonny MV & Hall MN (2009) Growth and aging: a common molecular mechanism. *Aging (Albany NY)* 1(4):357-362.
58. Ma XM & Blenis J (2009) Molecular mechanisms of mTOR-mediated translational control. *Nat Rev Mol Cell Biol* 10(5):307-318.
59. Jonasch E*, et al.* (2012) State of the science: an update on renal cell carcinoma. *Mol Cancer Res* 10(7):859-880.
60. Eble JN SG, Epstein JI, et al (eds): ed (2004) *Pathology and Genetics of Tumors of the Urinary System and Male Genital Organs.*).
61. Zhang J*, et al.* (2007) Solid renal cortical tumors: differentiation with CT. *Radiology* 244(2):494-504.
62. von Teichman A*, et al.* (2011) VHL mutations and dysregulation of pVHL- and PTEN-controlled pathways in multilocular cystic renal cell carcinoma. *Mod Pathol* 24(4):571-578.
63. Lubensky IA*, et al.* (1996) Allelic deletions of the VHL gene detected in multiple microscopic clear cell renal lesions in von Hippel-Lindau disease patients. *Am J Pathol* 149(6):2089-2094.
64. Walther MM, Lubensky IA, Venzon D, Zbar B, & Linehan WM (1995) Prevalence of microscopic lesions in grossly normal renal parenchyma from patients with von Hippel-Lindau disease, sporadic renal cell carcinoma and no renal disease: clinical implications. *J Urol* 154(6):2010-2014; discussion 2014-2015.
65. Montani M*, et al.* (2010) VHL-gene deletion in single renal tubular epithelial cells and renal tubular cysts: further evidence for a cyst-dependent progression pathway of clear cell renal carcinoma in von Hippel-Lindau disease. *Am J Surg Pathol* 34(6):806-815.
66. Thoma CR, Frew IJ, & Krek W (2007) The VHL tumor suppressor: riding tandem with GSK3beta in primary cilium maintenance. *Cell Cycle* 6(15):1809-1813.
67. Krajewski KM, Giardino AA, Zukotynski K, Van den Abbeele AD, & Pedrosa I (2011) Imaging in renal cell carcinoma. *Hematol Oncol Clin North Am* 25(4):687-715.
68. TCGA (2013) Comprehensive molecular characterization of clear cell renal cell carcinoma. *Nature* 499(7456):43-49.
69. Kondo K, Kim WY, Lechpammer M, & Kaelin WG, Jr. (2003) Inhibition of HIF2alpha is sufficient to suppress pVHL-defective tumor growth. *PLoS Biol* 1(3):E83.

70. Raval RR*, et al.* (2005) Contrasting properties of hypoxia-inducible factor 1 (HIF-1) and HIF-2 in von Hippel-Lindau-associated renal cell carcinoma. *Mol Cell Biol* 25(13):5675-5686.
71. Zimmer M, Doucette D, Siddiqui N, & Iliopoulos O (2004) Inhibition of hypoxia-inducible factor is sufficient for growth suppression of VHL-/- tumors. *Mol Cancer Res* 2(2):89-95.
72. Mack FA, Patel JH, Biju MP, Haase VH, & Simon MC (2005) Decreased growth of Vhl-/- fibrosarcomas is associated with elevated levels of cyclin kinase inhibitors p21 and p27. *Mol Cell Biol* 25(11):4565-4578.
73. Mack FA*, et al.* (2003) Loss of pVHL is sufficient to cause HIF dysregulation in primary cells but does not promote tumor growth. *Cancer Cell* 3(1):75-88.
74. Gordan JD, Bertout JA, Hu CJ, Diehl JA, & Simon MC (2007) HIF-2alpha promotes hypoxic cell proliferation by enhancing c-myc transcriptional activity. *Cancer Cell* 11(4):335-347.
75. Koshiji M*, et al.* (2004) HIF-1alpha induces cell cycle arrest by functionally counteracting Myc. *EMBO J* 23(9):1949-1956.
76. Gordan JD*, et al.* (2008) HIF-alpha effects on c-Myc distinguish two subtypes of sporadic VHL-deficient clear cell renal carcinoma. *Cancer Cell* 14(6):435-446.
77. Monzon FA*, et al.* (2011) Chromosome 14q loss defines a molecular subtype of clear-cell renal cell carcinoma associated with poor prognosis. *Mod Pathol* 24(11):1470-1479.
78. Shen C*, et al.* (2011) Genetic and functional studies implicate HIF1alpha as a 14q kidney cancer suppressor gene. *Cancer Discov* 1(3):222-235.
79. Koh MY, Darnay BG, & Powis G (2008) Hypoxia-associated factor, a novel E3-ubiquitin ligase, binds and ubiquitinates hypoxia-inducible factor 1alpha, leading to its oxygen-independent degradation. *Mol Cell Biol* 28(23):7081-7095.
80. Koh MY, Lemos R, Jr., Liu X, & Powis G (2011) The hypoxia-associated factor switches cells from HIF-1alpha- to HIF-2alpha-dependent signaling promoting stem cell characteristics, aggressive tumor growth and invasion. *Cancer Res* 71(11):4015-4027.
81. Menrad H*, et al.* (2010) Roles of hypoxia-inducible factor-1alpha (HIF-1alpha) versus HIF-2alpha in the survival of hepatocellular tumor spheroids. *Hepatology* 51(6):2183-2192.
82. Toschi A, Lee E, Gadir N, Ohh M, & Foster DA (2008) Differential dependence of hypoxia-inducible factors 1 alpha and 2 alpha on mTORC1 and mTORC2. *J Biol Chem* 283(50):34495-34499.
83. Hildebrandt F, Benzing T, & Katsanis N (2011) Ciliopathies. *N Engl J Med* 364(16):1533-1543.
84. Schraml P*, et al.* (2009) Sporadic clear cell renal cell carcinoma but not the papillary type is characterized by severely reduced frequency of primary cilia. *Mod Pathol* 22(1):31-36.
85. Kobayashi T & Dynlacht BD (2011) Regulating the transition from centriole to basal body. *J Cell Biol* 193(3):435-444.
86. Ishikawa H & Marshall WF (2011) Ciliogenesis: building the cell's antenna. *Nat Rev Mol Cell Biol* 12(4):222-234.
87. Avery AK, Beckstead J, Renshaw AA, & Corless CL (2000) Use of antibodies to RCC and CD10 in the differential diagnosis of renal neoplasms. *Am J Surg Pathol* 24(2):203-210.
88. Bakshi N, Kunju LP, Giordano T, & Shah RB (2007) Expression of renal cell carcinoma antigen (RCC) in renal epithelial and nonrenal tumors: diagnostic Implications. *Appl Immunohistochem Mol Morphol* 15(3):310-315.
89. Droz D*, et al.* (1990) Expression of the human nephron differentiation molecules in renal cell carcinomas. *Am J Pathol* 137(4):895-905.
90. Mazal PR*, et al.* (2005) Expression of aquaporins and PAX-2 compared to CD10 and cytokeratin 7 in renal neoplasms: a tissue microarray study. *Mod Pathol* 18(4):535-540.

91. Paraf F*, et al.* (2000) Renal lesions in von Hippel-Lindau disease: immunohistochemical expression of nephron differentiation molecules, adhesion molecules and apoptosis proteins. *Histopathology* 36(5):457-465.
92. Schaub TP*, et al.* (1999) Expression of the MRP2 gene-encoded conjugate export pump in human kidney proximal tubules and in renal cell carcinoma. *J Am Soc Nephrol* 10(6):1159-1169.
93. Straube T*, et al.* (2011) Changes in the expression and subcellular distribution of galectin-3 in clear cell renal cell carcinoma. *J Exp Clin Cancer Res* 30:89.
94. Patel V*, et al.* (2008) Acute kidney injury and aberrant planar cell polarity induce cyst formation in mice lacking renal cilia. *Hum Mol Genet* 17(11):1578-1590.
95. Pazour GJ & Witman GB (2003) The vertebrate primary cilium is a sensory organelle. *Curr Opin Cell Biol* 15(1):105-110.
96. Satir P & Christensen ST (2007) Overview of structure and function of mammalian cilia. *Annu Rev Physiol* 69:377-400.
97. Tucker RW, Pardee AB, & Fujiwara K (1979) Centriole ciliation is related to quiescence and DNA synthesis in 3T3 cells. *Cell* 17(3):527-535.
98. Sorokin S (1962) Centrioles and the formation of rudimentary cilia by fibroblasts and smooth muscle cells. *J Cell Biol* 15:363-377.
99. Sorokin SP (1968) Reconstructions of centriole formation and ciliogenesis in mammalian lungs. *J Cell Sci* 3(2):207-230.
100. Rosenbaum JL & Child FM (1967) Flagellar regeneration in protozoan flagellates. *J Cell Biol* 34(1):345-364.
101. Marshall WF & Rosenbaum JL (2001) Intraflagellar transport balances continuous turnover of outer doublet microtubules: implications for flagellar length control. *J Cell Biol* 155(3):405-414.
102. Song L & Dentler WL (2001) Flagellar protein dynamics in Chlamydomonas. *J Biol Chem* 276(32):29754-29763.
103. Stephens RE (1997) Synthesis and turnover of embryonic sea urchin ciliary proteins during selective inhibition of tubulin synthesis and assembly. *Mol Biol Cell* 8(11):2187-2198.
104. Singla V & Reiter JF (2006) The primary cilium as the cell's antenna: signaling at a sensory organelle. *Science* 313(5787):629-633.
105. Pazour GJ, Wilkerson CG, & Witman GB (1998) A dynein light chain is essential for the retrograde particle movement of intraflagellar transport (IFT). *J Cell Biol* 141(4):979-992.
106. Porter ME, Bower R, Knott JA, Byrd P, & Dentler W (1999) Cytoplasmic dynein heavy chain 1b is required for flagellar assembly in Chlamydomonas. *Mol Biol Cell* 10(3):693-712.
107. Schafer JC, Haycraft CJ, Thomas JH, Yoder BK, & Swoboda P (2003) XBX-1 encodes a dynein light intermediate chain required for retrograde intraflagellar transport and cilia assembly in Caenorhabditis elegans. *Mol Biol Cell* 14(5):2057-2070.
108. Snow JJ*, et al.* (2004) Two anterograde intraflagellar transport motors cooperate to build sensory cilia on C. elegans neurons. *Nat Cell Biol* 6(11):1109-1113.
109. Cole DG*, et al.* (1998) Chlamydomonas kinesin-II-dependent intraflagellar transport (IFT): IFT particles contain proteins required for ciliary assembly in Caenorhabditis elegans sensory neurons. *J Cell Biol* 141(4):993-1008.
110. Pazour GJ*, et al.* (2000) Chlamydomonas IFT88 and its mouse homologue, polycystic kidney disease gene tg737, are required for assembly of cilia and flagella. *J Cell Biol* 151(3):709-718.
111. Piperno G*, et al.* (1998) Distinct mutants of retrograde intraflagellar transport (IFT) share similar morphological and molecular defects. *J Cell Biol* 143(6):1591-1601.
112. Eggenschwiler JT & Anderson KV (2007) Cilia and developmental signaling. *Annu Rev Cell Dev Biol* 23:345-373.
113. Sharma N, Berbari NF, & Yoder BK (2008) Ciliary dysfunction in developmental abnormalities and diseases. *Curr Top Dev Biol* 85:371-427.

114. Barker AR, Thomas R, & Dawe HR (2013) Meckel-Gruber syndrome and the role of primary cilia in kidney, skeleton and central nervous system development. *Organogenesis* 10(1).
115. Girard D & Petrovsky N (2011) Alstrom syndrome: insights into the pathogenesis of metabolic disorders. *Nat Rev Endocrinol* 7(2):77-88.
116. Romani M, Micalizzi A, & Valente EM (2013) Joubert syndrome: congenital cerebellar ataxia with the molar tooth. *Lancet Neurol* 12(9):894-905.
117. Praetorius HA & Spring KR (2001) Bending the MDCK cell primary cilium increases intracellular calcium. *J Membr Biol* 184(1):71-79.
118. Abd-El-Barr MM*, et al.* (2007) Impaired photoreceptor protein transport and synaptic transmission in a mouse model of Bardet-Biedl syndrome. *Vision Res* 47(27):3394-3407.
119. Hildebrandt F, Attanasio M, & Otto E (2009) Nephronophthisis: disease mechanisms of a ciliopathy. *J Am Soc Nephrol* 20(1):23-35.
120. Kulaga HM*, et al.* (2004) Loss of BBS proteins causes anosmia in humans and defects in olfactory cilia structure and function in the mouse. *Nat Genet* 36(9):994-998.
121. Christensen ST, Pedersen LB, Schneider L, & Satir P (2007) Sensory cilia and integration of signal transduction in human health and disease. *Traffic* 8(2):97-109.
122. Christensen ST, Pedersen SF, Satir P, Veland IR, & Schneider L (2008) The primary cilium coordinates signaling pathways in cell cycle control and migration during development and tissue repair. *Curr Top Dev Biol* 85:261-301.
123. Praetorius HA & Leipziger J (2009) Released nucleotides amplify the cilium-dependent, flow-induced [Ca2+]i response in MDCK cells. *Acta Physiol (Oxf)* 197(3):241-251.
124. Wong SY & Reiter JF (2008) The primary cilium at the crossroads of mammalian hedgehog signaling. *Curr Top Dev Biol* 85:225-260.
125. Wang Y, McMahon AP, & Allen BL (2007) Shifting paradigms in Hedgehog signaling. *Curr Opin Cell Biol* 19(2):159-165.
126. Ruiz i Altaba A, Mas C, & Stecca B (2007) The Gli code: an information nexus regulating cell fate, stemness and cancer. *Trends Cell Biol* 17(9):438-447.
127. Haycraft CJ*, et al.* (2005) Gli2 and Gli3 localize to cilia and require the intraflagellar transport protein polaris for processing and function. *PLoS Genet* 1(4):e53.
128. Huangfu D*, et al.* (2003) Hedgehog signalling in the mouse requires intraflagellar transport proteins. *Nature* 426(6962):83-87.
129. Corbit KC*, et al.* (2005) Vertebrate Smoothened functions at the primary cilium. *Nature* 437(7061):1018-1021.
130. May SR*, et al.* (2005) Loss of the retrograde motor for IFT disrupts localization of Smo to cilia and prevents the expression of both activator and repressor functions of Gli. *Dev Biol* 287(2):378-389.
131. Liu A, Wang B, & Niswander LA (2005) Mouse intraflagellar transport proteins regulate both the activator and repressor functions of Gli transcription factors. *Development* 132(13):3103-3111.
132. Giles RH*, et al.* (2006) Interplay between VHL/HIF1alpha and Wnt/beta-catenin pathways during colorectal tumorigenesis. *Oncogene* 25(21):3065-3070.
133. Giles RH, van Es JH, & Clevers H (2003) Caught up in a Wnt storm: Wnt signaling in cancer. *Biochim Biophys Acta* 1653(1):1-24.
134. Saadi-Kheddouci S*, et al.* (2001) Early development of polycystic kidney disease in transgenic mice expressing an activated mutant of the beta-catenin gene. *Oncogene* 20(42):5972-5981.
135. Gong Y, Mo C, & Fraser SE (2004) Planar cell polarity signalling controls cell division orientation during zebrafish gastrulation. *Nature* 430(7000):689-693.
136. Simons M*, et al.* (2005) Inversin, the gene product mutated in nephronophthisis type II, functions as a molecular switch between Wnt signaling pathways. *Nat Genet* 37(5):537-543.

137. Otto EA*, et al.* (2003) Mutations in INVS encoding inversin cause nephronophthisis type 2, linking renal cystic disease to the function of primary cilia and left-right axis determination. *Nat Genet* 34(4):413-420.
138. Fischer E*, et al.* (2006) Defective planar cell polarity in polycystic kidney disease. *Nat Genet* 38(1):21-23.
139. Ross AJ*, et al.* (2005) Disruption of Bardet-Biedl syndrome ciliary proteins perturbs planar cell polarity in vertebrates. *Nat Genet* 37(10):1135-1140.
140. Corbit KC*, et al.* (2008) Kif3a constrains beta-catenin-dependent Wnt signalling through dual ciliary and non-ciliary mechanisms. *Nat Cell Biol* 10(1):70-76.
141. Jonassen JA, San Agustin J, Follit JA, & Pazour GJ (2008) Deletion of IFT20 in the mouse kidney causes misorientation of the mitotic spindle and cystic kidney disease. *J Cell Biol* 183(3):377-384.
142. Davenport JR*, et al.* (2007) Disruption of intraflagellar transport in adult mice leads to obesity and slow-onset cystic kidney disease. *Curr Biol* 17(18):1586-1594.
143. Takakura A*, et al.* (2009) Renal injury is a third hit promoting rapid development of adult polycystic kidney disease. *Hum Mol Genet* 18(14):2523-2531.
144. Thoma CR*, et al.* (2009) VHL loss causes spindle misorientation and chromosome instability. *Nat Cell Biol* 11(8):994-1001.
145. Hell MP, Duda M, Weber TC, Moch H, & Krek W (2014) Tumor Suppressor VHL Functions in the Control of Mitotic Fidelity. *Cancer Res*.
146. Ansley SJ*, et al.* (2003) Basal body dysfunction is a likely cause of pleiotropic Bardet-Biedl syndrome. *Nature* 425(6958):628-633.
147. Harris PC (2009) 2008 Homer W. Smith Award: insights into the pathogenesis of polycystic kidney disease from gene discovery. *J Am Soc Nephrol* 20(6):1188-1198.
148. Geng L*, et al.* (1996) Identification and localization of polycystin, the PKD1 gene product. *J Clin Invest* 98(12):2674-2682.
149. Mochizuki T*, et al.* (1996) PKD2, a gene for polycystic kidney disease that encodes an integral membrane protein. *Science* 272(5266):1339-1342.
150. Yoder BK, Hou X, & Guay-Woodford LM (2002) The polycystic kidney disease proteins, polycystin-1, polycystin-2, polaris, and cystin, are co-localized in renal cilia. *J Am Soc Nephrol* 13(10):2508-2516.
151. Hurd TW & Hildebrandt F (2011) Mechanisms of nephronophthisis and related ciliopathies. *Nephron Exp Nephrol* 118(1):e9-14.
152. Fliegauf M*, et al.* (2006) Nephrocystin specifically localizes to the transition zone of renal and respiratory cilia and photoreceptor connecting cilia. *J Am Soc Nephrol* 17(9):2424-2433.
153. Fraser FC & Lytwyn A (1981) Spectrum of anomalies in the Meckel syndrome, or: "Maybe there is a malformation syndrome with at least one constant anomaly". *Am J Med Genet* 9(1):67-73.
154. Avner ED, Woychik RP, Dell KM, & Sweeney WE (1999) Cellular pathophysiology of cystic kidney disease: insight into future therapies. *Int J Dev Biol* 43(5):457-461.
155. Horikawa Y*, et al.* (1997) Mutation in hepatocyte nuclear factor-1 beta gene (TCF2) associated with MODY. *Nat Genet* 17(4):384-385.
156. Zhang MZ*, et al.* (2004) PKHD1 protein encoded by the gene for autosomal recessive polycystic kidney disease associates with basal bodies and primary cilia in renal epithelial cells. *Proc Natl Acad Sci U S A* 101(8):2311-2316.
157. Bisceglia M, Galliani CA, Senger C, Stallone C, & Sessa A (2006) Renal cystic diseases: a review. *Adv Anat Pathol* 13(1):26-56.
158. Hildebrandt F & Zhou W (2007) Nephronophthisis-associated ciliopathies. *J Am Soc Nephrol* 18(6):1855-1871.
159. Gunay-Aygun M (2009) Liver and kidney disease in ciliopathies. *Am J Med Genet C Semin Med Genet* 151C(4):296-306.
160. Moyer JH*, et al.* (1994) Candidate gene associated with a mutation causing recessive polycystic kidney disease in mice. *Science* 264(5163):1329-1333.
161. Boulter C*, et al.* (2001) Cardiovascular, skeletal, and renal defects in mice with a targeted disruption of the Pkd1 gene. *Proc Natl Acad Sci U S A* 98(21):12174-12179.

162. Lu W*, et al.* (1997) Perinatal lethality with kidney and pancreas defects in mice with a targetted Pkd1 mutation. *Nat Genet* 17(2):179-181.
163. Piontek K, Menezes LF, Garcia-Gonzalez MA, Huso DL, & Germino GG (2007) A critical developmental switch defines the kinetics of kidney cyst formation after loss of Pkd1. *Nat Med* 13(12):1490-1495.
164. Shibazaki S*, et al.* (2008) Cyst formation and activation of the extracellular regulated kinase pathway after kidney specific inactivation of Pkd1. *Hum Mol Genet* 17(11):1505-1516.
165. Pazour GJ, San Agustin JT, Follit JA, Rosenbaum JL, & Witman GB (2002) Polycystin-2 localizes to kidney cilia and the ciliary level is elevated in orpk mice with polycystic kidney disease. *Curr Biol* 12(11):R378-380.
166. Lin F*, et al.* (2003) Kidney-specific inactivation of the KIF3A subunit of kinesin-II inhibits renal ciliogenesis and produces polycystic kidney disease. *Proc Natl Acad Sci U S A* 100(9):5286-5291.
167. Marszalek JR, Ruiz-Lozano P, Roberts E, Chien KR, & Goldstein LS (1999) Situs inversus and embryonic ciliary morphogenesis defects in mouse mutants lacking the KIF3A subunit of kinesin-II. *Proc Natl Acad Sci U S A* 96(9):5043-5048.
168. Takeda S*, et al.* (1999) Left-right asymmetry and kinesin superfamily protein KIF3A: new insights in determination of laterality and mesoderm induction by kif3A-/- mice analysis. *J Cell Biol* 145(4):825-836.
169. Jonassen JA, SanAgustin J, Baker SP, & Pazour GJ (2012) Disruption of IFT complex A causes cystic kidneys without mitotic spindle misorientation. *J Am Soc Nephrol* 23(4):641-651.
170. Nishimura DY*, et al.* (2004) Bbs2-null mice have neurosensory deficits, a defect in social dominance, and retinopathy associated with mislocalization of rhodopsin. *Proc Natl Acad Sci U S A* 101(47):16588-16593.
171. Nachury MV*, et al.* (2007) A core complex of BBS proteins cooperates with the GTPase Rab8 to promote ciliary membrane biogenesis. *Cell* 129(6):1201-1213.
172. Solomon D & Schwartz A (1988) Renal pathology in von Hippel-Lindau disease. *Hum Pathol* 19(9):1072-1079.
173. Esteban MA, Harten SK, Tran MG, & Maxwell PH (2006) Formation of primary cilia in the renal epithelium is regulated by the von Hippel-Lindau tumor suppressor protein. *J Am Soc Nephrol* 17(7):1801-1806.
174. Lutz MS & Burk RD (2006) Primary cilium formation requires von hippel-lindau gene function in renal-derived cells. *Cancer Res* 66(14):6903-6907.
175. Schermer B*, et al.* (2006) The von Hippel-Lindau tumor suppressor protein controls ciliogenesis by orienting microtubule growth. *J Cell Biol* 175(4):547-554.
176. Lolkema MP*, et al.* (2007) The von Hippel-Lindau tumour suppressor interacts with microtubules through kinesin-2. *FEBS Lett* 581(24):4571-4576.
177. Mans DA*, et al.* (2008) Mobility of the von Hippel-Lindau tumour suppressor protein is regulated by kinesin-2. *Exp Cell Res* 314(6):1229-1236.
178. Lolkema MP*, et al.* (2008) Allele-specific regulation of primary cilia function by the von Hippel-Lindau tumor suppressor. *Eur J Hum Genet* 16(1):73-78.
179. Fan S*, et al.* (2004) Polarity proteins control ciliogenesis via kinesin motor interactions. *Curr Biol* 14(16):1451-1461.
180. Okuda H*, et al.* (1999) Direct interaction of the beta-domain of VHL tumor suppressor protein with the regulatory domain of atypical PKC isotypes. *Biochem Biophys Res Commun* 263(2):491-497.
181. Wilson NF & Lefebvre PA (2004) Regulation of flagellar assembly by glycogen synthase kinase 3 in Chlamydomonas reinhardtii. *Eukaryot Cell* 3(5):1307-1319.
182. Hergovich A*, et al.* (2006) Priming-dependent phosphorylation and regulation of the tumor suppressor pVHL by glycogen synthase kinase 3. *Mol Cell Biol* 26(15):5784-5796.
183. Cross DA, Alessi DR, Cohen P, Andjelkovich M, & Hemmings BA (1995) Inhibition of glycogen synthase kinase-3 by insulin mediated by protein kinase B. *Nature* 378(6559):785-789.

184. Zhang HH, Lipovsky AI, Dibble CC, Sahin M, & Manning BD (2006) S6K1 regulates GSK3 under conditions of mTOR-dependent feedback inhibition of Akt. *Mol Cell* 24(2):185-197.
185. Shin Lee J, Seok Kim H, Bok Kim Y, Cheol Lee M, & Soo Park C (2003) Expression of PTEN in renal cell carcinoma and its relation to tumor behavior and growth. *J Surg Oncol* 84(3):166-172.
186. Elliott JC & Dover SD (1982) X-ray microtomography. *J Microsc* 126(Pt 2):211-213.
187. Ritman EL (2011) Current status of developments and applications of micro-CT. *Annu Rev Biomed Eng* 13:531-552.
188. Schambach SJ, Bag S, Schilling L, Groden C, & Brockmann MA (2010) Application of micro-CT in small animal imaging. *Methods* 50(1):2-13.
189. Ohta S*, et al.* (2006) MicroCT for high-resolution imaging of ectopic pheochromocytoma tumors in the liver of nude mice. *Int J Cancer* 119(9):2236-2241.
190. Badea CT, Drangova M, Holdsworth DW, & Johnson GA (2008) In vivo small-animal imaging using micro-CT and digital subtraction angiography. *Phys Med Biol* 53(19):R319-350.
191. Almajdub M, Magnier L, Juillard L, & Janier M (2008) Kidney volume quantification using contrast-enhanced in vivo X-ray micro-CT in mice. *Contrast Media Mol Imaging* 3(3):120-126.
192. Degenhardt K, Wright AC, Horng D, Padmanabhan A, & Epstein JA (2010) Rapid 3D phenotyping of cardiovascular development in mouse embryos by micro-CT with iodine staining. *Circ Cardiovasc Imaging* 3(3):314-322.
193. Phelps ME, Gado MH, & Hoffman EJ (1975) Correlation of effective atomic number and electron density with attenuation coefficients measured with polychromatic x rays. *Radiology* 117(3 Pt 1):585-588.
194. Vogel J (1997) Measurement of cardiac output in small laboratory animals using recordings of blood conductivity. *Am J Physiol* 273(5 Pt 2):H2520-2527.
195. Kiessling F*, et al.* (2004) Volumetric computed tomography (VCT): a new technology for noninvasive, high-resolution monitoring of tumor angiogenesis. *Nat Med* 10(10):1133-1138.
196. Yamada KM & Cukierman E (2007) Modeling tissue morphogenesis and cancer in 3D. *Cell* 130(4):601-610.
197. Debnath J*, et al.* (2002) The role of apoptosis in creating and maintaining luminal space within normal and oncogene-expressing mammary acini. *Cell* 111(1):29-40.
198. Guo Q*, et al.* (2008) The microenvironmental determinants for kidney epithelial cyst morphogenesis. *Eur J Cell Biol* 87(4):251-266.
199. Leung CT & Brugge JS (2012) Outgrowth of single oncogene-expressing cells from suppressive epithelial environments. *Nature* 482(7385):410-413.
200. Bowes RC, 3rd, Lightfoot RT, Van De Water B, & Stevens JL (1999) Hepatocyte growth factor induces tubulogenesis of primary renal proximal tubular epithelial cells. *J Cell Physiol* 180(1):81-90.
201. Miya M*, et al.* (2011) Enhancement of in vitro human tubulogenesis by endothelial cell-derived factors: implications for in vivo tubular regeneration after injury. *Am J Physiol Renal Physiol* 301(2):F387-395.
202. Montesano R, Ghzili H, Carrozzino F, Rossier BC, & Feraille E (2009) cAMP-dependent chloride secretion mediates tubule enlargement and cyst formation by cultured mammalian collecting duct cells. *Am J Physiol Renal Physiol* 296(2):F446-457.
203. Petersen OW, Ronnov-Jessen L, Howlett AR, & Bissell MJ (1992) Interaction with basement membrane serves to rapidly distinguish growth and differentiation pattern of normal and malignant human breast epithelial cells. *Proc Natl Acad Sci U S A* 89(19):9064-9068.
204. Vichai V & Kirtikara K (2006) Sulforhodamine B colorimetric assay for cytotoxicity screening. *Nat Protoc* 1(3):1112-1116.
205. Lee GY, Kenny PA, Lee EH, & Bissell MJ (2007) Three-dimensional culture models of normal and malignant breast epithelial cells. *Nat Methods* 4(4):359-365.

206. Shao X, Somlo S, & Igarashi P (2002) Epithelial-specific Cre/lox recombination in the developing kidney and genitourinary tract. *J Am Soc Nephrol* 13(7):1837-1846.
207. Haase VH, Glickman JN, Socolovsky M, & Jaenisch R (2001) Vascular tumors in livers with targeted inactivation of the von Hippel-Lindau tumor suppressor. *Proc Natl Acad Sci U S A* 98(4):1583-1588.
208. Ryan HE*, et al.* (2000) Hypoxia-inducible factor-1alpha is a positive factor in solid tumor growth. *Cancer Res* 60(15):4010-4015.
209. Boehlke C*, et al.* (2010) Primary cilia regulate mTORC1 activity and cell size through Lkb1. *Nat Cell Biol* 12(11):1115-1122.
210. Linehan WM, Srinivasan R, & Schmidt LS (2010) The genetic basis of kidney cancer: a metabolic disease. *Nat Rev Urol* 7(5):277-285.
211. Semenza GL (2007) HIF-1 mediates the Warburg effect in clear cell renal carcinoma. *J Bioenerg Biomembr* 39(3):231-234.
212. Martin-Belmonte F*, et al.* (2007) PTEN-mediated apical segregation of phosphoinositides controls epithelial morphogenesis through Cdc42. *Cell* 128(2):383-397.
213. Mroue R & Bissell MJ (2013) Three-dimensional cultures of mouse mammary epithelial cells. *Methods Mol Biol* 945:221-250.
214. Ma M, Tian X, Igarashi P, Pazour GJ, & Somlo S (2013) Loss of cilia suppresses cyst growth in genetic models of autosomal dominant polycystic kidney disease. *Nat Genet* 45(9):1004-1012.
215. Berbari NF, O'Connor AK, Haycraft CJ, & Yoder BK (2009) The primary cilium as a complex signaling center. *Curr Biol* 19(13):R526-535.
216. Frew IJ & Krek W (2008) pVHL: a multipurpose adaptor protein. *Sci Signal* 1(24):pe30.
217. Bernhardt WM*, et al.* (2007) Involvement of hypoxia-inducible transcription factors in polycystic kidney disease. *Am J Pathol* 170(3):830-842.
218. Deere JD*, et al.* (2010) Viral decay kinetics in the highly active antiretroviral therapy-treated rhesus macaque model of AIDS. *PLoS One* 5(7):e11640.
219. Rowe I*, et al.* (2013) Defective glucose metabolism in polycystic kidney disease identifies a new therapeutic strategy. *Nat Med* 19(4):488-493.
220. Shillingford JM*, et al.* (2006) The mTOR pathway is regulated by polycystin-1, and its inhibition reverses renal cystogenesis in polycystic kidney disease. *Proc Natl Acad Sci U S A* 103(14):5466-5471.
221. Fischer E & Pontoglio M (2009) Planar cell polarity and cilia. *Semin Cell Dev Biol* 20(8):998-1005.
222. Xu R*, et al.* (2013) Polycystic kidneys have decreased vascular density: a micro-CT study. *Microcirculation* 20(2):183-189.

Grants & Awards

March 2014 Travel reimbursement of the Cancer Biology Ph.D program and the Swiss Physiological Society for the Keystone Symposium: Cilia, Development and Human Disease

April 2013 Poster award from the Cancer Network Zurich

List of Publications

"Pharmacological potential of RNAi--focus on miRNA" Pfeifer A. and **Lehmann H.**; Pharmacol Ther. 2010 Jun; 126(217-27)